2018-12-01

Development of a Simplified Analysis Approach for Predicting Pile Deflections of Piers Subjected to Lateral Spread Displacements and Application to a Pier Damaged During the 2010 Maule, Chile, M8.8 Earthquake

Logan Matthew Palmer
Brigham Young University

Development of a Simplified Analysis Approach for Predicting Pile Deflections of Piers Subjected to Lateral Spread Displacements and Application to a Pier Damaged During the 2010 Maule, Chile, M8.8 Earthquake

Logan Matthew Palmer

A thesis submitted to the faculty of
Brigham Young University
in partial fulfillment of the requirements for the degree of

Master of Science

Kevin W. Franke, Chair
Kyle M. Rollins
Paul W. Richards

Department of Civil and Environmental Engineering

Brigham Young University

ABSTRACT

Development of a Simplified Analysis Approach for Predicting Pile Deflections of Piers Subjected to Lateral Spread Displacements and Application to a Pier Damaged During the 2010 Maule, Chile, M8.8 Earthquake

Logan Matthew Palmer
Department of Civil and Environmental Engineering, BYU
Master of Science

The 2010, moment magnitude 8.8 earthquake that occurred near Maule, Chile caused major damages to several piers in the Port of Coronel located approximately 160 kilometers (100 miles) to the South of the earthquake epicenter. One of the piers, the North Pier, experienced significant lateral spreading that was caused from liquefaction of the soils at the approach zone of the pier. Damages from lateral spreading and liquefaction effects consisted of sheet pile welding ruptures of the cross-support beams, stiffener buckling, pile displacements, pile rotations, and pier deck displacement. Researchers analyzed the North Pier after the earthquake and documented in detail the damage caused by lateral spread displacements.

This study introduces a simplified performance-based procedure called the "Simplified Modeling Procedure" that is used for the analysis of piles supporting a pier that are exposed to lateral spread displacements. The procedure uses the software LPILE, a common program for analyzing a single pile under lateral loading conditions, to evaluate a more complex multi-pile pier design. Instead of analyzing each of the piles in a given pier individually, the procedure utilizes what is known as a "Super Pile" approach to combine several piles into a single representative pile during the analysis. To ensure displacement compatibility between each "Super Pile" in the analysis, the "Super Piles" are assumed to be fully connected at the top of each "Super Pile" to the pier deck. The Simplified Modeling Procedure is developed and tested using the case study history of the North Pier from the Port of Coronel during the 2010 Maule earthquake.

The Simplified Modeling Procedure incorporates p-y springs with a lateral push-over analysis. This approach allows the analysis to be performed in a matter of seconds and allows the user to more easily draw the needed correlations between the rows of piles. This procedure helps identify that different rows of piles either contribute to the movement of the pier or contribute to the bracing of the pier. The procedure ultimately predicts the anticipated pier deck deflection by determining when all the pile rows and their respective shear forces are in equilibrium.

The Simplified Modeling Procedure predicted that the North Pier experienced deflections between approximately 0.31 meters (1.01 feet) and 0.38 meters (1.26 feet). The predicted deflections and rotations determined using the procedure were determined to be a relatively close representation of the observations made during the post-earthquake reconnaissance observations.

Keywords: Maule, Liquefaction, Lateral Spread, Simplified Modeling Procedure, Super Pile

ACKNOWLEDGEMENTS

I would like to thank everyone that has personally had a part of helping reach the completion of this thesis. It was not an easy task by any means, but I did it thanks to all the support and encouragement. It is a journey that I will never forget.

First, I would personally like to recognize the National Science Foundation (NSF) and thank them for providing the funding that went towards the research. In addition to the NSF, I would like to thank Northern Geotechnical Engineering and Keith Mobley for providing my tuition while I was attending classes. The provided supplemental funds from these sources allowed me to fulfill my dream of completing a master's degree.

I would also like to thank my professors, Dr. Franke and Dr. Rollins for their support and guidance throughout this process. Although there were times that I probably let them down, they never once gave up on me. They pushed me to the end and provided the knowledge I needed to complete everything.

Lastly, but most importantly, I am so grateful for my friends, family, and fellow students for all their support. When things got difficult and I became discouraged, they knew exactly how to get me back into the right mood and back on track. They were always willing to listen to all of my frustrations and nonsense. My wife and son, Hailey and Flint, became my life and sometimes my only source of joy throughout this journey. I am so grateful for both of you. You were a much-needed distraction and gave me the motivation that was needed to finish. Thanks for not giving up on me. We did it together! I love you!

TABLE OF CONTENTS

LIST OF TABLES

LIST OF FIGURES

1 INTRODUCTION

After a significantly large earthquake has occurred, there are damages to structures, often as a result of two earthquake effects: liquefaction and lateral spreading displacement. These effects can often result in significant damages to infrastructures that are founded in materials that undergo these effects (e.g. piers, bridges, etc.). These effects were observed in an earthquake (moment magnitude of 8.8) that occurred in 2010 near Maule, Chile. It has become custom after a large earthquake for various groups of reconnaissance teams to visit the damaged sites to better understand what happened and learn how to better prepare for future events. Part of the reconnaissance effort after an earthquake is to gather relevant data associated with liquefaction and lateral spread that can then be used for research in developing new concepts, new mitigation approaches, new standards of code, or even new procedures to predict and mitigate future effects.

This study had two primary focuses:

1. Can the reconnaissance data collected on the North Pier, located in the Port of Coronel, Chile be used to develop a "simplified" procedure to deterministically determine the anticipated displacements of a pier deck and the supporting piles that have been exposed to liquefaction and lateral spread displacements?

2. Can this procedure be performed using a common software package that is well known to many practicing engineers?

With these two things in mind, this study introduces an analysis method that can be used in the commonly known software, LPILE 2016. This analysis approach will subsequently be referred to as the "Simplified Modeling Procedure".

Before introducing the Simplified Modeling Procedure, this thesis will present a review of the foundational elements of liquefaction and lateral spreading. Additionally, a review of the 2010 Maule, Chile Earthquake and the reconnaissance efforts will be included for an understanding of the data presented in the procedure. Finally, the procedure will be presented and discussed in a step-by-step format along with its application to the North Pier. A step-by-step instructional format is used so that the procedure may be replicated and applied to future events.

2 REVIEW OF LIQUEFACTION

2.1 Introduction to Liquefaction

Liquefaction is a phenomenon when soils begin to act like a liquid. This is due to the increase in pore pressures from soil strains due to earthquake movements. Liquefaction of underlying soil layers can cause surficial lateral spreading during an earthquake. Surficial lateral spread displacements is one of the most destructive elements during seismic activity. Lateral spreading can lead to extreme damages to lifelines and structures. The horizontal movement associated with lateral spreading usually occurs because of sloping ground or a nearby free-face, like a body of water. The ability to properly predict liquefiable soils layers that could potential lead to lateral spread displacements can lead to better seismically resilient facilities and lifelines. As liquefaction is the cause of lateral spreading, this chapter will discuss and review liquefaction. Lateral spreading and its effects will then be further discussed in Chapter 3.

2.2 Liquefaction

The phenomenon of soil liquefaction experienced during earthquakes was often observed historically, but the term was not used in publication until 1953 by Mogami and Kubo (1953). The 1964 Portage, Alaska (Mw=9.2) and Niigata, Japan (Mw=7.5) earthquakes brought the phenomenon to the forefront of engineering interest and attention. Through extensive research, the mechanics of liquefaction are much better understood today, but, due to the complexity of this phenomenon, intense research is still ongoing. Each new case added to the body of research

clarifies and advances essential understanding necessary for predicting the onset and behavior of soil liquefaction.

Liquefaction is known to occur in saturated soils and is, therefore, typically observed in soils near rivers, bays, and other bodies of water (Kramer 1996). Sands are the most susceptible to the phenomenon of liquefaction because they rely on inter-particle friction for shear strength and stability. When an earthquake occurs, the ground motions cause the particles to reconfigure and either become more dense or loose, depending on how they are deposited before the earthquake. A dense soil tends to expand with earthquake ground motions while loose soils tend to contract. The formation of negative pore pressure in dense soils limits concern for liquefaction, eliminating the need for further discussion here. Conversely, loose soils that have the ability to contract are more likely to experience problems because of the formation of greater positive pore pressures. A quick understanding of effective stresses explains why the pore pressures are critical in these cases. Effective stress represents the pressure the soil actually feels when loaded. The closer to zero the effective stress becomes, the lower the shear strength and stiffness of the soil. Effective stress is a function of the total stress of the soil and the pore pressures between particles. Equation (2-1) is used to determine the effective stresses in soil.

$$\sigma' = \sigma - \mu \tag{2-1}$$

where σ' is the effective vertical stress, σ is the total vertical stress, and μ is the pore pressure.

Liquefaction occurs when the pore pressure generation is greater than the drainage capacity of a saturated, loose, soil. In this condition, water becomes trapped in the spaces

between particles resulting in a temporary, undrained soil condition. When the particles attempt to contract in an undrained condition, the pore pressures significantly increase while the inter-particle friction decreases. If the pore pressures increase and approach, or exceed, the total vertical stresses of the soil, the soil will begin to flow like a liquid, while the shear strength decreases to zero. After time, the water will drain and the pore pressures will dissipate leading to regained strength in the soil.

The phenomenon of liquefaction is exhibited in two general ways: flow liquefaction and cyclic mobility. Flow liquefaction can occur when the shear stress required for static equilibrium of a soil mass is greater than the shear strength of the soil in its liquefied state (Kramer, 1996). Flow liquefaction generally results in a sudden and catastrophic soil deformation, called flow failure. Flow liquefaction is the most extreme and most dangerous form of soil failure to infrastructure. Flow failures are found more commonly on sloping grounds where the soil becomes unstable under its own weight. In spite of being less common, these failures can result in very large soil displacements and can occur very quickly and without warning.

Cyclic mobility is much more common and is less extreme and dangerous. This expression of liquefaction occurs when the static shear stresses in the soil are less than the shear strength of the liquefied soil. Resulting cyclic mobility failures are driven by both cyclic and static shear stresses that develop incrementally in the soil during the earthquake (Kramer, 1996). This kind of failure is more common in areas of little to no slope. The effect of this failure is that the soil moves in lurches, like a ratcheting effect. Although cyclic mobility is considered less dangerous, it can still result in very large horizontal displacements that can be devastating to infrastructure.

The mechanics of liquefaction become better understood with each observed case history. As the available data increases, researchers have not only increased the understanding of the mechanics of liquefaction, but identified many different aspects of the phenomenon. Three main aspects should be considered when evaluating soils and their potential to experience liquefaction: liquefaction susceptibility, liquefaction initiation, and liquefaction effects.

2.3 Liquefaction Susceptibility

Not all soils are susceptible to liquefaction; as a result, certain soils can be neglected during liquefaction analysis. The challenge for researchers lies in identifying which layers of soil are susceptible and which are not. The most common criteria employed when evaluating the susceptibility of a soil to liquefy are historical criteria, geological criteria, compositional criteria, and state criteria (Kramer, 1996).

2.3.1 Historical Criteria

During past post-earthquake evaluations and research, investigators have demonstrated trends that indicate that a soil that has previously experienced liquefaction is more susceptible to repeated occurrences of liquefaction if environmental conditions have not been altered (Youd, 1984). Additionally, researchers have evaluated prehistoric conditions of liquefaction and have used resulting observations to predict future areas that are potentially susceptible to liquefaction. Identified prehistoric occurrences are referred to as “paleoliquefaction” (Obermeier and Pond, 1999). Understanding past occurrences, both paleo and more contemporary, can be beneficial to engineers, especially when determining site conditions for new construction in areas prone to seismic activity. Preventative steps can be taken to reduce liquefaction hazard.

2.3.2 Geological Criteria

The environment in which soils were deposited in the past is another critical criteria aiding the ability to predict potential liquefaction in specific areas. The susceptibility of deposited soils to liquefy is dependent on a combination of the geologic age of the soils and the hydrological environment (Youd and Hoose, 1978). Older deposits are less susceptible. For example, Holocene deposits (nearly 11,700 years ago to present) are more susceptible than Pleistocene (2.59 million years to 11,700 years ago or the last glacial period). Pre-Pleistocene deposits have rarely been observed to undergo liquefaction (Youd and Hoose, 1978). The type of hydrological deposit is also an important key to the evaluation of susceptibility. Loose, shallow, deposited soils (i.e. alluvial, fluvial, Aeolian, and man-made deposits) are particularly susceptible when saturated. Seismic reconfiguration and subsequently generated excess positive pore pressures initiates volume changes in soils with loose configuration, leading to liquefaction (see Section 2.2 for a more detailed explanation of this process).

2.3.3 Compositional Criteria

The size, shape, and gradation of the soil particles all impact the susceptibility of a soil to liquefy. Soils that resist volume change (i.e. well-graded soils with greater amounts of fines) are less susceptible to liquefaction. Soils comprised of cementitious elements, such as carbonatious soils are also less likely to be susceptible. Soils that are liquefiable must undergo volume change (i.e. strain) to trigger pore pressure generation and liquefaction. Soils that are loose and have contractive volume changes that generate excess positive pore pressures are more prone to liquefaction.

Originally researchers assumed that only sands were able to experience this phenomenon. However, research has shown this phenomenon is not limited to just sand, but also gravels and silts. Liquefaction has been observed during field studies for gravels (Coulter and Miglaccio, 1966; Wong et al.,1975; Chen et al., 2009) and coarse non-plastic silts (Ishihara, 1984; Ishihara, 1985). Although research has demonstrated that fine grained soils can liquefy, it is difficult to produce the necessary high pore pressures needed for the development of liquefaction and therefore, are typically categorized as non-susceptible. Additionally, low-plastic clays undergo a strain softening process called "cyclic softening" (Idriss and Boulanger, 2008) which is similar to liquefaction but doesn't have the same destructive effects (Youd et al., 2009).

2.3.4 State Criteria

Even if a soil meets all of the preceding criteria for liquefaction susceptibility, its susceptibility to liquefaction remains dependent on the initial relative density and effective confining stress. (Kramer, 1996). Excess pore pressure drives the liquefaction process and therefore, these initial conditions, or "states", determine whether a soil will dilate or contract under cyclic loading (earthquakes). These criteria ultimately help determine whether or not a soil is susceptible to liquefaction. Additionally, the state in which soils are susceptible to either flow liquefaction or cyclic mobility are different. These relationships are further explained with the critical void ratio observation originally made by Casagrande (1936).

2.3.4.1 Critical Void Ratio

While performing experiments with drained triaxial tests of sands, Casagrande (1936) observed that two samples consisting of the same sand and undergoing the same effective confining pressure would both contract and dilate depending on whether the sand was initially

loosely or densely compacted. However, his observations showed that both conditions converged to the same void ratio when sheared in the drained condition, regardless of the initial density. He further predicted that if the same soil were to be sheared in the undrained condition, the soil would still converge to the same void ratio. He identified this resulting void ratio as the critical void ratio (CVR) of a soil. A CVR line for a particular soil type can be created for all possible void ratios and confining stress combinations. It is important to note that each type of soil has a unique CVR line. Additionally, when a CVR line is plotted it creates a boundary that delineates "loose" contractive behavior (above the line) from "dense" dilative behavior (below the line). Subsequently, points plotted above the CVR were considered to be susceptible to liquefaction and those plotted below the CVR line were not considered to be susceptible. Figure 2-1 shows this behavior and an example of a CVR line.

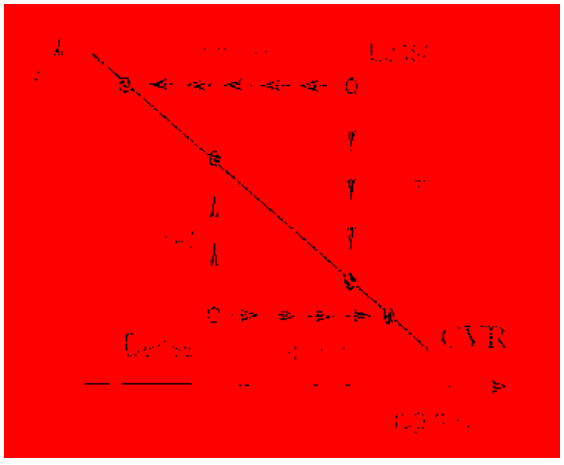

Figure 2-1: Behavior of Initially Loose and Dense Specimen Under Drained and Undrained Conditions for Logarithmic Effective Confining Stress (after Kramer, 1996)

Unfortunately, the liquefaction failure of the Fort Peck Dam in 1938 demonstrated that Casagrande's theory of the CVR line was critically flawed or incomplete. The soil from the dam plotted below the CVR line which, according to Casagrande's theory, indicated that the soil should have been non-susceptible to liquefaction (Middlebrooks, 1942).

2.3.4.2 Steady State of Deformation

After the Fort Peck Dam failure and discovery of the flaw in Casagrande's theory, Castro (1969) began studying the CVR theory further and made some important discoveries. He conducted static and cyclic triaxial tests on both isotropically and anisotropically consolidated sands. From these tests, Castro observed that loose soils would first reach peak strength at small shear strains and then suddenly collapse and begin to flow rapidly at large strains. These soils ended with low residual strength due to the generation of positive pore pressures. He referred to this behavior as "liquefaction". He also observed that dense soils would initially contract very slightly before dilating, resulting in large residual strength at smaller strains due to the generation of negative pore pressures. Castro called this behavior "dilation". Lastly, intermediate dense soils would follow the trend of loose soils initially and undergo strain softening. Though with further straining, soils would begin to dilate and regain strength similar to the behavior of dense soils. He referred to this behavior of intermediate dense soils as "limited liquefaction". Figure 2-2 shows a plot of these observations.

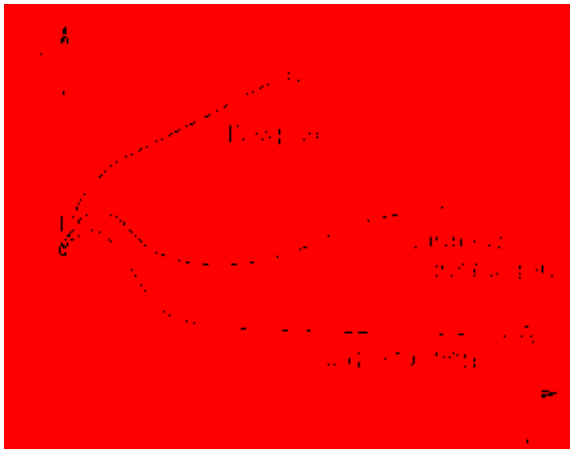

Figure 2-2: Castro (1969) Observations of A) Loose, B) Dense, and C) Medium Dense Soils (after Kramer, 1996)

Castro also noticed that there was a unique relationship between void ratio and effective confining pressure at large strains. This observed relationship plotted roughly parallel to but just below the CVR line. He called this new line the steady state line (SSL). The difference between the two lines was attributed to the development of the flow structure under stress-controlled conditions (Kramer, 1996). Later research further defined that the state at which soil flowed continuously under either constant shear stress, effective confining pressure, pressure, or velocity would be referred to as the "steady state of deformation" (Castro and Poulos, 1977; Poulos, 1981). Another term defined from this research was the strength of the soil in this state. This strength is referred to as the steady state strength, S_{su}. The SSL can also be expressed in terms of the S_{su}. Similar to the CVR line, a soil that plots above the SSL and has static shear stress greater that $S_{su,}$ is considered to be susceptible to flow liquefaction. A comparison of the CVR and SSL line can be seen in Figure 2-3.

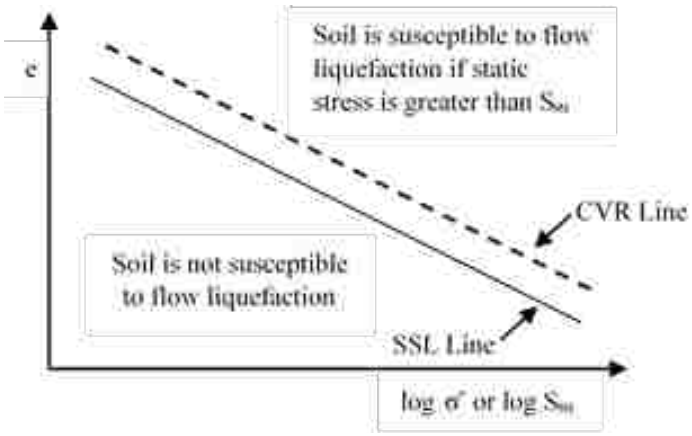

Figure 2-3: Comparison of the CVR and SSL Lines (after Kramer, 1996 Recreated w/ Modifications)

Castro's observations of the SSL line in defining susceptible and non-susceptible soils can only be applied to flow liquefaction. Cyclic mobility, on the other hand, can occur in both loose and dense soils and therefore soils undergoing cyclic mobility can plot both above and below the SSL (Kramer, 1996).

2.4 Liquefaction Initiation

Even if a soil is classified as being susceptible to liquefaction, it does not necessarily mean that the soil will, in fact, liquefy under a given level of seismic loading. Initiation of liquefaction is dependent the duration and the amplitude of the loading from a seismic event. For liquefaction to initiate, significantly large and/or long ground motions from seismic activity must alter the state of the soil enough to create a zero effective stress condition. Identifying the state of the soil when liquefaction is triggered is critical to understanding initiation of liquefaction (Kramer, 1996). Both flow liquefaction and cyclic mobility failures differ in their processes of

initiation mechanics. Due to these differences, both liquefaction failures will be briefly introduced and discussed here.

2.4.1 Flow Liquefaction Surface

Although less common, flow liquefaction is possibly the most dangerous of all the possible liquefaction failures. This type of failure is initiated when the initial shear stress state of the soil is greater than the steady state strength and the duration and/or amplitude of the loading is sufficient enough to push the stress path to the flow liquefaction surface (FLS). The FLS was first observed during triaxial tests performed by Hanzawa et al. (1979) while testing five soil samples that were initially consolidated to the same void ratio but exposed to different effective pressures. The soil stress paths during monotonic loading were plotted and it was determined that, at the peak of each stress path, there was a failure surface that the soils would reach before rapidly converging to S_{SU} on the Mohr-Coulomb failure envelope. Figure 2-4 shows the observations made by Hanzawa et al. (1979) during monotonic loading conditions.

From Figure 2-4 the line created by connecting all the failure points along the stress paths of soils C,D, and E can be used to define the FLS in p-q space. The FLS represents a boundary of stability in undrained shear conditions, and is effectively the boundary at which flow liquefaction is initiated. Vaid and Chern (1983) were the first to show that flow liquefaction will initiate if the stress condition in an element of soil reaches the FLS by monotonic or cyclic loading. Additionally, Figure 2-4 shows that points that initially plot below the SSL (soils A and B), experience dilative behavior and don't ever reach the FLS. They therefore do not undergo flow liquefaction, but ultimately converge to S_{SU} on the Mohr-Coulomb failure envelope.

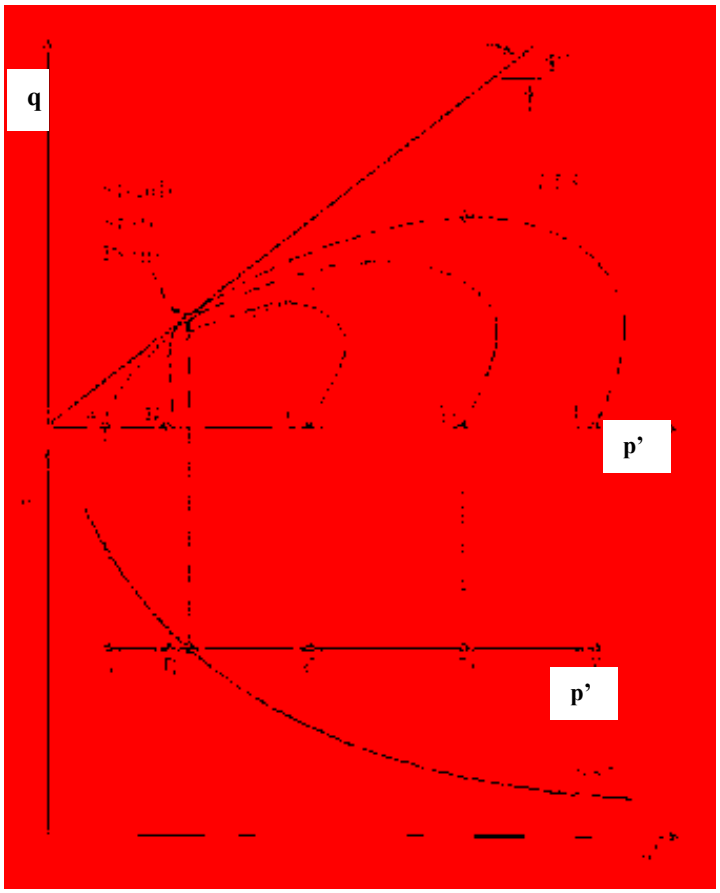

Figure 2-4: Flow Liquefaction Surface (after Kramer, 1996)

Flow liquefaction is triggered throughout two different stages. In the first stage, the generation of sufficient excess pore pressure is needed to move the stress path from the initial condition to the FLS. This excess pore pressure is generated from either monotonic or cyclic loading. In the second stage, the stress path of the soil converges rapidly towards S_{SU}, usually from static stresses associated with the soil's own weight. The first stage occurs under stress-controlled conditions while the second stage is inevitable if the FLS is reached (Kramer, 1996). Figure 2-5 shows the zone in which the stress state is associated with flow liquefaction.

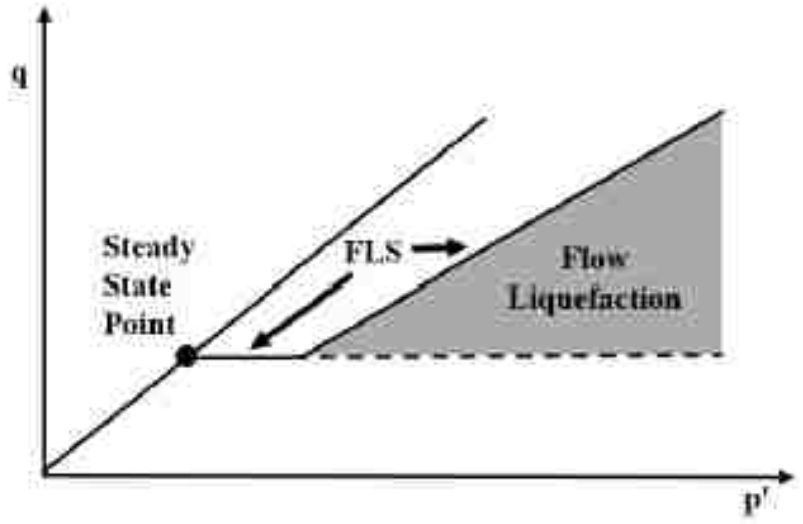

Figure 2-5: Zone Susceptible to Flow Liquefaction Failure (after Kramer, 1996)

2.4.2 Cyclic Mobility

Cyclic mobility is a more common result of soil liquefaction failure. Unlike flow liquefaction, this type of failure occurs when the initial shear stress state of the soil is less than the S_{SU}. As previously mentioned, cyclic mobility can occur with loose or dense soils at low or high effective confining pressures. Figure 2-6 illustrates the stress state zone associated with cyclic mobility.

Cyclic mobility occurs when undrained cyclic loading conditions cause pore pressure build up, initiating a gradual loss of strength of the soil. Kramer (1996) presents three cyclic loading conditions that can explain the gradual loss of strength. These three conditions presented by Kramer can be seen in Figure 2-7.

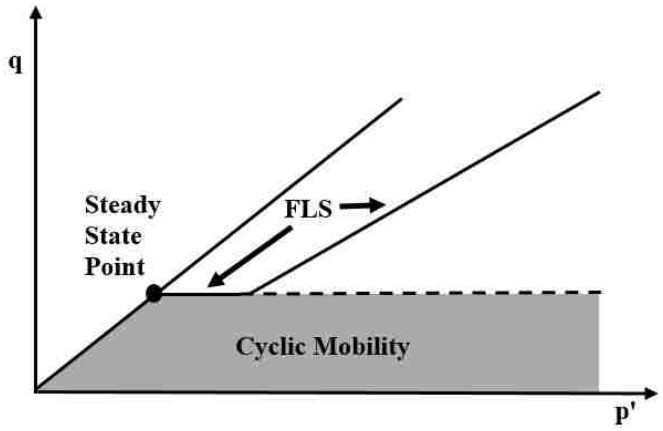

Figure 2-6: Zone Susceptible to Cyclic Mobility Failure (after Kramer, 1996)

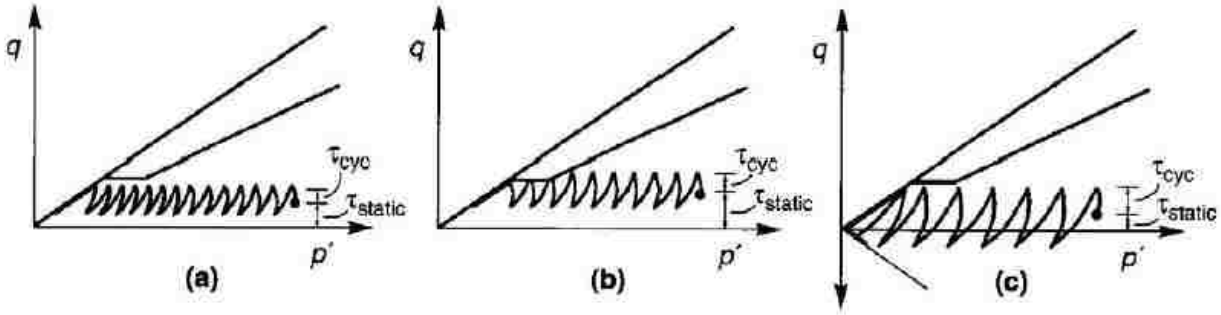

Figure 2-7: Three Cases of Cyclic Mobility Presented by Kramer (1996)

The first condition (Figure 2-7a) occurs when $\tau_{static} - \tau_{cyclic} > 0$ and $\tau_{static} + \tau_{cyclic} < S_{SU}$. In this condition, the soil is in constant compression, has no stress reversal, and does not ever exceed the S_{SU}. As can be seen on the chart, the effective stress path moves to the left until it reaches the failure envelope. This loading condition is accompanied with gradual strength loss and an increase in the permanent shear strains.

The second condition (Figure 2-7b) occurs when $\tau_{static} - \tau_{cyclic} > 0$ and $\tau_{static} + \tau_{cyclic} > S_{SU}$. In this condition there is no stress reversal, like in the first condition, but S_{SU} is momentarily exceeded due to larger stress loads. Once again, the stress path moves to the left with additional loading. Since S_{SU} is exceeded, the stress path will eventually reach the FLS, after which the rate of pore pressure generation will increase as it continues to the failure envelope. The result will be a period of instability (liquefaction) where significant permanent strain may develop.

The third and final condition (Figure 2-7c) occurs when $\tau_{static} - \tau_{cyclic} < 0$ and $\tau_{static} + \tau_{cyclic} < S_{SU}$. In this condition, the S_{SU} is never exceeded, but instead, the stresses undergo a reversal of compressional and extensional loading. Dobry et al. (1982) and Mohamad and Dobry (1986) have shown that when this kind of stress reversal occurs, the rate of pore pressure generation increases rapidly which ultimately leads to liquefaction failure. As with the first two conditions, the stress path continues until the failure envelope is reached.

Unlike flow liquefaction failure, there is no clear point where cyclic mobility is initiated. Instead, permanent strains and the associated deformations accumulate incrementally throughout the loading process. The magnitude of the strains and deformations are dependent on the duration, amplitude, and frequency of the ground motions during seismic activity.

2.4.3 Assessing the Potential of Liquefaction Initiation

There are two primary types of hazard assessments used in practice today: the Cyclic Stress Approach and the Cyclic Strain Approach (Kramer, 1996). Each has specific advantages and limitations, but engineers most commonly apply the cyclic stress approach because stresses

are generally easier to predict in the soil than strains. It is not uncommon to apply both approaches on important projects for conservatism and/or redundancy.

2.4.3.1 Cyclic Stress Approach

The cyclic stress approach compares the earthquake-induced loading with the liquefaction resistance of the soil. These two factors, earthquake loading and soil resistance, are both expressed in terms of cyclic shear stresses labeled cyclic stress ratio (CSR) and cyclic resistance ratio (CRR), respectively. Liquefaction is expected to occur at locations where the loading exceeds the resistance (Kramer, 1996). This process compares the CRR to the CSR to determine the factor of safety against liquefaction (FS_L). The equation used for this process is shown in Equation (2-2):

$$FS_L = \frac{\tau_{cyc,L}}{\tau_{cyc}} = \frac{CRR}{CSR} \tag{2-2}$$

where $\tau_{cyc,L}$ is the cyclic shear stress required to initiate liquefaction that is determined in the lab and τ_{cyc} is the equivalent cyclic shear stress induced by the earthquake loading.

Models using different in-situ tests to compute CRR have been developed for convenience and ease. Models for the cone penetrometer test (CPT) have been developed by Douglas et al. (1981), Robertson and Campanella (1985), Seed and De Alba (1986), Mitchell and Tseng (1990), Martin (1992), Kayen et al. (1992), Ishihara (1993), Carraro et al. (2003), Ku et al. (2004), Andrus et al. (2004), and Moss et al. (2006). Additionally, the shear wave velocity (Stokoe et al., 1988; Tokimatsu et al., 1991; Finn et al., 1991; Kayen et al., 1992; Suzuki et al.,

2004; Andrus et al., 2004), the dilatometer index (Marchetti, 1982; Robertson and Campanella, 1986; Reyna and Chameau, 1991), and the standard penetration test (SPT) (Seed et al., 1983, 1985; Youd et al., 2001; Cetin et al., 2004; Idriss and Boulanger, 2008) have been used to compute CRR values. Although CPT methods are gaining popularity, SPT-based methods are generally the most used by engineers due to the widespread use of the SPT for site characterization.

Three different seismic stress approaches using SPT-based evaluations have been presented in recent years by Youd et al. 2001, Cetin et al. 2004, and Idriss and Boulanger 2010. These three approaches will be further discussed in Section 2.4.4.

2.4.3.2 Cyclic Strain Approach

In an effort to develop a more robust approach, procedures using cyclic strains instead of cyclic stresses were developed by Dobry and Ladd (1980), Dobry et al. (1982, 1984), and Vasquez-Herrera and Dobry (1988). This approach is based on experimental evidence from Silver and Seed (1971) and Youd (1972) that shows densification of dry sands to be controlled by cyclic strains rather than cyclic stresses and that pore pressure generation is fundamentally more related to cyclic strains than cyclic stresses. The cyclic strain approach is an alternative to the cyclic stress approach and is more challenging to use due to the difficulty predicting accurate strains accumulated from seismic loading (Seed, 1980). Because of these limitations, this approach merits only brief consideration here. The overall procedure of this approach will not be further discussed in this thesis.

2.4.4 SPT-Based Evaluation of Liquefaction Initiation

After the 1964 Portage, Alaska and Niigata, Japan Earthquakes, Seed and Idriss (1971) published what they called the "Simplified Procedure" for predicting liquefaction. This procedure quickly gained popularity because of its simpler approach. The process has been reevaluated and altered throughout the years to match current research and knowledge of liquefaction. The 1996 and 1998 National Center for Earthquake Engineering Research (NCEER) as well as the National Science Foundation (NSF) workshops brought experts together in an attempt to reach a unified agreement on a procedure to be used by engineers in practice. The agreed-upon procedure formed the foundation of modern procedures and was eventually published as Youd et al. (2001). More recently, two different deterministic procedures using SPT-based evaluation were presented by Cetin et al. (2004) and Boulanger and Idriss (2014). Each of these approaches has been heavily debated among engineers because of their apparent differences. In spite of this debate, each is still widely used by engineers based on experience and preference.

2.4.4.1 Youd et al. 2001 Approach

This approach uses the same equation as the Simplified Procedure (Seed and Idriss, 1971) to find the CSR determined during the NCEER and NSF conferences, with only minor changes to the calculation of the shear stress reduction factor (r_d). As mentioned previously with the seismic stress approach, CSR and CRR are the foundational elements needed to determine the factor of safety against liquefaction. CSR is defined by the Youd et. al. (2001) procedure as:

$$CSR = 0.65\left(\frac{\sigma_{vo}}{\sigma'_{vo}}\right)\left(\frac{a_{max}}{g}\right)\cdot r_d \qquad (2\text{-}3)$$

where σ_{vo} is the total vertical stress, σ_{vo} is the effective vertical stress, a_{max} is the maximum horizontal ground acceleration in units of g, and r_d is the stress reduction factor. The stress reduction factor with depth (z) can be defined as:

$$r_d = 1.0 - 0.00765z \; for \; z \leq 9.15m \tag{2-4}$$

$$r_d = 1.174 - 0.0267z \; for \; 9.15m \; < z \leq 23m \tag{2-5}$$

For the CRR value estimated from SPT resistance, Youd et al. (2001) recommends that standard corrections (overburden pressure, hammer energy, borehole diameter, rod length, sampling liner, and fines content) to the blow counts ($N1_{60cs}$) be performed to maintain consistency between all methods of SPT testing. The CRR value used in this procedure is also standardized to a 7.5 magnitude earthquake and can be defined as shown in Equation (2-6).

$$CRR_{7.5} = \frac{1}{34(N1_{60cs})} + \frac{N1_{60}}{135} + \frac{50}{(10(N1_{60cs})+45)^2} - \frac{1}{200} \tag{2-6}$$

To correct the CRR for magnitudes other than 7.5, CRR can be adjusted by a magnitude scaling factor (MSF) and an overburden correction factor labeled as K_σ.

$$CRR_{M,\sigma'_v} = CRR_{M=7.5,\sigma'_v=1} \cdot MSF \cdot K_\sigma \quad (2\text{-}7)$$

The Seed and Idriss (1982) MSF factor was later modified by Idriss to be defined as:

$$MSF = \frac{10^{2.24}}{M_w{}^{2.56}} \quad (2\text{-}8)$$

where M_w is the magnitude of the earthquake that the FS_L should be scaled to. The K_σ factor developed by Boulanger (2003) can be defined as:

$$K_\sigma = 1 - C_\sigma \ln\left(\frac{\sigma'_v}{P_a}\right) \leq 1.1 \quad (2\text{-}9)$$

where:

$$C_\sigma = \frac{1}{18.9 - 2.55\sqrt{N1_{60,cs}}} \leq 0.3;\ N1_{60,cs} \leq 37 \quad (2\text{-}10)$$

Once CSR and CRR have been calculated, the factor of safety against liquefaction (FS_L) can be determined. A safety factor value less than one indicates that the soil, at the specific site

and depth of interest, has potential to liquefy during an earthquake. The FS_L can be determined by:

$$FS_L = (\frac{CRR_{7.5}}{CSR})(MSF) \quad (2\text{-}11)$$

2.4.4.2 Cetin et al. 2004 Approach

The Cetin et al. (2004) approach aims to more accurately evaluate the CSR by revising the evaluation of the r_d factor, accounting for fines content in blow counts and magnitude correlations. The revised recommendations for the r_d factor in this approach were developed based on a larger number of site response cases (2,153 sites). Additionally, they are based on more realistic site stratigraphies from actual liquefied/nonliquified case histories. Cetin et al. (2004) addressed and incorporated the effects of key seismic source, motion, and soil factors such as moment, intensity, and stiffness.

The new recommendation for the r_d by Cetin et al. (2004) for depths greater than 20m is the following:

$$r_d = \frac{[1+\frac{-23.013-2.949(a_{max})+0.999(M_W)+0.0525(V^*_{s,12m})}{16.258+0.201(e^{0.341(-d+0.0785(V^*_{s,12m})+7.586)})}]}{[1+\frac{-23.013-2.949(a_{max})+0.999(M_W)+0.0525(V^*_{s,12m})}{16.258+0.201(e^{0.341(0.0785(V^*_{s,12m})+7.586)})}]} \pm \sigma_{\varepsilon,rd} \quad (2\text{-}12)$$

For depths less than 20m, the following equation is to be used:

$$r_d = \frac{\left[1+\frac{-23.013-2.949(a_{max})+0.999(M_W)+0.0525(V^*_{s,12m})}{16.258+0.201(e^{0.341(-20+0.0785(V^*_{s,12m})+7.586)})}\right]}{\left[1+\frac{-23.013-2.949(a_{max})+0.999(M_W)+0.0525(V^*_{s,12m})}{16.258+0.201(e^{0.341(0.0785(V^*_{s,12m})+7.586)})}\right]} - 0.0046(d-20) \pm \sigma_{\varepsilon,rd} \quad (2\text{-}13)$$

where a_{max} is the maximum horizontal ground acceleration, M_w is the moment magnitude of the earthquake in question, d is the depth (meters), $V^*_{s,12m}$ is the shear wave velocity(m/sec) in the upper 12m of soil, and $\sigma_{\varepsilon,rd}$ is the standard deviation. For very soft soils, a minimum value of 120 m/s should be used for the stiffness factor with a maximum value of 250 m/s for very stiff soils. The standard deviation that is to be used with these equations (Equations (2-9) and (2-10)) is:

$$\sigma_{\varepsilon,rd} = d^{0.8500}(0.0198)\ for\ d < 12m \quad (2\text{-}14)$$

$$\sigma_{\varepsilon,rd} = 12^{0.8500}(0.0198)\ for\ d \geq 12m \quad (2\text{-}15)$$

Cetin et al. (2004) developed an equation for computing CRR using Bayesian statistical analysis with hundreds of case histories were liquefaction was either known to have occurred or to have not occurred. The CRR equation is given as:

$$CRR = \exp\left[\frac{N_{1,60}\cdot(1+0.004\cdot FC)-29.53\cdot\ln(M_w)-3.70\cdot\ln\left(\frac{\sigma'_v}{P_a}\right)+0.05\cdot FC+16.85+2.70\cdot\varphi^{-1}(P_L)}{13.32}\right] \quad (2\text{-}16)$$

where $N_{1,60}$ is the SPT blowcount corrected for hammer energy and overburden, FC is the fines content in percent ($5 \leq FC \leq 35$), M_w is the moment magnitude of the design earthquake, σ'_v is the effective vertical stress at the depth of interest, P_a is atmospheric pressure (= 1atm = 100 kPa = 1 tsf) and has units consistent with the effective vertical stress, P_L is the probability of liquefaction in decimals (common to use 15% or 0.15), and $\varphi^{-1}(P_L)$ is the inverse of the standard cumulative normal distribution (i.e. mean = 0, standard deviation = 1). Figure 2-8 shows a plot of these CRR curves for both (a) probabilistic liquefaction evaluation, and (b) deterministic liquefaction evaluation (i.e. P_L is assumed to be 15%).

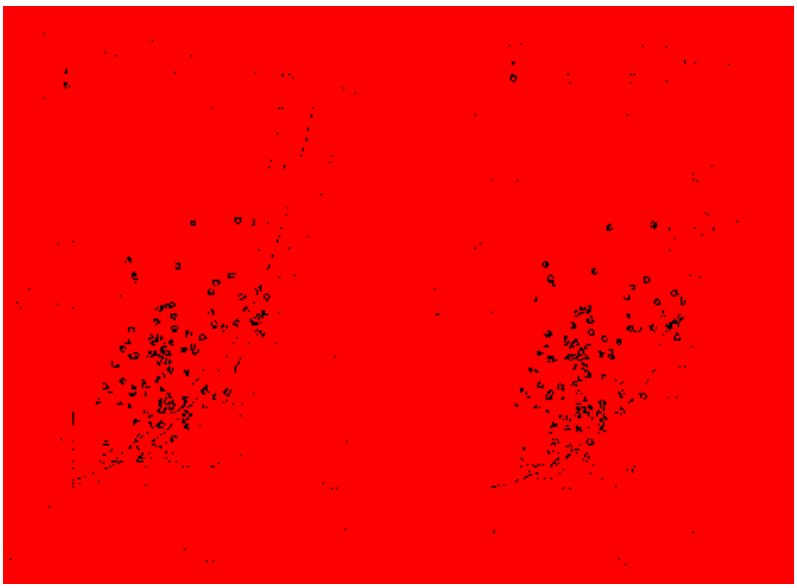

Figure 2-8: (a) Probabilistic SPT-Based CRR Correlation for Mw=7.5 and σ'_v = 1atm, and (b) Deterministic SPT-Based CRR Correlation for Mw – 7.5 and σ'_v = 1atm (After Cetin et al., 2004)

Lastly, Cetin et al. (2004) recommends correcting the CSR for both duration and over burden stress using a duration weighting factor (DWF_M) and over burden factor (K_σ) for use in FS_L. Using equation 2-3 for CSR, the corrected CSR (CSR_{eq}) is to be calculated as:

$$CSR_{eq} = \frac{CSR}{DWF \cdot K_\sigma} \tag{2-17}$$

where DWF can be determined using equation 2-18 or referencing Figure 2-9:

$$DWF \approx e^{(-0.3353 \cdot M_W + 2.5281)}; (5.5 \leq M_W \leq 8.5) \tag{2-18}$$

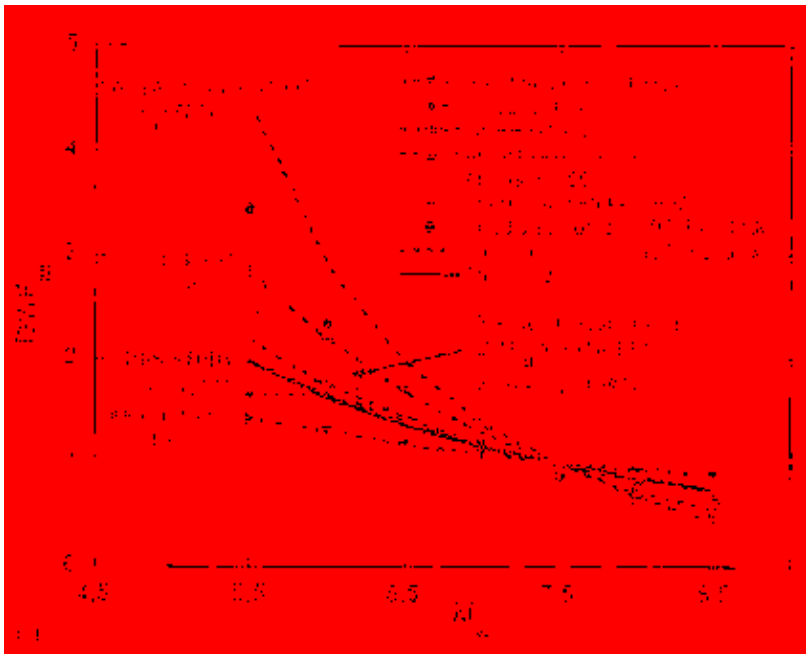

Figure 2-9: Recommendations for Duration Weighting Factor (Cetin et al., 2004 is Labeled as THIS STUDY) (after Cetin et al., 2004)

Cetin et al. (2004) defined K_σ as:

$$K_\sigma = \left(\frac{\sigma_v'}{P_a}\right)^{f-1} \tag{2-19}$$

where P_a is in the same units as the effective overburden pressure, σ_v' ; and f is a function of relative density and is equal to 0.8 for loose soils, 0.7 for medium-dense soils, and 0.6 for dense soils. Cetin et al. (2004) state that this relationship is valid for effective overburden pressures greater than about 0.3 atmospheres.

The factor of safety against liquefaction triggering can be computed as:

$$FS_L = \frac{CRR}{CSR_{eq}} \tag{2-20}$$

2.4.4.3 Boulanger and Idriss 2014 Approach

The Boulanger and Idriss (2014) approach incorporates several hundred parametric site response analyses. This approach follows the same framework as Youd et al. (2001) and Cetin et al. (2004) in calculating FS_L. The difference is the redefined approaches to determining previously used parameters r_d, MSF, and CRR.

The CSR is calculated using the same approach as Youd et al. (2001) using Equation (2-3) with a new r_d value. Boulanger and Idriss (2014) suggested that the r_d parameter be determined using the following equation:

$$r_d = \exp[\alpha(z) + \beta(z) \cdot M] \tag{2-21}$$

where:

$$\alpha(z) = -1.012 - 1.126 \sin(\frac{z}{11.73} + 5.133) \tag{2-22}$$

$$\beta(z) = 0.106 + 0.118 \sin(\frac{z}{11.28} + 5.142) \tag{2-23}$$

This approach also introduced a different approach to determining the clean sands equivalent resistance ($N1_{60,cs}$) by introducing new correction factors and also accounting for fine content (FC). The $N1_{60,cs}$ parameter is used, similar to the other two methods, to determine the CRR, however, the value is based on a few case histories that were interpreted differently. Equation (2-18) is the definition of this parameter used in the Boulanger and Idriss (2014) approach.

$$N1_{60,cs} = N1_{60} + \Delta N1_{60} \tag{2-24}$$

where:

$$N1_{60} = C_N C_E C_R C_B C_S N_m \tag{2-25}$$

$$\Delta N1_{60} = exp\left(1.63 + \frac{9.7}{FC+0.01} - \left(\frac{15.7}{FC+0.01}\right)^2\right) \tag{2-26}$$

The correction factors used to determine the $N1_{60}$ value are used to account for the differences in SPT testing methods. The C_N factor accounts for the overburden, $C_E = \frac{ER_m}{60\%}$ (ER_m is the measured efficiency of the free fall energy) accounts for the efficiency of the hammer, C_R is the rod correction factor, C_B is the correction for nonstandard boring diameter, C_S is the correction for using split spoons without liners, and N_m is the measured field blow count.

C_R can be determined using Table 2-1, and C_B and C_S are typically 1.0 with standard practices. C_N can be more difficult to determine because it has to be solved iteratively. The equation for C_N is presented in Equation 2-27.

Table 2-1: Rod Correction Factors

Rod Length [m]	C_R
< 3	0.75
3 - 4	0.80
4 - 6	0.85
6 - 10	0.95
10 - 30	1.00

$$C_N = \left(\frac{P_a}{\sigma'_v}\right)^m \leq 1.7 \tag{2-27}$$

where:

$$m = 0.784 - 0.0768\sqrt{N1_{60}} \; ; N1_{60} \leq 46 \tag{2-28}$$

The CRR is standardized to a 7.5 magnitude earthquake and one atmospheric pressure. The CRR for this approach is denoted as $CRR_{M=7.5,\sigma'_v=1}$ and can be defined as:

$$CRR_{M=7.5,\sigma'_v=1} = \exp\left(\left(\frac{N1_{60,cs}}{14.1}\right) + \left(\frac{N1_{60,cs}}{126}\right)^2 - \left(\frac{N1_{60,cs}}{23.6}\right)^3 + \left(\frac{N1_{60,cs}}{25.4}\right)^4 - 2.8\right) \tag{2-29}$$

To correct the CRR for magnitudes other than 7.5, it can be adjusted by MSF and an overburden correction factor developed by Boulanger (2003), labeled as K_σ.

$$CRR_{M,\sigma'_v} = CRR_{M=7.5,\sigma'_v=1} \cdot MSF \cdot K_\sigma \quad (2\text{-}30)$$

The following equations are used to calculate MSF and K_σ that then can be used to correct the CRR to the correct magnitude.

$$MSF = 6.9 \exp\left(\frac{-M}{4}\right) - 0.058 \leq 1.8 \quad (2\text{-}31)$$

and

$$K_\sigma = 1 - C_\sigma \ln\left(\frac{\sigma'_v}{P_a}\right) \leq 1.1 \quad (2\text{-}32)$$

where:

$$C_\sigma = \frac{1}{18.9 - 2.55\sqrt{N1_{60,cs}}} \leq 0.3;\ N1_{60,cs} \leq 37 \quad (2\text{-}33)$$

The FS_L then can be determined using the same equation as the simplified methods equation, which is:

$$FS_L = \frac{CRR_{M,\sigma'_v}}{CSR} \quad (2\text{-}34)$$

In general, if the FS_L is greater than one, meaning that CRR is greater than CSR, the soil is predicted to not experience liquefaction. When CRR and CSR are plotted with depth, it can be easily identified which layers are predicted to trigger liquefaction by identifying where CSR is greater than CRR. An example of this kind of plot is provided in Figure 2-10.

2.5 Liquefaction Effects

The effects of liquefaction have many different physical manifestations, all of which can be very destructive to structures. Once the liquefaction hazard potential has been identified for a site, the extent and type of liquefaction effects can be considered and methods of mitigation can be determined. Baska (2002) identified the most observed liquefaction effects as the alteration of ground motions, ground surface settlement, loss of bearing capacity, increased lateral pressure on walls, flow failure, ground oscillation, and lateral spread. Although each of these effects have serious consequences, the ones associated with cyclic mobility are the most relevant and will be briefly discussed here.

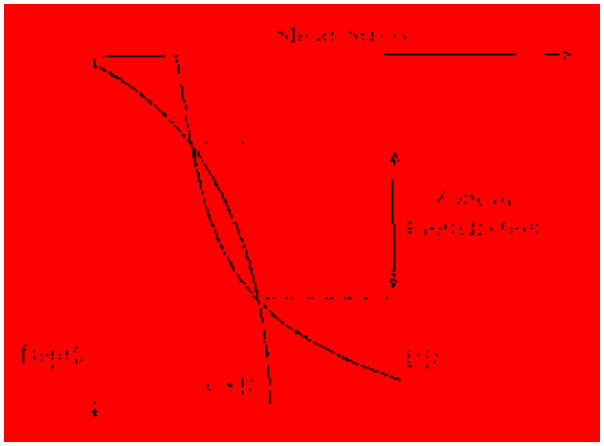

Figure 2-10: Example of Plotted CSR and CRR vs Depth to Determine Zone of Liquefaction (after Kramer, 1996)

One of the more common effect of liquefaction related to cyclic mobility is the settlement of liquefied soils. As previously mentioned, soils that liquefy generate excess pore pressures by trying to consolidate during an earthquake. This mode forces water from the pore space to the surface. This results in a denser configuration of the soil, which is manifested as settlement at the ground surface. This settlement effect from liquefaction can induce significant vertical settlement in structures and lifelines that can render them inoperable and unsound.

The loss of bearing capacity in the soil, another liquefaction effect, can also be extremely damaging. The reduced shear strength of the soil during soil liquefaction can severely reduce the resistance of the soil to vertical pressures induced from structures. This lack of resistance can result in toppling of structure as was seen in the famous 1964 Niigata, Japan earthquake where the reinforced concrete Kawagishi-cho Apartment building toppled because of global bearing capacity failure. Despite the extreme tilting, the building suffered very little structural damage. Figure 2-11 shows a picture of the Kawagishi-cho Apartment building and other neighboring buildings after experiencing bearing capacity failure. Additionally, the loss of bearing capacity can cause buried light-weight utility structures, such as gas tanks or septic tanks, to rise to the surface due to them being less dense than the effected liquefied soil.

The most important effect of liquefaction relevant to this study is lateral spread displacements. This phenomenon is very common and very expensive because it has contributed to significant economic damage in many earthquakes. Lateral spread is the movement of blocks of mostly intact, surficial soil that is displaced down slope or towards a free face that has formed in liquefied soil (Bartlett and Youd, 1995). The resulting horizontal deformations can be as large as 10m and be very damaging to infrastructure and lifelines. A deeper review of this phenomenon is provided in the next chapter.

Figure 2-11: Example of Bearing Capacity Failure During the 1964 Niigata, Japan Earthquake (Photo from quakeinfo.ucsd.edu/)

The most important effect of liquefaction relevant to this study is lateral spread displacements. This phenomenon is very common and very expensive because it has contributed to significant economic damage in many earthquakes. Lateral spread is the movement of blocks of mostly intact, surficial soil that is displaced down slope or towards a free face that has formed in liquefied soil (Bartlett and Youd, 1995). The resulting horizontal deformations can be as large as 10m and be very damaging to infrastructure and lifelines. A deeper review of this phenomenon is provided in the next chapter.

2.6 Chapter Summary

Liquefaction is an important, interesting, complex, and controversial topic in geotechnical earthquake engineering (Kramer, 1996). This phenomenon occurs due to excess pore pressures that are generated during seismic ground motions, which reduces the soil's strength and makes it act like a liquid.

There are three criteria that are important in determining the potential of liquefaction at a site: liquefaction susceptibility, liquefaction initiation, and liquefaction effects. The

susceptibility of a particular soil to the phenomenon of liquefaction can be assessed by examining the historic, geologic, compositional, and state condition of the soil. Generally, soils that are susceptible to liquefaction are cohesionless, low in fines content, uniform in grain size distribution, and saturated. Additionally, the initial state of a soil can help determine the expected behavior during seismic activity. Loose soils tend to contract, generate excess pore pressures, and lose strength that results in liquefaction while dense soils tend to dilate and gain strength.

Even if a soil is classified as being susceptible to liquefaction, it does not necessarily mean that the soil will, in fact, liquefy. Initiation is dependent on the duration and the amplitude of the loading from seismic events. There are two types of liquefaction: flow liquefaction and cyclic mobility. The initiation mechanics of these two liquefaction types are different. Soils above the SSL line are considered to be loose and have contractive behavior and those below are dense and have dilative behavior. A soil is likely to experience flow liquefaction if it plots above the SSL line and will not if plotted below the line. Cyclic mobility can occur in both loose and dense soils. Liquefaction occurs if the earthquake loading drives the stress path of a soil to the FLS. Additionally, various approaches have been presented that evaluate the CRR verses the CSR using SPT data. This evaluation can be used to calculate the factor of safety against liquefaction (FS_L) at each depth. When the FS_L is less than one, the soil at that depth is predicted to liquefy. When the CSS and CSR verses depth is plotted, the zones of liquefaction can easily be determined.

Shallow soils that experience liquefaction are likely to have diverse and extensive destructive effects on infrastructure and lifelines. This chapter discussed three effects associated with cyclic mobility: settlement, loss of bearing capacity, and lateral spread. These effects should be considered when performing a liquefaction hazard analysis on any particular site.

3 REVIEW OF LATERAL SPREAD

3.1 Introduction

The term lateral spread describes the permanent horizontal deformations of soils that have not completely failed but have been sufficiently weakened, allowing movement to occur under seismic driving forces. Common sites of lateral spreading occur on gently sloping ground or near a free-face. The greatest deformations have been observed to be located near free faces such as rivers and open bodies of water. Cumulatively, deformations from lateral spread have caused more damage than any other liquefaction-induced ground failure (National Research Council, 1985). Horizontal deformations can range in magnitude from a few millimeters to, in extreme cases, more than 10 meters (Coulter and Migliaccio, 1966). It is important to note that lateral spreading will only occur when soils have liquefied. Therefore, if seismic activity does not trigger liquefaction, lateral spreading will not occur. Additionally, an interesting feature of lateral spreading is that it may look like a slope failure, but the mechanics of the soil indicate that the surface soil in fact does not lose strength like normal slope failures would.

Lateral spread often causes excessive structural damage, which has resulted in significant economic losses throughout the world. The most damaging economic losses are not limited exclusively to structural damage, but also to waterlines, lifelines, bridges, roads, and piers because they prevent assistance to affected peoples and areas following earthquakes. Understanding what kinds of damages have been recorded from historical events promotes

understanding of the importance of predicting displacements and possible damages during events. As the theory of lateral spread is improved from the study of historical cases, the more prepared engineers can be in designing appropriate structures and lifelines.

In the 1906 earthquake in San Francisco, California, buildings, bridges, and roads were destroyed by lateral spreading. Although these damages were significant, the most significant and greatest damage occurred with the shearing of pipelines that prevented firefighters from extinguishing fires caused by the earthquake (Youd and Hoose, 1978). This unforeseen complication led to a large number of non-direct earthquake deaths (Bartlett and Youd, 1995).

In 1964, the lateral spread effects of the earthquake located at Prince William Sound, Alaska damaged several coastal communities. The displacements experienced at the city of Valdez forced the entire city to be relocated (Coulter and Migliaccio, 1966). In the same year, another large magnitude earthquake struck Niigata, Japan which resulted in lateral spread displacements causing the banks of the Shinano River to displace as much as 10 meters into the river channel (Hamada et al., 1986). This change in the river severely damaged facilities along the waterfront. Once again, in the more recent 1989 Loma Prieta earthquake, the Moss Landing Marine Laboratory was totaled from the results of one meter of lateral spreading at the site (Boulanger et al., 1997). These are just a few of the case histories that have aided engineers to learn and establish further research goals to help with the understanding and prediction of the likelihood of lateral spreading from seismic activity and liquefaction.

3.2 Lateral Spread Experimental Studies

Lateral spread is extremely complicated like liquefaction and predicting the extent of the horizontal displacements is not easy. The mechanics of the process are neither well understood

nor easily quantifiable. These challenges have led researchers to conduct several types of laboratory experiments to attempt to better understand what is happening. As is the case for most experiments that are properly conducted, new fundamental discoveries opened up new revealed insights to the governing mechanics.

Throughout the years of research, there have been different methods of experiments performed to better understand lateral spreading. Some of the most beneficial experiments have come from shake tables, centrifuges, and many other small-scale laboratory tests. Shake tables have been used for many different experiments, including earthquake experiments to test liquefaction of soils. Soils are placed on the table and then subjected to accelerations from harmonic waves that mimic equivalent earthquake ground motions. Such experiments can be viable sources of data because shake table lengths can be as large as several meters and can accommodate large amounts of soils for these experiments.

There are two main shake table experiments from history that shaped the research in characterizing lateral spread. The first was performed at the Kanazawa University in Japan by Miyajima et al. (1991) and the second was conducted by Sasaki et al. (1991). From these two experiments, various relationships between average displacements, duration of soil liquefaction, velocity of ground deformation, thickness of sand layers, and slope of sand layers were developed. Based on these relationships, researchers have concluded that lateral spread is mostly correlated to the thickness of the liquefiable layer and the slope of the soil at the surface. Additionally, the greatest displacements occurred near the bottom of the liquefied layer and only during actual shaking is when lateral displacements were observed.

Although not initially used to determine characteristics of lateral spreading, centrifuge experiments have gradually migrated to be used for lateral spread research. In 1998, researchers

Toboada-Urtuzuastegui and Dobry began to conduct experiments to model earthquake-induced lateral spread in sands at the Rensselaer Polytechnic Institute. This form of experimentation is used to simulate gravity-induced stresses in soil deposits using reduced scaled loadings. Unlike the larger models produced from shake table experiments, this procedure can be beneficial by using small models that have been scaled down. It is important however, to be aware that scaling factors are used and need to be properly accounted for. From the various experiments performed with this method, researchers have concluded that experiments show that downslope spikes in pore pressures correspond with upslope spikes in accelerations. Similar to the shake table experiments, researchers recognized that the maximum lateral ground displacements were a function of soil density, penetration resistance, ground-surface geometry, thickness of the liquefied layer, and the duration and intensity of ground shaking. They also observed that the liquefiable sands that were tested would dilate and gain strength with lateral deformation. Additionally, there was a decrease in pore pressures as the accumulation of shear strains increased. These observed results lead to a densification of the liquefied sands. As the liquefied sands densified, the induced accelerations of the experiment would peak as the accelerations no longer were filtered out by loose liquefied sands.

Other studies were conducted using smaller scale laboratory experiments. Some of the laboratory testing experiments consisted of undrained torsional testing (Yasuada et al., 1994 and Shamoto et al., 1997), undrained triaxial testing (Nakase et al., 1997), and undrained cyclic direct simple shear tests (Wu, 2002). These tests confirmed many of the conclusions that were previously made through the shake table and centrifuge experiments. Wu (2002) discovered the most notable difference while performing the undrained cyclic direct simple shear tests. He noticed that the direction of the loading in some samples resulted in different behaviors. When

loaded in one direction, the sample would undergo cyclic mobility while the other direction would cause it to experience flow liquefaction. He concluded that the directivity of the ground motions can affect the liquefaction behavior of the soil.

3.3 Analytical Methods for Lateral Spread Prediction

Contemporary understanding of soil mechanics and fundamental science theories have encouraged further development of currently utilize analytical methods for calculating lateral spread. These methods typically involve closed-form mathematical solutions that make them relatively complex and harder to perform. However, they prove to be very promising as models and computing tools improve. Through the years, many different analytical methods have been developed, however, the three methods that will be reviewed in this thesis are the most commonly known: numerical models, elastic beam model, and Newmark sliding block.

3.3.1 Numerical Models

Numerical models represent systems of interest with a two- or three-dimensional mesh of nodes and elements. The displacements and forces at each of the individual nodes can be determined iteratively from calculations of the surrounding nodes. These models can be either finite element or finite difference type models. Both approaches can be used on fairly complex systems and account for various soil parameters for better accuracy. Because numerical models require a constitutive model based on the mechanics and stress-strain behavior in the soils, there is a challenge because of the complexity of soil mechanics and the uncertainty in properly predicting residual strengths and stress/strain behaviors.

With the introduction of computers, numerical models gradually became more sophisticated, accurate, and useful. The first models were developed in the late 1970s and further refined through to the 1980s (Zienkiewicz et al., 1978; Zienkiewicz and Shiomi, 1984; Finn et al., 1986; Shiomi et al., 1987). More modern models (Gu et al., 1994; Yang, 2000; Yang et al., 2003; Arduino et al., 2006; Valsamis et al., 2010; Zhang and Wang, 2012) have further advanced the original models through increased computational power of computers, input from additional research, greater understanding of soils, and modern testing technology more accurately determining the characteristics of soils. These advances are allowing numerical models to be more representative of complicated systems and are making them more universal in research.

3.3.2 Elastic Beam Models

Originally proposed by Hamada et al. (1987), the Elastic Beam method was first used by researchers in an attempt to predict permanent displacements measured during the 7.7 magnitude earthquake at Maeyama Hills near Nishiro City, Japan in 1983. They used this method to simplify large areas that would be difficult to analyze with more complicated methods. This procedure simplifies the analysis by treating the soil profile as if it were a board floating on water. The unsaturated soil layers are assessed as the board with the liquefied soil layer being the water with no friction between the layers. Traditional means, such as gravity and boundary conditions, control the movement of the unsaturated soils. The co-authors of this research (Towhata et al., 1991; 1992; Yasuda et al., 1991) performed additional research, however little additional information was added to this procedure and has remained this way since.

3.3.3 Newmark Sliding Block

As lateral spreading most often occurs on sloping grounds, a method that treats the soil profile as a single block on an inclined plane was introduced and proposed by Newmark (1965). Frictional forces between the solid block and the plane are the only parameters that resist the sliding block. When there are sufficient external forces introduced, the driving forces on the soil block will overcome the frictional force that is preventing the block from sliding. This method was first introduced for seismic slope stability, however, further research allowed for this procedure to be incorporated into predictive lateral spread models (Dobry and Bazier, 1991; Byrne, 1991; Byrne et al., 1992; Toboadao et al., 1996; Olson and Johnson, 2008) and semi-empirical models (Bray and Travasarou, 2007; Saygili and Rathje, 2008). It can be effectively used for estimating lateral spread displacements by back calculating mobilized strength ratios. Caution should be observed when using these models for lateral spread displacement as these models were developed using specific bounds. Extrapolation outside these bounds would be unwise, as the data would likely be erroneous.

3.4 Empirical Methods for Lateral Spread Prediction

Empirical methods are developed from statistical data developed from earthquake case histories. One common statistical regression method is multi-linear regression (MLR), and it is used to create linear relationships between lateral deformations and certain quantifiable soil parameters. These models are widely used by practicing engineers because they are established independently of physics and soil mechanics, and are instead developed solely from case history data.

It is important that the collected data is accurate and of quality, which can be very difficult to achieve after an earthquake. Inaccurate data flaws the resulting values of empirical models. Additionally, the primary data incorporated into these models has traditionally come from two sources: Japan and the Western United States. Since the data primarily comes from these two sources, not all variations of earthquakes are accounted for and the models may not properly represent the predicted deformation. For example, each model has a range of acceptable inputs, as well as a range of predicted lateral spread displacements. Therefore, if the parameter inputs of interest do not fall within these ranges, the results would need to be extrapolated and provide less accurate data sets.

Despite challenges created by data limitation, with a little training and experience, empirical methods can be used with great results. In fact, they are widely used in practice due to simplicity of execution and rapid prediction of displacements, especially with the use of a spreadsheet. Additionally, these models require little knowledge of the soil profile, the mechanics, and the relationships used in their development in order to acquire practical results. Three of the most commonly used empirical models by engineers in practice today will be examined along with their limitations and benefits.

3.4.1 Youd et al. (2002) Procedure (Six-Parameter MLR Model)

Bartlett and Youd (1992, 1995) began to estimate lateral spreading displacements with the incorporation of a wider range of earthquake factors such as PGA, duration, magnitude, and source distance. Additionally, they incorporated topographical factors (ground slope, distance, and height of free face), geological factors (liquefaction layer thickness and depth in stratum), and soil factors (residual strength, mean grain size, fines content). In order to come up with their

empirical model, 448 horizontal displacement vectors were compiled from seven case histories: 1906 San Francisco (California), 1964 Portage (Alaska), 1964 Niigata (Japan), 1971 San Fernando (California), 1979 Imperial Valley (California), 1983 Nihonkai-Chubu (Japan), and the 1987 Superstition Hills (California) earthquakes. Their model considered two possible site geometry cases of lateral spread: ground slope case and free face case. Their procedure cannot assess both cases at once and therefore; the seven case histories were divided accordingly during their analyses. If a site is characterized by both free-face and gently sloping ground cases, both conditions should be assessed independently, and the larger of the two predicted displacement results should govern the analysis. Using these case studies, they used MLR to determine the combination of all the considered factors that would maximize the regression accuracy (R^2). Research by Youd et al. (2002) updated the model by removing incorrect measures of ground displacements from the 1983 Nihinkai-Chubu earthquake, adding three additional case histories: 1983 Borah Peak (Idaho), 1989 Loma Prieta (California), and 1995 Hyogo-Ken Nanbu (Japan) to the data set. The updated data also changed the form of the equation to include an R^* term which accounts for near-field earthquake events when source-site distance (R) becomes small. The model was regressed again in stepwise MLR procedure and the regression coefficients were re-evaluated.

Equation (3-1) shows the general six-parameter equation that was developed from the research by Youd et al. (2002).

$$\log D_H = b_0 + b_1 M + b_2 \log R^* + b_3 R + b_4 \log W + b_5 \log S + b_6 \log T_{15} \qquad (3\text{-}1)$$

$$+ b_7 \log(100 - F_{15}) + b_8 \log(D50_{15} + 0.1)$$

The earthquake terms that regressed most efficiently were magnitude (M) and source-site distance (R) and were therefore used in the equation. All the terms used in the equation can be defined as: D_H = lateral spread displacement (m); M = earthquake moment magnitude; R = horizontal source-to-site distance (km); R^* = distance parameter to account for near-field earthquake events; W = free-face ratio (%); S = slope gradient (%); T_{15} = cumulative thickness (m) of saturated granular or silt layers with $(N_1)_{60} < 15\,\frac{blows}{ft}$; F_{15} = the mean fines content of the soil comprising the T_{15} parameter (%); and $D50_{15}$ = the mean grain size of the soil comprising the T_{15} parameter (mm). The $b_0 - b_8$ regression coefficients and the R^* value to be used in the equation can be determined from Table 3-1 and Equation (3-2), respectively. The model's ability to match the data expressed with the combined coefficients result in an R^2 value of 82.6% and a standard deviation of 0.197.

Table 3-1: Regression Coefficients for the Youd et al. (2002) MLR Empirical Model (after Youd et al., 2002)

Geometry Case	b_0	b_1	b_2	b_3	b_4	b_5	b_6	b_7	b_8
Ground Slope	-16.213	1.532	-1.406	-0.012	0	0.338	0.540	3.413	-0.795
Free Face	-16.713	1.532	-1.406	-0.012	0.592	0	0.540	3.413	-0.795

$$R^* = R + 10^{0.89M-5.64} \qquad (3\text{-}2)$$

Figure 3-1 shows a diagram of how to determine the free-face ratio (W) and slope gradient (S) at a site. It is important to note that the soil where L < 5H is considered the "slump

zone". The slump zone is where flow liquefaction or slope failure is more likely to govern failure at the site, not lateral spread.

Figure 3-1: Diagram to Determine Site Geometry Terms to be Used in Youd et al. (2002) Procedure (after Bartlett and Youd, 1992)

Additionally, it should be noted that limitations on the terms used in Equation (3-1) were recommended by Youd et al. (2002) to ensure that the displacement results were not extrapolated and outside the model bounds. The recommended ranges of the parameters for this procedure are given in

Table 3-2 and Figure 3-2. A new term is introduced (Z_T) as well, which is defined as the depth to the top of the liquefiable layer.

3.4.2 Bardet et al. (2002) Procedure (Four-Parameter MLR Model)

Bardet et al. (2002) made observations during research that lateral spread displacements were not strictly confined to small isolated locations, but instead can extend over areas as large as several square kilometers. This observation led to the development of another MLR model

that avoids the use of certain complex soil parameters and instead focuses more on the seismic loading and site geometry characteristics. This procedure incorporates only four-parameters and is specific to predicting ground displacements over large areas.

Table 3-2: Recommended Ranges for Terms Used in Youd et al. (2002) Procedure (after Youd et al., 2002)

Term	Range
D_H (m)	0 to 6.0
M	6.0 to 8.0
R (km)	0.2 to 100
W (%)	1 to 20
S (%)	0.1 to 6
T_{15} (m)	1 to 15
Z_T (m)	1 to 10

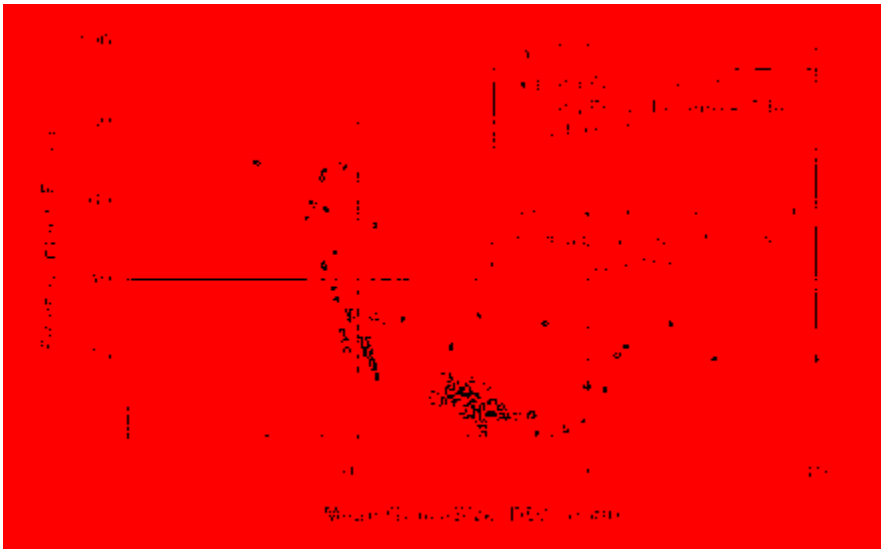

Figure 3-2: Limitation Bounds for F_{15} and $D50_{15}$ Terms for the Youd et al. (2002) Procedure (after Youd et al., 2002).

The four-parameter MLR model was regressed using the same data collected and analyzed by Bartlett and Youd (1992, 1995). One of the major differences in how Bardet et al. (2002) used the data was that they divided the earthquake case histories up according to the magnitude of displacement to create two separate predictive relationships. The first set used the entire range of displacements to create a general equation (Data Set A). The second set was only the case histories that had displacement magnitudes of 2m or less (Data Set B). Additionally, they believed that the F_{15} and $D50_{15}$ terms used in the Youd et al. (2002) model were more difficult to obtain from borehole data over a large area and also had the largest change for uncertainty; therefore, they suggested to remove these terms from the equations. Similar to the Youd et al. (2002) model, each of the models have specific regression coefficients depending of the site condition (free-face or ground slope).

$$\log(D_H + 0.01) = b_0 + b_{off} + b_1 M + b_2 \log(R) + b_3 R + \log(W) + b_5 \log(S) + b_6 \log(T_{15}) \quad (3\text{-}3)$$

The general equation developed to predict lateral spread displacements from the Bardet et al. (2002) research is shown in Equation (3-3). The terms used in the equation can be defined as: D = median computed lateral spread displacement (m); M = earthquake moment magnitude; R = horizontal distance to the nearest seismic energy source or nearest fault rupture (km); W = free-face ratio (%) (also defined on Figure 3-1); S = ground slope (%); and T_{15} = cumulative thickness (m) of saturated granular or silt layers with $(N_1)_{60} < 15 \frac{blows}{ft}$. The regression coefficients for the specific site conditions for both Data Set A and Data Set B can be seen in

Table 3-3 and Table 3-4, respectively. The model's ability to match the data expressed in the combined coefficients resulted in R^2 values of 64.3% for both Data Set A and B (Bardet et al., 2002) and a standard deviation of 0.290. The lower R^2 shows that generally there is a loss in accuracy when the F_{15} and $D50_{15}$ terms are removed. Additionally, the R^2 results indicate that there is no benefit to using one equation over the other, as they demonstrate similar accuracy.

Table 3-3: Data Set A Regression Coefficients used with the Bardet et al. (2002) Procedure (after Bardet et al., 2002)

Geometry Case	b_0	b_{off}	b_1	b_2	b_3	b_4	b_5	b_6
Ground Slope (GS4-A)	-6.815	0	1.017	-0.278	-0.026	0	0.454	0.558
Free Face (FF4-A)	-6.815	-0.465	1.017	-0.278	-0.026	0.497	0	0.558

Table 3-4: Data Set B Regression Coefficients used with the Bardet et al. (2002) Procedure (after Bardet et al., 2002)

Geometry Case	b_0	b_{off}	b_1	b_2	b_3	b_4	b_5	b_6
Ground Slope (GS4-B)	-6.747	0	1.001	-0.289	-0.021	0	0.203	0.289
Free Face (FF4-B)	-6.747	-0.162	1.001	-0.289	-0.021	0.090	0	0.289

As was the case with Youd et al. (2002), there are limitations for the specific terms in each data set used in the Bardet et al. (2002) procedure. These limitations prevent engineers from extrapolating data outside the models bounds and resulting in unrealistic magnitudes of predicted lateral spread displacements. These limitations are presented in Table 3-5.

Table 3-5: Limitations of the Terms used in Bardet et al. (2002) Procedure (after Bardet et al., 2002)

Term	Range	
	Data Set A	Data Set B
D_H (m)	0 to 10.15	0 to 1.99
M	6.4 to 9.2	6.4 to 9.2
R (km)	0.2 to 100	0.2 to 100
W (%)	1.64 to 55.68	1.64 t0 48.98
S (%)	0.05 to 5.90	0.05 to 2.50
T_{15} (m)	0.2 to 19.7	0.2 to 13.6

The last term that needs to be addressed is the sensitivity of the term R (source-site distance) in the model. Bardet et al. (2002) did not use the R^* value that Youd et al. (2002) proposed to prevent unreasonably large predicted displacements when the R value is small. Instead, Bardet et al. (2002) suggests limitations be applied to the R term based on the seismic magnitude (M) proposed by Bartlett and Youd (1995). These limitations are shown in Table 3-6.

3.4.3 Zhang et al. (2012) Procedure

The main objective of the Zhang et al. (2012) procedure was to expand the bounds and application of empirical models to countries other than the western United States and Japan. This model, unlike Youd et al. (2002), accounts for the difference in fault types (i.e. subduction, strike-slip, reverse, and normal) of all the earthquake case histories used. Because of the variation in fault types, this procedure replaces the moment magnitude (M) and site-source distance (R) with a parameter that can conveniently be determined for different seismic regions. This new term is called the pseudo spectral displacement (SD). The SD is calculated using a local strong motion attenuation relationship to find the spectral acceleration (m/s^2) at a period of

0.5 seconds and dividing that acceleration by $(4\pi)^2$. The use of local attenuation relationships allows the model to be specifically tailored to the seismic source of any location without the need to develop a specific model for that location. Additionally, the dataset used for regression eliminated the Portage, Alaska 1964 earthquake case history from the Youd et al. (2002) database because of the larger 9.2 magnitude that was unrepresentative of common magnitudes. The general equation for this method and the corresponding coefficients for the free-face and ground slope cases are shown in Equation (3-4) and Table 3-7, respectively. This equation results in an R^2 value of 76.8% and a standard deviation of 0.18.

Table 3-6: Recommended Minimum R-Values for Various Earthquake Magnitudes (after Bartlett and Youd, 1995)

Magnitude (M)	Minimum R (km)
6.0	0.5
6.5	1
7.0	5
7.5	10
8.0	20-30

The terms used in the equation are the same as in the Youd et al. (2002) model and are again defined as: D_H = lateral spread displacement (m); SD = pseudo spectral displacement (m) (found by SA(0.5s)/$(4\pi)^2$); W = free-face ratio (%); S = slope gradient (%); T_{15} = cumulative thickness (m) of saturated granular or silt layers with $(N_1)_{60} < 15\frac{blows}{ft}$; F_{15} = the mean fines

content of the soil comprising the T_{15} parameter (%); and $D50_{15}$ = the mean grain size of the soil comprising the T_{15} parameter (mm).

$$\log D_H = b_0 \log SD + b_1 \log W + b_2 \log S + b_3 T_{15} + b_4 \log(100 - F_{15}) + b_5 \log(D50_{15} + 0.1) + b_6 \quad (3\text{-}4)$$

Table 3-7: Regression Coefficients to be used for Zhang et al. (2012)

Geometry Case	b_0	b_1	b_2	b_3	b_4	b_5	b_6
Ground Slope (GSZ)	1.8619	0	0.4591	0.0197	2.4643	-0.8382	-2.7096
Free Face (FFZ)	1.8619	0.6080	0	0.0342	2.4643	-0.8382	-3.4443

After deriving the equation, the equation was tested using lateral spread case histories from the 1999 Kocaeli, Turkey and 1987 Edgecumbe, New Zealand earthquakes. The model predicted the lateral spread displacements for these two earthquakes very well. This procedure is not recommended when working on sites outside the western United States and Japan.

3.4.4 Gillins and Bartlett (2014) Procedure

Just like Bardet et al. (2002), Gillins and Bartlett (2014) recognized that the $D50_{15}$ and F_{15} terms are often not reported in borehole logs or are more uncertain. The way Gillins and Bartlett address this problem was by introducing indices based on the qualitative soil descriptions or general USCS symbol included on the boring logs. To do so, soils indices (SI) were assigned. These values range from 1 to 6 and are meant to describe all expected soil types. The corresponding SI values used in this procedure are presented in Table 3-8.

To incorporate the SI values into the MLR model, Gillins and Bartlett (2014) defined a new variable known as x_i (unitless), which is defined as the thickness of the layers in the site profile that comprises T_{15} with SI = i divided by the total cumulative thickness of T_{15} (i.e. if a soil index of 3 is not represented in a boring, the value of the variable x_3=0). Using the Youd et al. (2002) database again, the general regression equation to be used for this procedure is given in Equation (3-5) with the corresponding regression coefficients provided in Table 3-9. The other terms used in the equation can be defined as: D = median computed lateral spread displacement (m); M = earthquake moment magnitude; R = horizontal distance to the nearest seismic energy source or nearest fault rupture (km); W = free-face ratio (%); S = ground slope (%); and T_{15} = cumulative thickness (m) of saturated granular or silt layers with $(N_1)_{60} < 15\frac{blows}{ft}$. This model has an R^2 value of 79.0% with a standard deviation of 0.2232.

Table 3-8: Soil Indices used in Gillins and Bartlett (2014) (after Gillins and Bartlett, 2014)

Typical Soil Descriptions in Database	General USCS Symbol	Soil Index *SI*
Silty gravel with sand, silty gravel, fine gravel	GM	1
Very coarse sand, sand and gravel, gravelly sand	GM-SP	2
Coarse sand, sand with some gravel	SP	2
Sand, medium to fine sand, sand with some silt	SP-SM	3
Fine sand, sand with silt	SM	4
Very fine sand, silty sand, dirty sand, silty/clayey sand	SM-ML	4
Sandy silt, silt with sand	ML	5
Nonliquefiable material (not part of T_{15})	CL	6

$$\log D_H = b_0 + b_{off} + b_1 M + b_2 \log(R) + b_3 \mathrm{R} + b_4 \log(W) + b_5 \log(S) \qquad (3\text{-}5)$$

$$+ b_6 \log(T_{15}) + b_7 x_1 + b_8 x_2 + b_9 x_3 + b_{10} x_4 + b_{11} x_5$$

Table 3-9: Regression Coefficients to be used for Gillins and Bartlett (2014) (after Gillins and Bartlet, 2014)

Geometry Case	b_0	b_{off}	b_1	b_2	b_3	b_4	b_5
Ground Slope (GSGB)	-8.208	0	1.318	-1.073	-0.016	0	0.337
Free Face (FFGB)	-8.208	-0.344	1.318	-1.073	-0.016	0.445	0

Geometry Case	b_6	b_7	b_8	b_9	b_{10}	b_{11}
Ground Slope (GSGB)	0.592	-0.683	-0.200	0.252	-0.040	-0.535
Free Face (FFGB)	0.592	-0.683	-0.200	0.252	-0.040	-0.535

3.4.5 Comparison of Empirical Procedures

The models were all regressed with the same database originally compiled by Bartlett and Youd (1992, 1995). Since each method utilized the dataset differently and applied different parameters to the models, the accuracy of the regressions is important to understanding their practicality. The statistical regression term, R^2, is what is universally used by researchers to determine the accuracy of their models. R^2 is a measure of what percentage of the used database is captured correctly by the developed model after regression. For these empirical procedures, the higher the R^2 value of a model, the more accurate the model is in predicting the lateral spread displacement magnitude. Additionally, despite the widespread acceptance and implementation of the predictive models, the estimated displacements do not directly account for the uncertainty and spread in the data. It is important to note that these models are regressed from case history

data with significant scatter. This scatter has led engineers and researchers to apply a standard deviation to the models to attempt to account for the uncertainty in the dataset. Both the regression accuracy and standard deviations of the discussed empirical models are given in Table 3-10.

Table 3-10: Regression Accuracy (R^2) and Standard Deviation (σ_{logD}) Comparison for Empirical Models

Model	R^2	σ_{logD}
Youd et al. (2002)	82.6%	0.1970
Bardet et al. (2002)	64.3%	0.2900
Zhang et al. (2012)	76.8%	0.1800
Gillin and Bartlett (2014)	79.0%	0.2232

Comparing the data, it can be seen that the models that have the highest regression accuracies are the Youd et al. (2002), Zhang et al. (2012), and Gillin and Bartlett (2014) models. The small difference in accuracy is not large enough to be significant, meaning that these three models are equally reliable and accurate. However, there are differences in their difficulty and application that need to be considered when choosing which model to use. As previously mentioned in the descriptions of each model, the Youd et al. (2002) model is a six-parameter model that utilizes both the F_{15} and $D50_{15}$ parameters. These terms are more uncertain and more difficult to obtain which makes the model harder to use. The Zhang et al. (2012) model is derived for use in locations other than the United States and Japan and uses the SD term instead of moment magnitude (m) and site-source distance (R). The Gillin and Bartlett (2014) model simplified the models by neglecting the more complex F_{15} and $D50_{15}$ terms and instead used the

simpler, x_i terms, which increase its accuracy but maintaining simplicity in the application. Additionally, the Bardet et al. (2002) model has a lower regression accuracy due the use of fewer (four) parameters in the model and is used less frequently. With all of these models, caution is to be used in applying parameters. The models were created with specific limitations and ranges. Extrapolation outside the bounds of each individual model is not recommended.

3.5 Chapter Summary

Lateral spread is a horizontal deformation effect of soil that is triggered by cyclic mobility in liquefiable soils. Because lateral spread is an effect of liquefactions, liquefaction susceptibility should be evaluated before predicting any lateral spread displacements. Typical regions where lateral spread occurs are in areas that have either a free-face or gently sloped ground.

Significant research has been performed in order to better understand the mechanics driving liquefaction induced lateral spread. From this research, it has been determined that there are strong correlations between lateral spread displacements and site-specific parameters such as: seismic loading parameters (magnitude and source-site distance), soil parameters (fines content, particle size, liquefaction layer thickness, and $(N1)_{60}$ blow counts), and site geometry (slope and distance to free-face).

These correlations have led to the development of both analytical and empirical lateral spread prediction models. Analytical models attempt to predict the magnitude of displacement based on the understanding of the fundamentals of soil mechanics of liquid soils. Although analytical models incorporate the most current research and understanding of liquefaction and

are more fundamentally correct, they have not been used as frequently in practice as empirical models.

Empirical models have been developed by incorporating database case history information from earthquakes where lateral spread occurred. These models have been derived without the consideration of soil mechanics and used case histories only from the western United States and Japan which make them more limited in their use. However, models have been developed to account for both of these limitation in different capacities. The most useful thing with these models is that they have made predicting displacements simpler by reducing the amount of parameters used in the models. Because of the uncertainty of the varied parameters used in these models for regression, statistical relationships have been developed with them in order to determine their precision. Although these models don't consider the same parameters as analytical models, they have been used more in practice by engineers due to their ease of use along with relatively high accuracies.

4 EQUIVALENT SINGLE PILE SUMMARY

4.1 Soil-Pile Interactions

Many researchers have developed different methodologies to analyze soil-pile interactions resulting from any given lateral spread event. There are two types of response loading analyses: inertial and kinematic. Inertial loading is caused by the inertial reaction of the mass from the overlying structure being transmitted to the foundation with kinematic loading a result of free-field displacement of the soil surrounding the foundation. While some research has shown that a combination of inertial and kinematic loading could provide the most critical scenario for a given structure and its foundation, most engineers prefer to analyze the two scenarios independently and allow the most critical scenario to govern the design (Franke, 2011). Inertial loading was neglected in this study because this study is primarily concerned with lateral spreading and its effects on piles, which is considered to be kinematic loading.

Some of the methodologies are more complex than others. These methodologies range from a simplistic generalization of lateral pressures and are considered limit equilibrium methods (e.g., Ledezma and Bray, 2010; He et al., 2009; and Gonzalez et al., 2005) while others are more advanced numerical models (e.g., Cheng and Jeremic, 2009; Lam et al., 2009; and Arduino et al., 2006).

A popular method among engineers for evaluating pile response is known as a Beam-on-Winkler Foundation (BWF) method. This method uses p-y soil springs to represent the lateral

resistance of the soil. Due to the ability and ease for this method to predict pile displacements, this method is often preferred over the more simplistic limit equilibrium methods and more complex numerical models (Juirnarongrit and Ashford, 2006). This method has been demonstrated both in laboratory and in the field to provide reasonable representation of the soil response (inertial and kinematic) of single piles as well as pile groups (Wilson et al., 2000; Tokimatsu et al., 2001; Ashford and Rollins, 2002; Boulanger et al., 2003; Tokimatsu and Suzuki, 2004; Brandenberg, 2005; Rollins et al. 2005; Weaver et al. 2005; Juirnarongrit and Ashford 2006; Brandenberg et al. 2007).

Using p-y soil springs as well as the BWF methodology, Juirnarongrit and Ashford (2006) were the first to identify a simpler procedure for computing the average response of a pile group by the use of an equivalents single pile. The works of Juirnarongrit and Ashford (2006) is based on the original works of Mokwa (1999) and Mokwa and Duncan (2003).

4.2 p-y Analysis Methodology

Juirnarongrit and Ashford (2006) acknowledge that the BWF procedure can be used for both inertial as well as kinematic loading of a pile. They also summarize the original BWF p-y procedure for analyzing the kinematic loading of a pile that was presented by Reese et al. (2000). The resulting p-y curves for this procedure are illustrated in Figure 4-1.

Reese et al. (2000) explained that if the soil surrounding a pile is stationary, then the p-y curve (curve 1) for that soil is symmetrical about the p-axis. If the soil surrounding the pile moves relative to the pile, then the soil curve (curve 2) is understood to be offset by the soil movement.

If the pile movement, y_p , is less than the soil movement, y_s , then the soil is understood to be applying a driving force (p_1) to the pile. If $y_p > y_s$, the soil is understood to be providing a resistance force (p_2) to the pile. Therefore, the response of the pile from kinematic loading, using a p-y analysis, must be computed by applying a free-field soils movement boundary condition to the soils springs in the BWF model. Figure 4-2 shows an illustration of this analysis.

Figure 4-1: Depiction of p-y Curves for Kinematic Loading of Piles (after Juirnarongrit and Ashford, 2006; Modified from Reese et al., 2000)

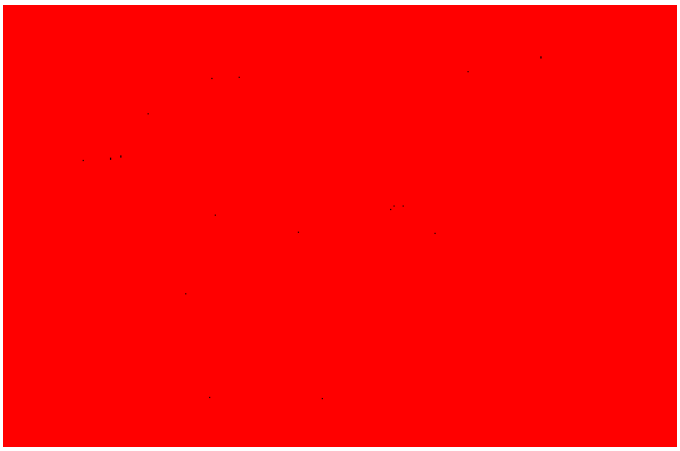

Figure 4-2: p-y Analysis for Kinematic Loading (after Juirnarongrit and Ashford, 2006)

The pile response for the p-y soil springs can be computed by solving the following differential equation:

$$EI\frac{d^4y_p}{dz^4} - p(y_p - y_s) = 0 \quad (4\text{-}1)$$

where:

EI = pile stiffness

p = soil reaction per unit length of pile

y_p = pile displacement

y_s = soil displacement

z = depth

This equation can be solved by using finite difference or finite element methods. The software used for this study, LPILE v2016 (ENSOFT) utilizes a finite difference method to solve the equation.

4.3 p-y Development for Soil Layering

Due to the relatively high cost and complexity to perform a site specific lateral load pile test (e.g. Hales, 2003; Bowles, 2005), engineers often choose to use already published p-y curves that represent general soil types. Although these published curves are not site specific, they were still developed through the same field testing methods on several different sites. Some of these

curve include: Matlock (1970) for general soft clays, Reese et al. (1974) for general sands, and Reese et al. (1975) for general stiff clay beneath the water table. These curves require the user to specify soil properties in order to produce the representative p-y curve. Some of the properties include friction angle, undrained strength, confining stresses, and p-y modulus. The produced p-y curves and behavior are only as accurate as the properties used for each curve.

p-y curves for typically behaving soils (i.e. sands and clays) are usually well accepted among engineers, however, soils experiencing behaviors such as liquefaction cause the p-y curves to become more questionable and engineers are more uncertain of their accuracy. This is due to the more complex behavior and variability of liquefiable soils. Franke and Rollins (2013) developed a simplified hybrid model that incorporates aspects of exiting p-y spring models with liquefied soil behaviors. The hybrid model is applicable to a wide range of soil types, relative densities, pile/shaft diameters, and loading conditions. Franke and Rollins (2013) compared their developed hybrid model with a variety of case histories involving single piles and determined that the hybrid model provided reasonable estimates of the response for both kinematic and inertial loadings.

The hybrid p-y model simply uses the lower predicted soil resistance from the Wang and Reese (1998) and Rollins et al. (2005) p-y models. Rollins et al. (2005) p-y model attempts to account for dilative effects that occur within a liquefied soil during phase transformation while the Wang and Reese (1998) p-y model attempts to account for the limiting residual shear strength of liquefied soils at large strains. The ultimate lateral soil resistance (p_{hybrid}) for the hybrid model presented by Franke and Rollins (2013) is calculated using the following equation:

$$p_{hybrid} = min(p_{clay}, p_{liq}) \tag{4-2}$$

Wang and Reese (1998) defines p_{clay} as:

$$p_{clay} = \begin{cases} p_{u,clay} \; for \; y > 8y_{50} \\ \frac{p_{u,clay}}{2}\left[\frac{y}{y_{50}}\right]^{1/3} \; for \; y \leq 8y_{50} \end{cases} \tag{4-3}$$

$$p_{u,clay} = min\left[\left(3 + \frac{\gamma'_{avg}}{c}z + \frac{J}{b}z\right)cb, 9cb\right] \tag{4-4}$$

where:.

y = relative differential displacement between the pile and soil

$y_{50} = 2.5\epsilon_{50}b$

ϵ_{50} = strain corresponding to one-half the maximum principal stress difference (recommended to by 0.05 for liquefied soils (Wang and Reese, 1998)

b= width of pile

J = model factor (typically 0.5 for soft soils)

γ'_{avg}= average effective unit weight of the soil

c = shear strength of the soil at depth z

z = depth of interest from ground surface [meters]

Rollins et al. (2005) defines p_{liq} as:

$$p_{liq} = min\begin{cases} p_{u,liq} \\ p_d A(By)^C \end{cases} \quad (4\text{-}5)$$

$$p_{u,liq} = min\left[p_d A(150B)^C, p_{d,max}\right] \quad (4\text{-}6)$$

where:

$$p_d = \begin{cases} \frac{b}{0.3m} \; for \; b < 0.3m \\ 3.81 \ln|b| + 5.6 \; for \; 0.3 \leq b \leq 2.6 \, m \\ 3.81 \ln|2.6| + 5.6 \;\; for \; b > 2.6m \end{cases}$$

$$A = 3x10^{-7}(z+1)^{6.05}$$

$$B = 2.8(z+1)^{0.11}$$

$$C = 2.85(z+1)^{-0.41}$$

A variation of four different scenarios can be experienced when determining the simplified hybrid p-y curve. The four general scenarios are illustrated in Figure 4-3 to Figure 4-6.

Figure 4-3: Dilative (Rollins et al. ,2005), Residual (Wang and Reese, 1998), and Hybrid (Franke and Rollins, 2013) p-y Curves (Scenario 1)

Figure 4-4: Dilative (Rollins et al. ,2005), Residual (Wang and Reese, 1998), and Hybrid (Franke and Rollins, 2013) p-y Curves (Scenario 2)

Figure 4-5: Dilative (Rollins et al. ,2005), Residual (Wang and Reese, 1998), and Hybrid (Franke and Rollins, 2013) p-y Curves (Scenario 3)

Figure 4-6: Dilative (Rollins et al. ,2005), Residual (Wang and Reese, 1998), and Hybrid (Franke and Rollins, 2013) p-y Curves (Scenario 4)

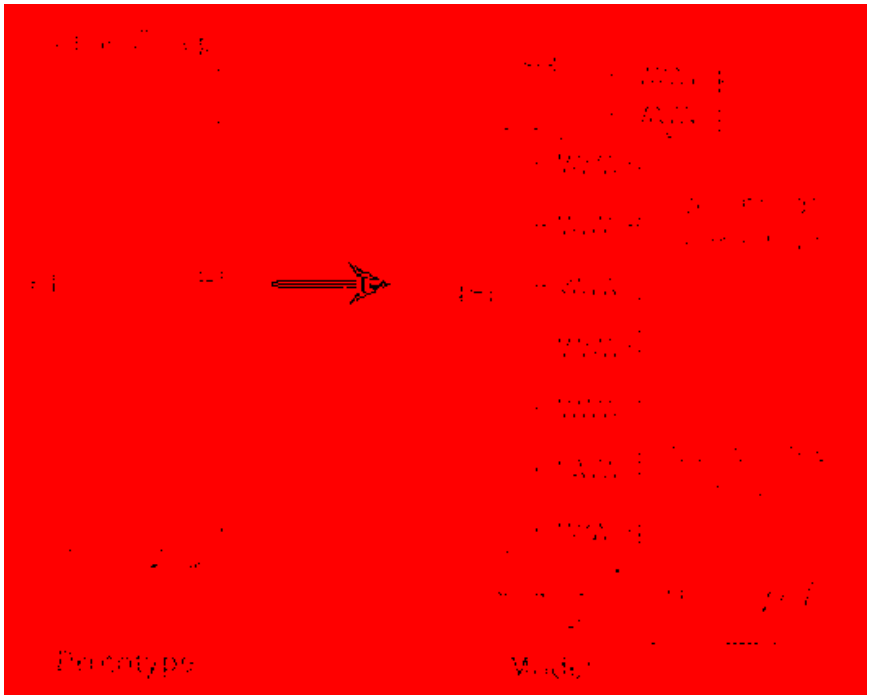

Figure 4-7: Equivalent Single Pile Model Demonstrated on a Simple Four-Pile Group Prototype (after Juirnarongrit and Ashford, 2006)

4.4 Equivalent Single Pile for Pile Groups

An equivalent single pile is intended to be used to provide the average response of an entire group of piles. This procedure was first summarized by Juirnarongrit and Ashford (2006) and is based on the original works of Mokwa (1999) and Mokwa and Duncan (2003). The procedure by Juirnarongrit and Ashford (2006) will be briefly explained to give background and support to the equivalent single pile procedure used in the study presented in this thesis. "Super Pile" is a name that will be used throughout the remainder of this report to identify when a group of piles have been converted to an equivalent single pile.

4.4.1 Development of the Equivalent Single Pile

Mokwa (1999) proposed that a pile group could be represented by a single equivalent pile to be used in analysis. The equivalent single pile is computed for a pile group by determining the flexural stiffness of a single pile in the group and then multiplying that stiffness by the number of total piles in the group. In addition, the procedure suggests that the p-y soil springs of the equivalent single pile be reduced with what is known as a p-multiplier value. This reduction in the p-y soil springs is to account for pile group (i.e. shadowing) effects. The concept of an equivalent single pile is presented in Figure 4-7.

The soil spring resistance for the equivalent single pile can be computed as:

$$P = \sum_{i=1}^{N} p_i (f_m)_i \qquad (4\text{-}7)$$

where:

$p_i = soil\ spring\ resistance\ of\ a\ single\ pile\ in\ the\ i^{th}\ row$

$(f_m)_i = group\ reduction\ p - multiplier\ for\ the\ i^{th}\ row$

Rollins et al. (2006) of Brigham Young University determined that there is a phenomenon called “shadowing” that occurs when rows of piles are close to each other. Results from full scale testing indicate that the average load for a pile within a closely spaced group will be substantially less than a single isolated pile with the same deflection. It was also noticed that

the leading pile row in the group carried significantly larger loads than the trailing rows of piles. The trailing rows experience less resistance because of the interference with the failure surface of the row of piles in front of them. The closer the rows of piles are to one another, the more resistance to horizontal loading they will develop. Rollins et al. (2006) study presented the group reduction factor for a given row in a group as:

$$f_m = 0.26 \ln \frac{S}{D} + 0.5 \leq 1.0 \ (Leading\ Row\ of\ Piles) \quad (4\text{-}8)$$

$$f_m = 0.52 \ln \frac{S}{D} \leq 1.0 \ (Second\ Row\ of\ Piles) \quad (4\text{-}9)$$

$$f_m = 0.60 \ln \frac{S}{D} - 0.25 \leq 1.0 \ (Third\ or\ Higher\ Row\ or\ Piles) \quad (4\text{-}10)$$

where:

$S = \ spacing\ of\ the\ piles\ (center\ to\ center)$

$D = diameter\ of\ the\ piles$

Rollins et al. (2006) determined that the shadowing effects are only significant if the spacing of the piles/rows (S) is less than 5.65 times the diameter (D) of the piles.

The equivalent single pile approach can easily be incorporated into a linear elastic pile response analysis; however, it is more difficult to incorporate the approach for a nonlinear pile response due to the algorithms that compute the flexural stiffness. Therefore, a guideline for

manually incorporating a simplified nonlinear approach for analysis using an equivalent single pile was presented by CalTrans (2011). The steps presented in that guideline are summarized as:

1) Develop a moment-curvature curve for a single pile. Φ

2) Scale the moment in the M-Φ curve by the number of piles in the pile group.

3) Determine the yield curvature, Φ_y, from the M-Φ plot and calculate the allowable curvature as $\Phi_a = 12(\Phi_y)$. Extend the M-Φ curve to point (Φ_a, 1.1 M_{max}).

4) M-EI values are calculated at several points along the curve using the fact that EI=M/Φ.

5) Input these values of M-EI as user-defined moment-stiffness curves in the software (i.e. LPILE).

A figure showing an M-Φ curve and an M-EI curve developed with this method is shown in Figure 4-8.

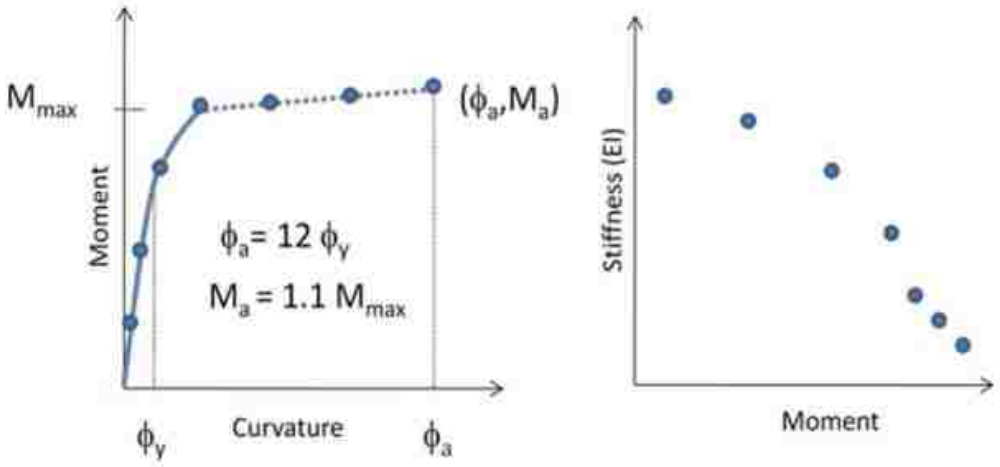

Figure 4-8: Equivalent Single Pile M-Φ Curve for Non-Linear Pile Response Analysis (After CalTrans, 2011)

4.4.2 Development of the Rotational Soil Spring

Mokwa (1999) and Mokwa and Duncan (2003) theorized that a rotational stiffness coefficient could be developed to describe the behavior of lateral spreading causing a rotation in the cap of the pile group. This rotation is caused by the back piles being pulled down while simultaneously the front rows are pulled up. Mokwa (1999) and Mokwa and Duncan (2003) suggested that the coefficient for rotational stiffness can be estimated as:

$$k_{m\theta} = \frac{M}{\theta} \tag{4-11}$$

where:

M = restraining moment to resist rotation

θ = angular rotation of the pile head

If a linear relationship is assumed between M and θ up to the ultimate restraining moment, then $k_{m\theta}$ can be estimated using the ultimate restraining moment, M_{ult}, and the ultimate angular rotation, θ_{ult}. This is demonstrated in Figure 4-9.

M_{ult} from a pile group can be computed as follows:

$$M_{ult} = \sum_{i=1}^{N} \left[(Q_s)_i + (Q_p)_i \right] x_i \tag{4-12}$$

where:

$(Q_s)_i$ = skin friction resistance for pile *i*

$(Q_p)_i$ = end bearing resistance for pile *I* (equals zero with upward moving piles)

X_i = moment arm for pile *i*

N = total number of piles in the pile group

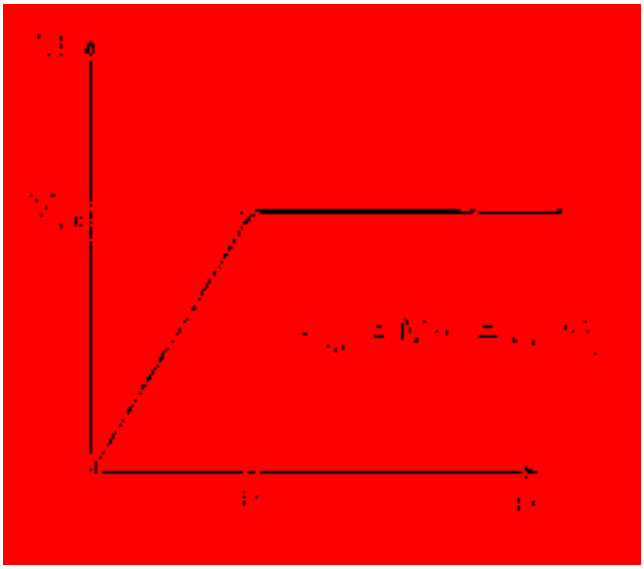

Figure 4-9: Linear Relationship Assumption between M_{ult} and θ_{ult} for Rotational Stiffness (after Juirnarangrit and Ashford, 2006)

4.4.2.1 Skin Friction Resistance $(Q_s)_i$

In order to estimate $(Q_s)_i$, Juirnarongrit and Ashford (2006) recommend using the α-method presented by Tomlinson (1994) for cohesive soils and the β-method by Esrig and Kirby

(1979) for cohesionless soils. It is assumed that the frictional resistance for both upward and downward moving piles will be equivalent in magnitude.

There have been multiple publications suggesting different methods for estimating α as a function of the undrained strength of cohesive soils. These publications vary largely which demonstrates the amount of uncertainty associated with the α-method for skin friction resistance (Franke, 2011). The most commonly used estimate for α is the relationship recommended by Kulhawy and Phoon (1993) and is defined as:

$$\alpha = \frac{\Psi}{\left(\frac{S_u}{P_a}\right)^{0.5}} \tag{4-13}$$

where:

Ψ = Factor equal to 0.5 for soil

S_u = undrained strength of the soil

p_a = atmospheric pressure (units consistent with S_u)

Each cohesive layer will have an individual estimated α value. The total skin resistance for a given pile *i* in cohesive soil can be computed as:

$$(Q_s)_i = \sum_{j=1}^{N} \alpha_j (S_u)_j \, (A_s)_{j,i} \tag{4-14}$$

where:

α_j = alpha factor for soil sublayer j

$(S_u)_j$ = undrained strength for soil sublayer j

$(A_s)_{j,i}$ = surface area of pile i in soil sublayer j

N = total number of cohesive soil sublayers

For cohesionless soils, it is suggested to use the β-method for estimating the skin frictional resistance of a pile. The β factor can be computed using the following equation:

$$\beta = K \tan \delta \tag{4-15}$$

where δ is the interface friction angle between the soil and the pile. K is the lateral earth pressure coefficient for the soil. K it typically estimated as the at-rest lateral earth pressure K_o:

$$K = K_o \approx 1 - \sin \emptyset \tag{4-16}$$

where:

$\emptyset =$ soil internal friction angle

Vertical pile group efficiency effects tend to reduce the skin friction for piles in cohesionless soils. Das (2004) summarized a group efficiency η-value that was first presented by Kishida and Meyerhof (1965). The η value is a function of the friction angle of the soil and the ratio of the pile diameter to the pile spacing, d/D. Kishida and Meyerhof (1965) presented a chart that can easily identify the group efficiency η-value (Figure 4-10).

Figure 4-10: Variation of Efficiency (η) of Pile Groups in Sand (based on Kishida and Meyerhof, 1965)

The total skin resistance for a given pile *i* in cohesionless soil can be computed as:

$$(Q_s)_i = \sum_{j=1}^{N} \eta_j \beta_j (\sigma'_v)_j \, (A_s)_{j,i} \tag{4-17}$$

4.4.2.2 End Bearing Resistance $\left(\mathrm{Q_p}\right)_\mathrm{i}$

The end bearing resistance is dependent on the type of soil the pile is founded in as well as if the pile is moving upward or downward during loading. If the pile is moving upward, the end bearing resistance, $\left(Q_\mathrm{p}\right)_i$, is zero and will not contribute to the resistance. If the pile is moving downward, $\left(Q_\mathrm{p}\right)_i$ can be approximated as:

$$\left(Q_\mathrm{p}\right)_i = \begin{cases} 9(S_u)_i \left(A_p\right)_i \ \ for\ cohesive\ soils \\ \left(q_p\right)_i \left(A_p\right)_i \approx \left[(\sigma'_v)_i \left(N_q\right)_i\right] \left(A_p\right)_i \leq 0.5(p_a)\tan(\emptyset_i)\left(A_p\right)_i \ \ for\ cohesionless\ soils \end{cases} \tag{4-18}$$

where:

$(S_u)_i$ = undrained shear strength of soil layer *i*

$\left(A_p\right)_i$ = cross-sectional area for a given pile tip (including the soil plug)

$(\sigma'_v)_i$ = effective vertical stress for soil layer *i*

$(N_q)_i$= bearing capacity factor for the end-bearing soil = $10^{0.0005\emptyset^2+0.0427\emptyset+0.0088}$ (after Meyerhof (1976))

$\emptyset$ = soil internal friction angle

When calculating the moment are, X_i, choosing the best datum about which to sum the moments can conveniently simplify the process. Juirnarongrit and Ashford (2006) suggest to sum the moments about the back row of piles (i.e. the piles moving downward) to eliminate the end-bearing resistance. This simplifies the calculation because the moment arm for the end-bearing resistance is equal to zero and therefore can be neglected. Figure 4-11 demonstrates this concept suggested by Juirnarongrit and Ashford (2006).

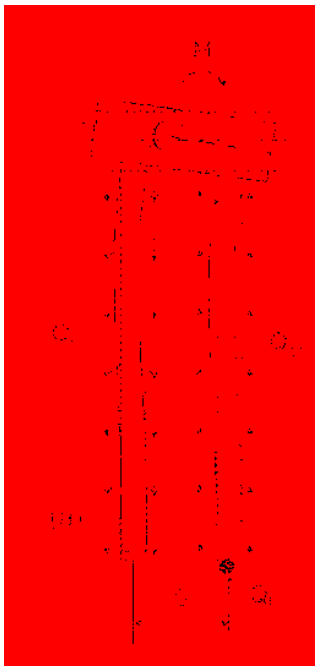

Figure 4-11: Demonstration of Summing the Moments about the Downward –Moving Piles (adapted from Juirnarongrit and Ashford, 2006)

Mokwa (1999) identified that there is an ultimate angle rotation of the pile cap and that it is dependent on whether or not the ends of the piles are free to move downward when loaded (i.e. frictional piles), or if they are fixed and can't move (i.e. end bearing piles) (Franke, 2011). This is demonstrated in Figure 4-12.

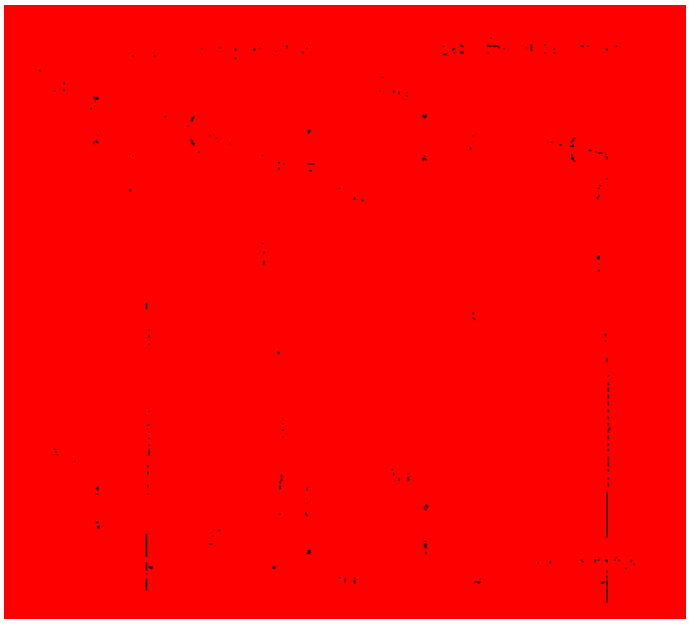

Figure 4-12: Ultimate Angular Rotation of the Pile Cap for a Frictional Pile Group and End Bearing Pile Group (after Juirnarongrit and Ashford, 2006; adapted from Mokwa and Duncan, 2003)

Irrespective of pile diameter and length, Juirnarongrit and Ashford (2006) suggested that the skin friction is fully mobilized when the pile displacement,Δ_{ult}, is 8 mm (0.315 inches or 0.026 feet).

4.5 Equivalent Single Pile Limitations

As is the case with many procedures, the equivalent single pile procedure has some limitations. The major limitation that applies to the study within this thesis is that this procedure

is not able to account for both battered and vertical piles at the same time. The procedure makes the assumption that the entire group of piles is either all battered or all vertical. As a standard of practice, most engineers neglect any battered piles in a group of piles. Battered piles often strengthen the group; therefore, neglecting these piles makes the group appear to be slightly weaker, which is a more conservative approach to the analysis. If it is desired to account for the battered piles along with vertical piles, a more sophisticated approach, such as a numerical model, should be performed.

5 "SIMPLIFIED MODELING PROCEDURE" FOR ANALYZING PIERS SUBJECT TO LATERAL SPREAD

5.1 Introduction

Using the principles presented in the previous chapters regarding liquefaction, lateral spreading, and equivalent single piles ("Super Piles"), the "Simplified Modeling Procedure" developed during this study will be presented in this chapter. This procedure is intended to provide engineers with a new approach to evaluating possible pile loads and anticipated displacements to piers due to lateral spread displacement. The term "pier" throughout the remainder of this thesis is to be understood as a cargo loading pier located near water that is made up of many supporting piles.

This chapter will first present the general assumptions made in applying the Simplified Modeling Procedure. The procedure will then be presented in a step-by-step format. Finally, each step of the procedure will be explained in more depth as to the importance and the needed details.

5.2 General Assumptions of the Simplified Modeling Procedure

Because the Simplified Modeling Procedure was developed and evaluated with only one case study and its specifics, caution should be used in interpreting its results until additional vetting can be performed. While developing this procedure, several assumptions were made in regards to the performance of the pier. These assumptions were made to either allow for certain

parts of the procedure to be performed (i.e. creating "Super Piles") or to simplify the overall analysis while still maintaining a representative model. These assumptions include:

a) All piles are treated as vertical. No battered piles are considered;

b) The magnitude of lateral spreading is assumed uniform across the entire head of the pier;

c) Kinematic loading from lateral spreading is the only external load that is applied to the piles. Inertial loads from the pier can also be added, but were neglected for simplification in this study.

d) The pier deck and piles move as a single unit, and pile connections at the pier are assumed partially fixed and partially pinned:

e) The piles are assumed to have elastic behavior (i.e. non-yielding);

f) The only damages considered on the piles occur between the pile connection and the pier deck (i.e. shearing from the pier deck supports); and

g) Each row of piles along the length of the pier can be modeled as a "Super Pile".

If these conditions are not similar to future analyses, then precautions should be made to the accuracy of the results until further evidence is confirmed of the approach working in other conditions.

5.3 Steps to the Simplified Modeling Procedure

A) Initialize the Model

1) Characterize the soils at the site;

2) Predict the amount of lateral spreading;

3) Create a two-dimensional geotechnical base model;

4) Determine "Super Pile" parameters;

5) Generate "Super Pile" model(s) in LPILE;

B) Run the Analysis

6) Perform push-over analysis on each "Super Pile";

7) Record the individual push-over analysis results; and

8) Determine the displacements where all shear forces reach equilibrium.

5.4 PART A – Initialize the Model

5.4.1 STEP 1 - Characterize the Soils at the Site

Characterization of the soils at the site of interest is the most critical component of creating a representative model. Because the procedure recommended in this study involves applied forces due to lateral spread, it is necessary to identify potential liquefiable layers upon which overlaying non-liquefiable soils may subsequently displace during earthquake ground motions. Soils can be investigated by the means of strategically placed Standard Penetration Testing (SPT) borings, Cone Penetration Testing (CPT) soundings, Vane Shear testing, dilatometer testing, and various other in-situ field tests to establish the different layer interfaces

and their respective geotechnical properties. Ideally, investigative borings and soundings should extend to depths of several hundreds of feet and should be performed with as little linear spacing as possible to establish a clear and more accurate soil profile. However, it is often difficult to get these ideal conditions due to the length of time and cost it can take to perform these investigations. Instead, multiple deeper investigations with greater lateral spacing from one another and intermittent shallower investigations to confirm layer uniformity can be implemented. Determining a sufficient soil profile for the site will require engineering judgement. During these investigations, it is important to follow general standards of practice consistent with the respective investigation methods to ensure more accurate collection of samples and the respective data.

Specific laboratory tests should be assigned to the various representative samples collected during the investigations to identify the more important soil parameters required to create the representative geotechnical base model. It is also important to identify parameters potentially necessary for the analysis of liquefaction and lateral spreading. These tests may include (but are not limited to): sieve analyses and/or minus #200 washes to evaluate fines content and grain size distributions, unit weights and water content, Atterberg limits on fine-grained soil samples to measure liquid limits and soil plasticity, and direct shears to obtain friction angle and cohesion.

An evaluation of the SPT borings, CPT soundings, and any other in-situ testing data should be performed collectively. All the results should be plotted so that the respective elevations are aligned. Once aligned, a direct comparison of the results can be made. This can be easily performed by creating a 2D layout (e.g. stick diagram) for each of the investigations. This plotting approach may assist the engineer in identifying continuous soil layers present at the site

of interest. Each continuous layer should also have the various soil parameters (e.g. SPT blow counts, unit weights, friction angles, grain size distribution, fines content, Atterberg limits, moisture contents, etc.) averaged across the layer in order to develop a representative profile of the site's soils.

Additionally, during the evaluation of the developed representative soil profile, it is important to identify which layers in the profile may be susceptible to liquefaction. If the representative soil profile results in little layer continuity or does not have potentially liquefiable layers, then it is likely that the site will not experience lateral spread. If this is the case, other potential hazards that could apply loading conditions to the piles should be considered. However, the elaboration on these other hazards and how to evaluate them is beyond the scope of this study.

Developing an accurate and representative soil profile is an art and requires experience. Each profile requires a significant amount of engineering judgement, and every engineer may develop different profiles for the same site by either different judgment or through implementing different methods.

5.4.2 STEP 2 - Predict the Amount of Lateral Spreading

If a continuous liquefiable layer is identified within the soil profile, the user then must predict the amount of lateral spread displacement that could occur.

There are several different methods to predict the lateral spreading at a site as was summarized in Chapter 3. Application of empirical models requires SPT or CPT data to determine the lateral spreading. It is important to understand the limitations and factors that go into any selected model prior to use. If possible, make a comparison between different models to evaluate and potentially incorporate epistemic uncertainty.

Lastly, assign the layers that will be affected by the lateral spreading and how displacements will be distributed through these layers. It is often assumed that the lateral spreads are linearly distributed across the liquefied layer. The lowest section of the layers will have very little or no deflection while the top of the layer will have experienced the full lateral spreading.

5.4.3 STEP 3 – Create a Two-Dimensional Geotechnical Base Model

By combining the geometric design of the pier, the site topography, and the two-dimensional representative soil profile along with the corresponding geotechnical properties, a geotechnical base model can be developed. For each pile group location along the pier, a one dimensional generalized soil profile and corresponding geotechnical properties can be developed for modeling. A simplified topographic profile of the site along the length of the pier can also be developed as part of the geotechnical base model.

The user should identify areas in the soil profile that are uniform from one pile location to the next. If there are variations in soil profiles between separate pile rows, determine if an average soil profile could still be made that would still result in a representative profile of the area.

5.4.4 STEP 4 - Determine "Super Pile" Parameters

5.4.4.1 "Super Pile" Moduli

Analyzing a large number of piles along a pier is a challenging task. To simplify the process, individual rows of piles could be grouped together into "Super Piles" for analysis. If the soil profile and pile parameters for a row are similar to other rows already established, the row does not need to be replicated into another "Super Pile". The similar rows will be accounted for

by simply multiplying the results by the number of similar rows. This greatly reduces the amount of required “Super Pile” models that are needed.

A “Super Pile” for a row is determined by establishing the number of piles acting within the specified row and multiplying that number with the value for the modulus of elasticity of a single pile within the row. This row can then be represented by a single “Super Pile” that uses the modified elastic modulus derived from combining the moduli of all the piles in the row. A more in-depth explanation for creating a “Super Pile” can be found in Chapter 4.

5.4.4.2 Check for Shadowing Effects

Shadowing effects are to be applied to the model by using a p-multiplier that reduces the p-y soil spring resistance on the pile. Determine if the spacing (S) of the piles is greater than or less than 5.65 times the diameter (D) of the piles. If $S \leq 5.65D$, then proceed to use equations 5-2 through 5-4 to determine the appropriate shadowing reduction factors to apply to the p-multiplier value in equation 5-1. The p-multiplier is then applied to the “Super Pile” to reduce the p-y soil spring values. If $S > 5.65D$ then shadowing effects can be neglected (P=1) and the p-y spring values are not affected when creating the “Super Piles”.

5.4.4.3 Other “Super Pile” Parameters

Just like with the soil profile, the more pile parameters that are identified and known, the more accurate the resulting model will be. Some of the parameters that are important in regards to the piles include: length [m/ft], diameter [mm/in.], wall thickness [mm/in.], elastic modulus [kPa/ksi], and rotational stiffness [kN*m/Rad or in*lb/degree]. Most of these parameters are easily obtained from reconnaissance efforts and through standard industry values. However, the rotational stiffness parameter of an object that is subject to rotation is more difficult to determine.

For this thesis, rotation stiffness was assumed to occur within the support beam connecting the pier deck and the individual piles. The rotational stiffness of the support beam (I-Beam) can be assessed using Equation (6-1).

$$Rotational\ Stiffness\ (\beta) = M_0/\theta \tag{6-1}$$

where:

M_0 = Bending moment of the support beam

θ = the resulting slope/curvature of the beam created by the applied moment

The support beam can be represented with a simple free body diagram of a cantilever scenario as is shown in Figure 5-1. The representative free body diagram shows the parameters of the steel support beam (E= Young's modulus or elastic modulus, I=Moment of Inertia), the depth of the beam (L), and the bending moment applied from the pile (M_o). The bending moment of the support beam is created when the pile is subject to lateral spread displacements. The displacements cause the attached pile to apply a moment to the support beam as it rotates.

Using the free-body diagram that represents the support beam, the slope (θ) or deflection can be determined using the equation shown in Equation (6-2).

$$\theta = \frac{M_o L}{EI} \tag{6-2}$$

When the slope equation is substituted into the rotational stiffness (β) equation (6-1), the following rotational stiffness equation results:

$$\beta = \frac{M}{\frac{M_o L}{EI}} = \frac{EI}{L} \tag{6-3}$$

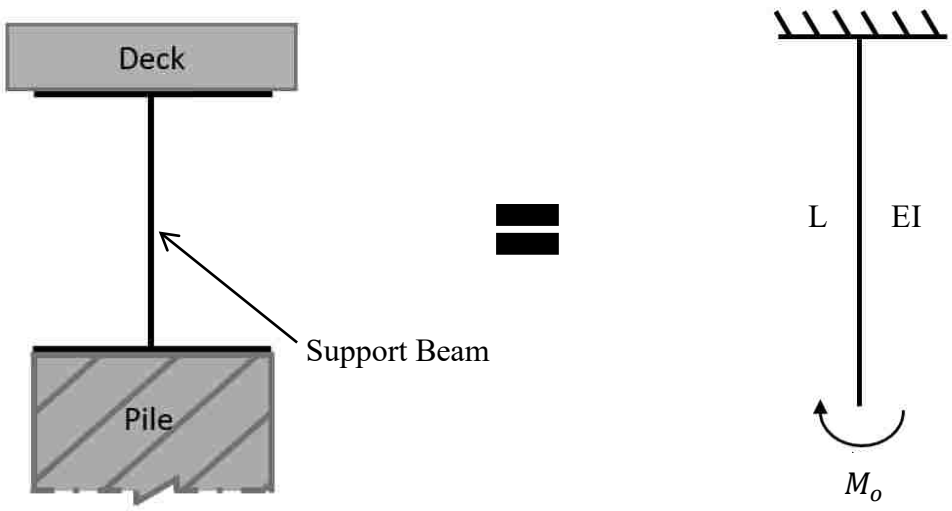

Figure 5-1: Free-Body Diagram Conversion of Piles

As can be seen, the bending moment of the support beam becomes obsolete in Equation (6-3) and the equation simplifies to a function comprised of the support beam properties only (Young's modulus or elastic modulus (E), moment of inertia (I), and the depth of the beam (L)).

This makes the equivalent rotational stiffness dependent strictly on the support beam itself and independent of the pile rotation from lateral spread or any other applied loads.

The orientation of support beams along a pier (i.e. perpendicular to the length of the pier) leads to the assumption that the beam is more likely to yield through the web of the beam along the x-axis or its weak axis. The different axes for the support beam are illustrated in Figure 5-2.

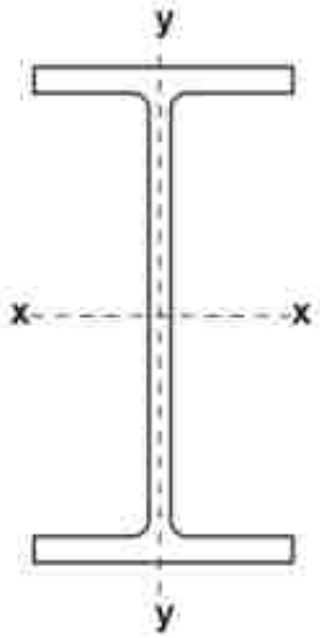

Figure 5-2: I-Beam Moment of Inertia Axes

Moment of inertia along the x axis (I_x) for the support beam (I-Beam) can be determined as:

$$I_x = \frac{L'(t_w)^3}{12} \quad (6\text{-}4)$$

where:

$$L' = effective\ length\ of\ the\ beam$$

$$t_w = web\ thickness$$

Once a rotational stiffness is determined, the user applies engineering judgment to determine if the value is large enough to be of significance. Typically, small rotational stiffness's (e.g. 100 kN*m/Rad or lower) can be neglected. However, if a larger value is determined, this value should then be implemented into the subsequent pile response analysis because the large stiffness will reduce the amount of deflection of the piles.

5.4.5 STEP 5 - Generate "Super Pile" Model(s) in LPILE

5.4.5.1 LPILE Overview

LPILE v2016 (ENSOFT) is a special-purpose program for analyzing a single pile (or drilled shaft) under lateral loading using p-y curves. LPILE solves the differential equation for a beam-column using nonlinear lateral load-transfer (p-y) curves. The program computes lateral deflection, bending moment, shear force, and soil response over the length of the pile. Different parameters can be applied to any analysis in order to more accurately produce results of the pile performance. The program also allows for different approaches to analyses to be performed. Two of the most used analyses are the push-over and pile buckling analyses.

LPILE has a wide range of selection for all kinds of parameters that allows the user to make an accurate model that can represent any condition needed. The following sections discuss the different settings that can be altered while setting up the model in LPILE.

5.4.5.2 Configure LPILE for the Model

5.4.5.2.1 Allow Soil Loads to be Applied

To allow the soil loads from lateral spreading to be applied to the pile in LPILE, the option to use *loading by single soil movement* needs to be toggled on in the program options dialog box, which will provide the user access to the *soil movements* tab on the main tool bar. Once inside the soil movements dialog box, the user can then input the desired profile of soil movement.

5.4.5.2.2 Other Options and Settings

Changes to the options and settings can be changed throughout the analysis to either simplify the process or to analyze a different portion of the analysis. The program options and settings are specifically chosen to optimize the program and allow the proper analysis to be utilized.

5.4.5.3 Select Section Type

LPILE allows for a variety of pile types to be selected and analyzed. This capability is useful because each pile type has its own unique set of parameters that LPILE already has programmed into the software so the user knows which parameters are required. LPILE will also provide warnings to alert the user if invalid values have been specified in the design. The section types that LPILE gives as options are variations of Elastic, Concrete, Steel, Pre-stressed Concrete, and Non-linear Bending sections.

5.4.5.4 Input Model Parameters for "Super Piles"

Once the configurations have been selected and toggled on, the respective parameters for the soil profile, rotational stiffness, "Super pile" parameters (i.e. Modulus of elasticity), and soil loads (i.e. lateral spreading) can all be added to create the "Super Pile" model(s) in LPILE. Each "Super Pile" needs its own individual model for analysis.

5.5 Part B - Run the Analysis

5.5.1 STEP 6 - Perform Push-Over Analysis on each "Super Pile"

Both force and strain compatibility must be achieved when analyzing all of the "Super Piles" in LPILE, however, analyzing force and strain compatibility sequentially in individual "Super Piles" in not recommended because it is very time consuming and much harder to make the needed correlations between each row of piles. Each compactible deflection is achieved with a different shear force for each individual "Super Pile", which leads to numerous calculations that slow down the process significantly. Rather than this sequential approach, a push-over analysis reverses the normal analysis by specifying various deflections as boundary conditions and then calculates the shear forces required to reach those deflections simultaneously. This type of analysis allows the calculations to be performed in a matter of seconds because the user can specify multiple deflections to be analyzed at one time. This approach allows the user to more easily draw the needed correlations between the rows because all the deflections are the same from on "Super Pile" to the next. To perform the push-over analysis in LPILE, the toggle box must be selected from the *Program Options and Settings* dialog box. The conventional analysis mode must be selected for the push-over analysis toggle to be available for selection.

The user must specify the range of the displacements that will be analyzed in the push-over analysis. Specific displacements should begin with zero and increase to a maximum deflection that is significantly past the yield point of the piles. The user must also carefully consider and select intervals to use between each deflection. The smaller the interval between each deflection, the more accurate the results will be, but the more calculation time will be required.

5.5.1.1 Understanding Shear Forces for Push-Over Analysis

The push-over analysis results can be confusing if the sign convention of the resulting shear forces is not understood. These results in LPILE must be understood to know where the shear forces are being applied in the system (i.e. pier deck acting on the pile, or pile acting on the pier deck). The push-over resulting forces are shown with respect of the pier deck acting on the piles. A typical positive shear force in the push-over analysis results indicates a pier deck shear force acting to the right while negative shear force indicates a pier deck shear force acting to the left as is shown in Figure 5-3.

In this analysis, with lateral spreading affecting the movement of the piles in the direction of the occurred spreading, a positive shear force applied from the pier deck on the pile forces the pile to deflect more to the right. Positive shear can also be seen as forcing the pile past the "natural state" deflection that would have resulted from the soil loads (i.e. lateral spreading) alone. In this state, as long as the pile has not yielded, the pile will behave like a spring and want return to the natural state deflection caused by the lateral spreading. Thus, the pile itself develops an opposite force (i.e. negative force) that it applies to the pier deck. This spring-like action of the piles resists the pier deck from permanently deflecting.

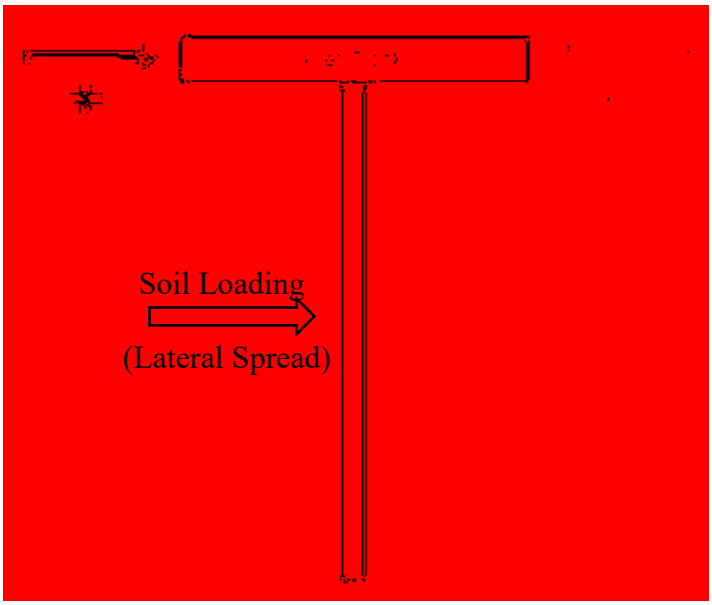

Figure 5-3: Typical Pier Deck Forces

In relation to the pile acting on the pier deck, positive forces that result from the push-over analysis are considered to be resisting forces (i.e. opposite) that the piles are applying to the pier deck. This is shown in Figure 5-4. The forces shown in the left image are what the pile feels from the pier deck acting on it, and represent the sign convention presented in the LPILE push-over analysis results. The forces shown in the image on the right represent the reacting forces applied from the piles to the pier deck.

Negative shear force resulting from the analysis can be seen as the pier deck resisting the lateral spreading deflection. Once again, as long as the pile has not yielded, the pile will act like a spring and want to return to the "Natural State" deflection. The pier deck force that is resisting the pile from fully deflecting to the "Nature State," causes a positive force on the pier deck due to the spring effect that has now developed in the pile. This is illustrated in Figure 5-5.

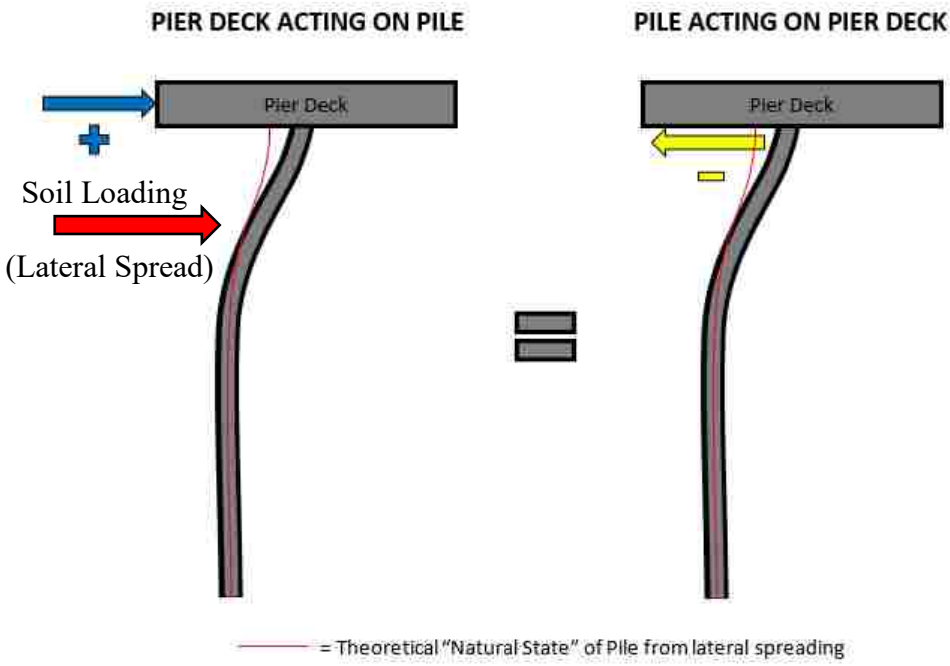

Figure 5-4: Positive Pier Deck Shear Forces and Equivalent Pile Shear Forces

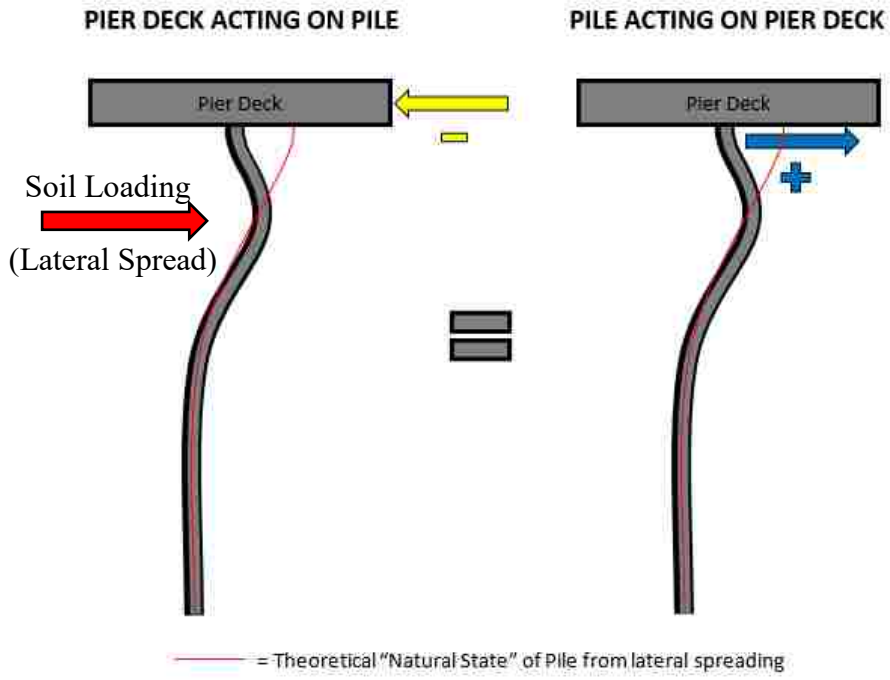

Figure 5-5: Negative Pier Deck Shear Forces and Equivalent Pile Shear Forces

5.5.2 STEP 7 – Record the Individual Push-Over Analysis Results

Record the push-over results from each individual "Super Pile" analysis into a simple spreadsheet that lists the magnitudes of shear force that were required to deflect the pile to each of the designated deflections. Ensure that sign conventions (+/-) are maintained while recording the values. Only the pile-head deflections and pile-head shear forces are required for the Simplified Modeling Procedure.

5.5.3 STEP 8 - Determine the Displacements where all Shear Forces Reach Equilibrium

Once all the results have been recorded, summate the shear force magnitudes for each deflection and determine at what deflection the shear forces are in equilibrium (i.e. summation of zero).

6 PORT OF CORONEL (MAULE, CHILE) CASE STUDY

6.1 Background of the North Pier

The North Pier located within the Port of Coronel (approximately 22 km southwest of Concepcion, Chile) was constructed in 1996 with additional expansions/upgrades performed in 2000 and 2004. The North Pier is used primarily for general bulk cargo. It is approximately 541 meters in length and upwards of 30 meters wide. Its design is that of a conventional pile-supported pier with 308 piles (vertical and battered). The reinforced concrete pier deck is supported by cross-support beams (I-beams) made up of 25.4 mm thick steel that are 0.9 m deep. The pile supports are hollow steel piles with a diameter of 50 centimeters and a wall thickness of 14 millimeters. Figure 6-1 shows the general dimensions for the support beams and the piles of the North Pier.

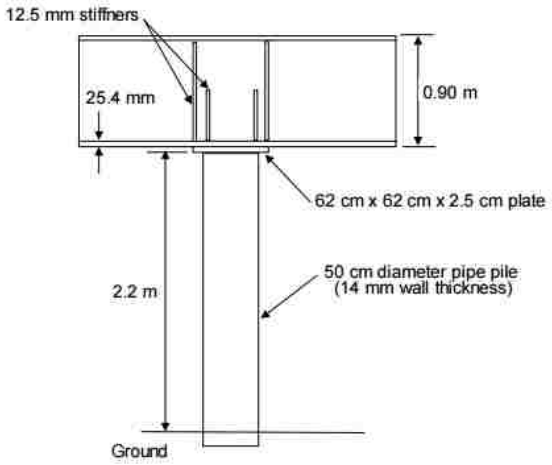

Figure 6-1: North Pier Pile and Pier Deck General Dimensions (Bray, et al. 2012)

SPT tests conducted during construction and each of the expansions/upgrades were used to characterize the seafloor and locate the depth of the bedrock along the length of the pier. From these tests, it was determined that liquefiable soils were located within the first 70 meters of the shoreline. The location of the Port of Coronel in relation to the epicenter of the 2010 earthquake is shown in Figure 6-2. Additionally, the piers in the Port of Coronel are shown in Figure 6-3 with the North Pier being labeled. The North Pier is used as the basis of this thesis and therefore, only the North Pier will be further discussed in detail.

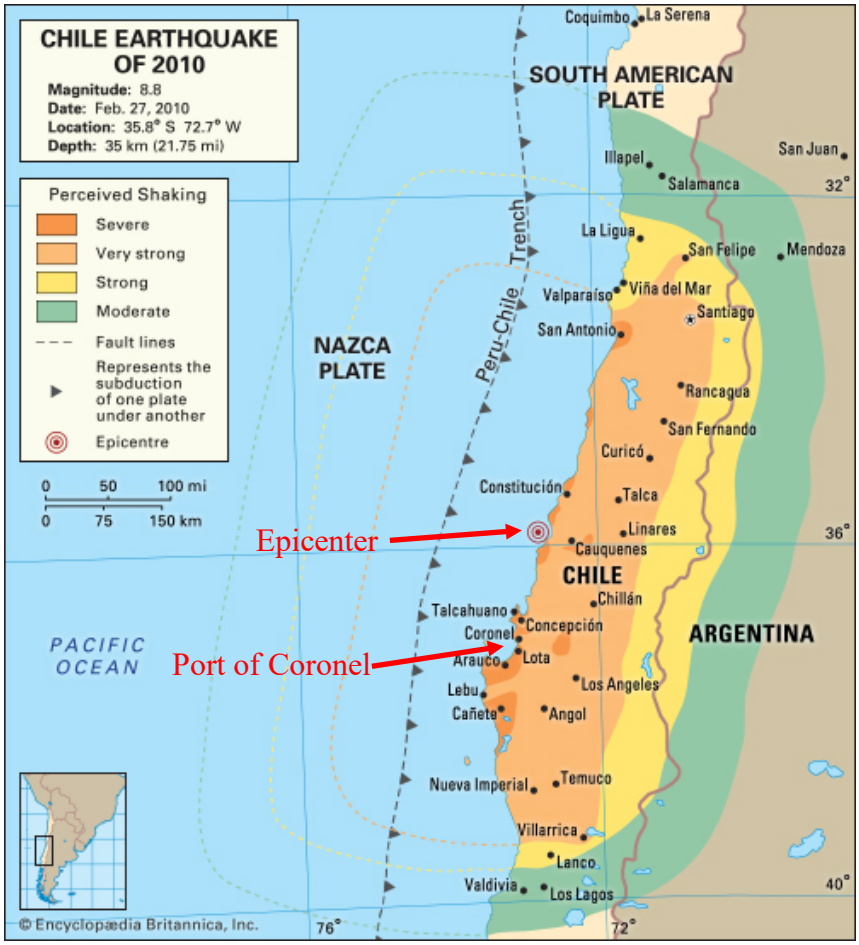

Figure 6-2: Location of the Port of Coronel to the Epicenter of Maule, Chile 2010 Earthquake (Pallardy, n.d.)

Figure 6-3: Port of Coronel and the Location of the North Pier (image from googlemaps.com)

6.2 North Pier Damages during the Maule 2010 Earthquake

On the 27th of February, 2010, a large offshore mega thrust earthquake of moment magnitude (M_w) 8.8 struck the central south region of Chile, affecting the Port of Coronel near Maule, Chile. The peak ground acceleration (PGA) occurred at Concepcion with a magnitude of 0.65g (6.38 m/s^2). The shaking from the earthquake lasted approximately two minutes as the Nazca Plate slipped under the South American Plate upwards of 10 meters over an area of approximately 500 km long and 100 km wide. In the first month following the main earthquake, there were 1,300 aftershocks of M_w 4.0 or greater and 19 of M_w 6.0-6.9. The locations of the

aftershocks the following month can be seen in Figure 6-4. The M_w 8.8 earthquake ranked as the fifth largest earthquake to date that had been recorded by a seismograph (Astroza et al., 2012). The results of both the earthquake and the subsequent tsunami lead to 486 deaths and approximately 370,000 homes were damaged (Bray and Frost, 2010). The ground shaking, liquefaction, and lateral spreading introduced from the large earthquake additionally damaged highways, railroads, airports, and ports, including the port of Coronel.

Figure 6-4: Location of the Epicenter of the Mw 8.8 Earthquake on February 27th, 2010 (White Star in Red Circle), and the Aftershocks that Occurred until March 25th, 2010 (Maule, n.d)

Shortly after the 2010 Earthquake, both the Geotechnical Extreme Events Reconnaissance team (GEER) and Earthquake Engineering Research Institute (EERI) visited several sites affected by the event. Lateral spread displacement magnitudes were measured and evaluated at several ports, including the Port of Coronel. Lateral spreading was observed at two of the piers (Fisherman's Pier and the North Pier) in the Port of Coronel. The results of the observed damages were described by Brunet et al., (2012). In 2014, additional SPT and CPT data was collected by research groups from Brigham Young University to more clearly and better characterize the soils above the bedrock plane along the length of each of the piers. These tests were done to better understand the lateral spreading effects due to the soil types. Figure 6-5 shows the approximate locations of both the pre earthquake borings as well as the 2014 borings performed near the North Pier.

Figure 6-5: Locations of Boreholes and Geotechnical Soundings near the North Pier (Ledezma & Tiznado, 2017)

The North Pier experienced damages from lateral spreading in the approach zone (first 145 meters of the pier to the shoreline). Lateral spreading was measured to be between 1.5 meters and 3.0 meters at the North Pier (Brunet et al., 2012). Several of the pile supports were observed to have rotated, had broken welds on the deck plates, and displaced seaward (same direction of the lateral spread effects). The reinforced concrete pier deck was observed to have significant pavement cracks and ground settlements. Since the piles were embedded in bedrock, displacement and rotation in the piles indicates the possibility of the piles experiencing unseen shear failure located within the underlying soil profile. Direct costs in damages for all the ports in southern Chile were estimated to be approximately US$285 million. The North Pier alone had approximately US$620 thousand in damages (Brunet et al., 2012). Damages observed at the Port of Coronel can be seen in Figure 6-6 and Figure 6-7 .

Figure 6-6: Toppled Containers at the Port of Coronel (GEER 2010)

Figure 6-7: Sink Hole at the Port of Coronel (GEER 2010)

As previously mentioned, the zone of liquefaction was determined to be in the first 70 meters of the shoreline. This encompasses the first 8 rows of piles. Consequently, and as expected, the first 8 rows are where the major damages to the pier were observed. Piles located further off shore along the pier were not subject to the same lateral spreading effects and were supported instead by a stronger soil profile. These piles stayed in place, with little to no damage, which caused compression forces in the deck when the first 8 rows moved seaward from lateral spread. Figure 6-8 shows a general plan of the pier and the location of the damages, an approach zone plan view, and an approach elevation view. These views also show the observed damages to the piles (rotation, displacement, ruptures). Additionally, Table 6-1 gives the numerical damages observed for each of the approach zone pile rows. An example of the rotations observed in the pile rows (row 3 is shown) can be seen in Figure 6-9.

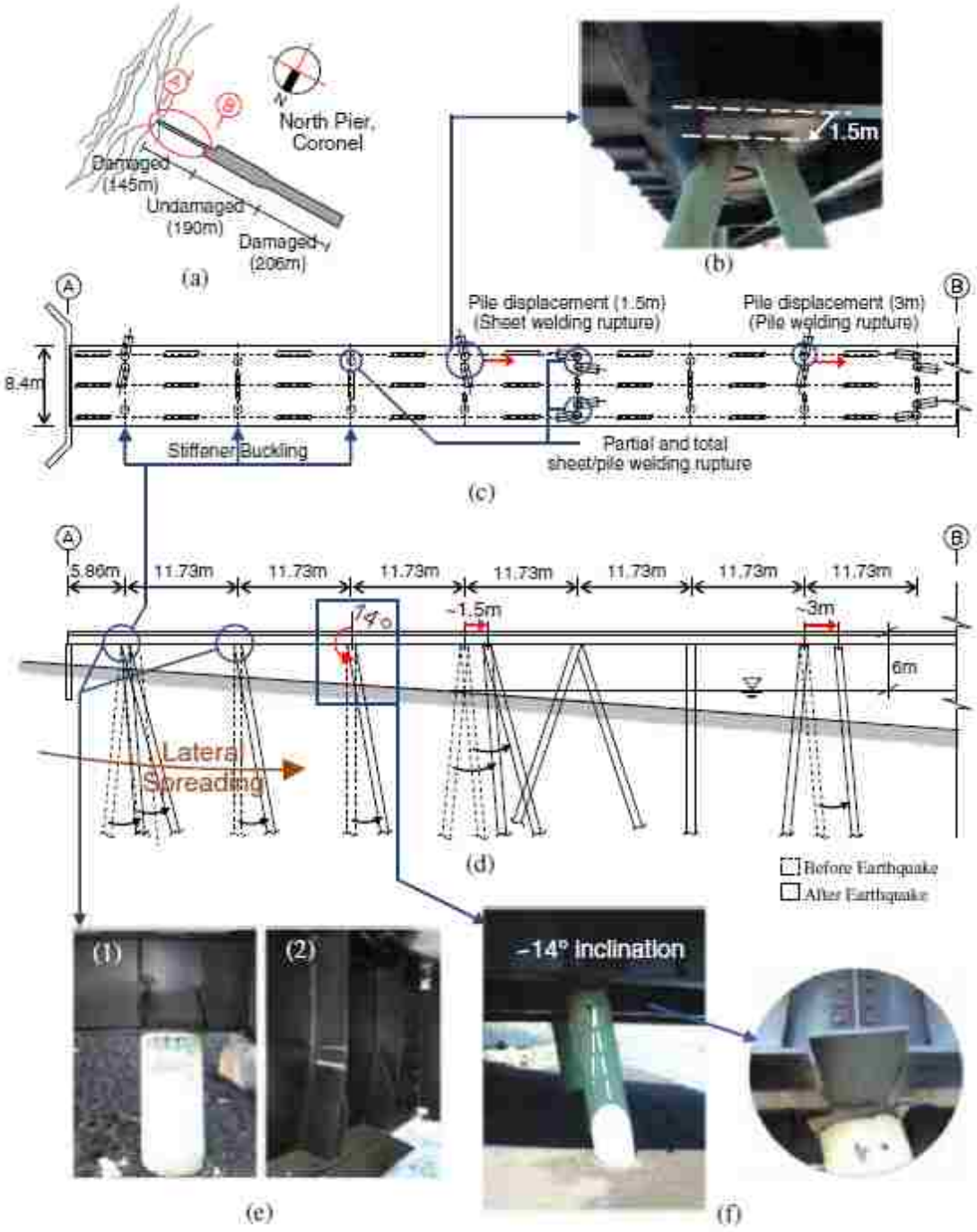

Figure 6-8: General, Plan, and Elevation Views of the Damages Observed at the North Pier (after Brunet et al., 2012)

Table 6-1: Numerical Values of Damages at the North Pier (Pile 3 shows both 2010 and 2014 results) (Tryon, 2014)

Pile Row	1	2	3	4	5	6	7	8
Evidence of Lateral Spread	Pile Rotation	Pile Rotation	Pile Rotation	Pile Displacement	Ruptured Welds	None	Pile Displacement	None
Pile Rotation (°)	11.7	15.3	12.2/14.0	-	-	-	-	-
Ground Displacement (m)	0.27	0.3	0.48/0.55	1.5	-	-	2-2.25	-
Flange Rotation (°)	10.4	12.8	10	-	-	-	-	-

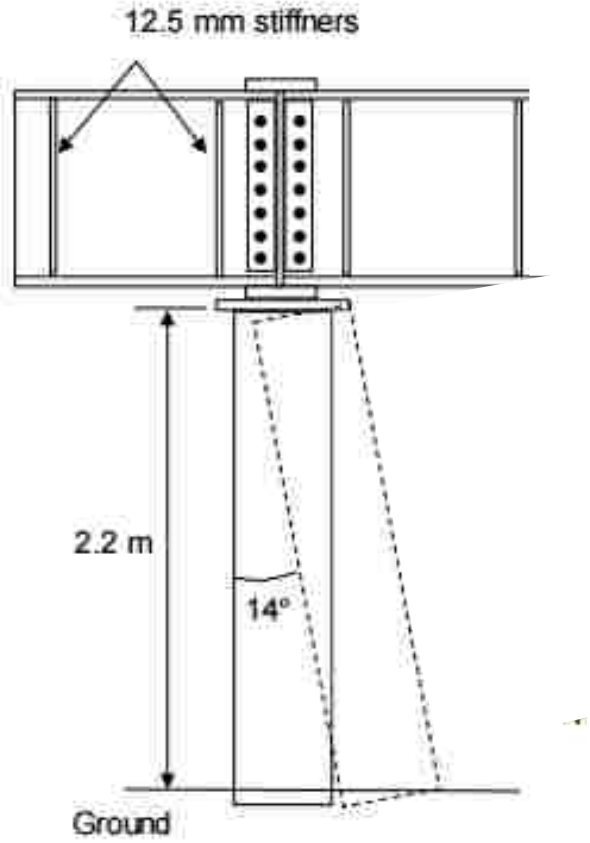

Figure 6-9: Pile Row 3 after the Earthquake (Bray et al., 2012)

7 VALIDATION OF THE "SIMPLIFIED MODELING PROCEDURE"

To test and validate the Simplified Modeling Procedure for analyzing piers impacted by lateral spread, the procedure is applied to the North Pier study from Chile, as described in Chapter 6.

7.1 STEP 1 - Characterize the Soils at the Site

In a previous study, Tryon (2014) of Brigham Young University provided additional information for the soil profile along the length of the North Pier. A combination of data collected from six borings was collected to develop a two-dimensional soil profile at the site (See appendix A).

Figure 7-1 presents an AutoCAD schematic created by Tryon (2014) that shows the soil profile and the approximate soil interfaces between each boring. This AutoCAD model was used, along with the data from the soil borings, to define the layering used in this study.

Each of the soil borings were evaluated and compared side by side to help determine the averages that led to the profile that was ultimately used in the analysis. Table 7-1 shows the soil classifications determined for each of the layers encountered in the respective SPT borings. The boring information has been organized so that the respective elevations of all the borings align. The final profile that was then created from taking the averages of the boring data is also shown in the same figure. It is important to note that this final representative profile can be interpreted

differently for each user. There is no one correct representative profile that should be used. Engineering judgment is important in determining a profile that works for each user.

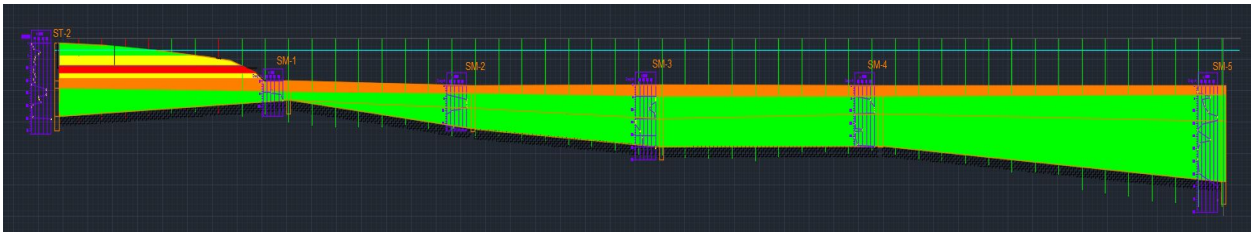

Figure 7-1: AutoCAD Soil Profile Depiction of the Soil and Topography at the North Pier Site at Coronel, Chile (Tryon, 2014)

The section towards the front of the pier was determined in the same way but from the single boring ST-2. The grade of this section was estimated by Tyron (2014) from field observations. It was determined that there was a clean sand layer along this section at a depth of 5.45-12.45 meters (17.9-40.8 feet) below grade that is highly susceptible to liquefaction.

The SPT values determined for each soil layer were correlated directly to their respective soil parameters for friction angle, unit weight, and undrained shear strength. The correlation graphs used were first presented by Bowles (1977) and Terzahgi & Peck (1967) and are provided in Figure 7-2 to Figure 7-4 and Table 7-2.

Additionally, Table 7-3 shows the correlated parameters that were determined for both the top and the bottom of each soil layer within the representative soil profile.

Table 7-1: Representative Soil Profile Spreadsheet

Depth [m]	SM-1 Profile	SM-2 Profile	SM-3 Profile	SM-4 Profile	SM-5 Profile
17.50	Lean CLAY (CL)	Lean CLAY (CL)	Clayey SAND (SC)	Lean CLAY (CL)	Silty SAND (SM)
18.50	Lean CLAY (CL)	Lean CLAY (CL)	Clayey SAND (SC)	Lean CLAY (CL)	Silty SAND (SM)
19.50	Lean CLAY (CL)	Lean CLAY (CL)	Clayey SAND (SC)	Lean CLAY (CL)	SILT (ML)
20.50	Lean CLAY (CL)	Lean CLAY (CL)	Clayey SAND (SC)	Lean CLAY (CL)	SILT (ML)
21.50	Silty SAND (SM)	Lean CLAY (CL)	Poorly Graded SAND With Silt (SP-SM)	Silty SAND (SM)	
22.50	Silty SAND (SM)	Poorly Graded SAND With Silt (SP-SM)	Poorly Graded SAND With Silt (SP-SM)	Silty SAND (SM)	
23.50	Silty SAND (SM)	Poorly Graded SAND With Silt (SP-SM)	Poorly Graded SAND With Silt (SP-SM)	Silty SAND (SM)	
24.50	Silty SAND (SM)	Poorly Graded SAND With Silt (SP-SM)	Poorly Graded SAND With Silt (SP-SM)	Silty SAND (SM)	
25.50	Elastic SILT (MH)	Poorly Graded SAND With Silt (SP-SM)	SILT (ML)	Silty SAND (SM)	
26.50	SILT (ML)	Poorly Graded SAND With Silt (SP-SM)	Silty SAND (SM)	Silty SAND (SM)	
27.50	SILT (ML)	Elastic SILT (MH)	Silty SAND (SM)	Silty SAND (SM)	
28.50	Elastic SILT (MH)	Elastic SILT (MH)	Silty SAND (SM)	Elastic SILT (MH)	
29.50	SILT (ML)	Elastic SILT (MH)	Silty SAND (SM)	Elastic SILT (MH)	
30.50		Elastic SILT (MH)	Silty SAND (SM)	Elastic SILT (MH)	
31.50		Elastic SILT (MH)	SILT (ML)	Elastic SILT (MH)	
32.50		Elastic SILT (MH)	Elastic SILT With Sand (MH)	Elastic SILT (MH)	
33.50		Silty CLAY (CL-ML)	Elastic SILT With Sand (MH)	Elastic SILT (MH)	
34.50		Silty CLAY (CL-ML)	SILT (ML)	Elastic SILT (MH)	
35.50		Silty CLAY (CL-ML)	SILT (ML)	Elastic SILT (MH)	
36.50			Elastic SILT (MH)	Elastic SILT (MH)	
37.50			Lean CLAY (CL)	Elastic SILT (MH)	
38.50			Lean CLAY (CL)	Elastic SILT (MH)	
39.50			Lean CLAY (CL)	Lean CLAY (CL)	
40.50			Lean CLAY (CL)	Lean CLAY (CL)	
41.50			Lean CLAY (CL)	Lean CLAY (CL)	
42.50			Elastic SILT With Sand (MH)		
43.50			Elastic SILT With Sand (MH)		
44.50			Elastic SILT With Sand (MH)		

Average Profile	Analysis	SPT
Clay w Free	Coh	6.4
Clay w Free	Coh	6.8
Clay w Free	Coh	7.2
Clay w Free	Coh	7.2
API Sand	Gran Low	87.7
API Sand	Gran Low	98.7
API Sand	Gran Low	99.1
API Sand	Gran Low	96.3
API Sand	Gran Low	99.3
API Sand	Gran Low	85.5
API Sand	Gran Low	77.7
API Sand	Gran Low	55.4
API Sand	Gran Low	57.7
API Sand	Gran Low	45.5
Elastic Silt	Coh	16.2
Elastic Silt	Coh	7.4
Elastic Silt	Coh	18.9
Elastic Silt	Coh	20.1
Elastic Silt	Coh	26.7
Elastic Silt	Coh	8.2
Clay	Coh	10.4
Clay	Coh	25.1
Clay	Coh	12.2
Rock		-
Rock		-
Rock		-
Rock		-
Rock		-

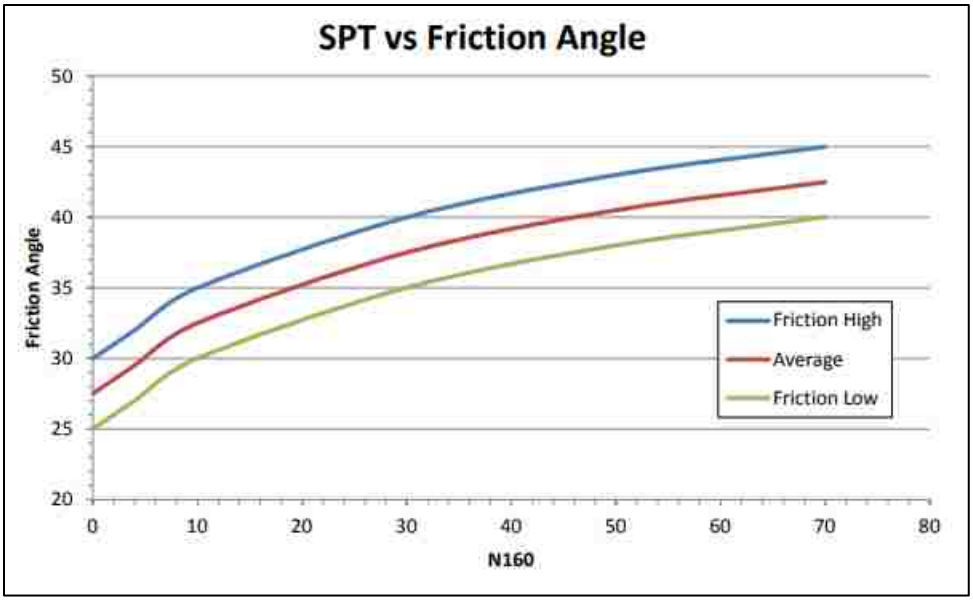

Figure 7-2: Correlation of SPT $N1_{60}$ with Friction Angle (After Bowles, 1977)

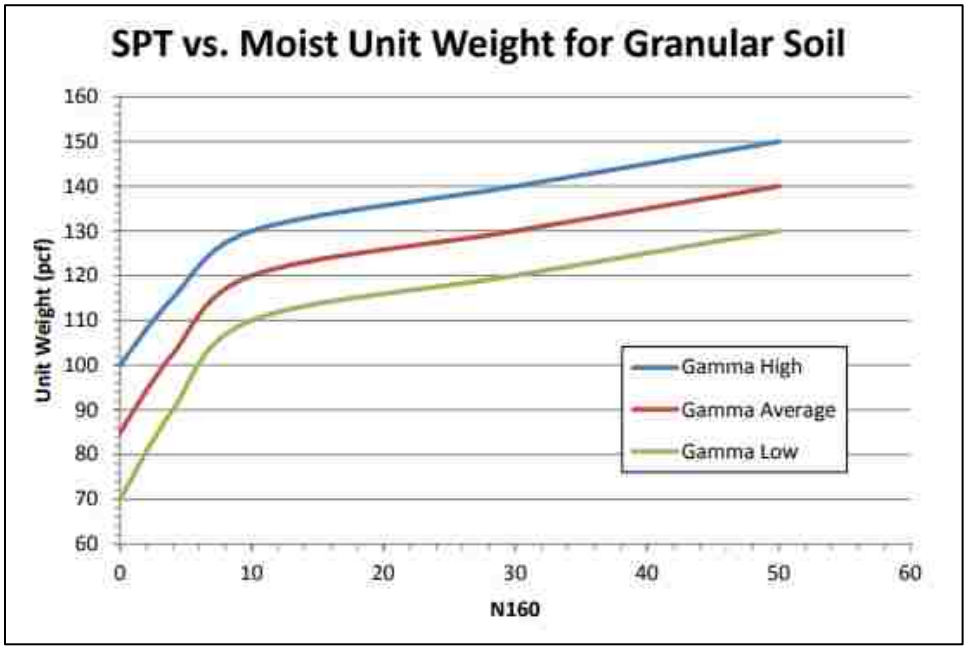

Figure 7-3: Correlation of SPT $N1_{60}$ with Unit Weight (Granular Soils) (After Bowles, 1977)

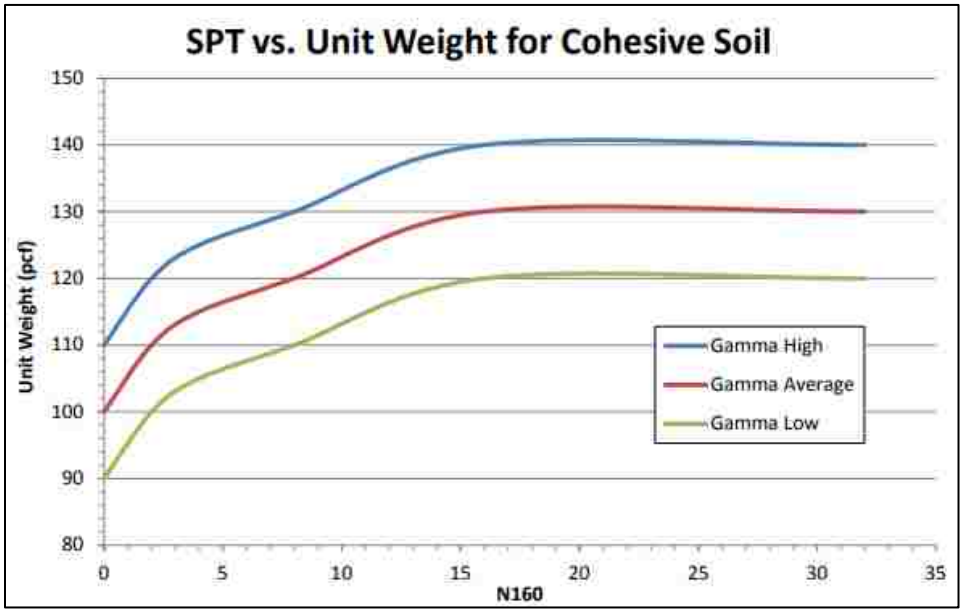

Figure 7-4: Correlation of SPT $N1_{60}$ with Unit Weight (Cohesive Soils) (After Bowles, 1977)

Table 7-2: Correlation of SPT $N1_{60}$ with Undrained Shear Strength (Cu) (Terzaghi & Peck, 1967)

Consistency	SPT - $N1_{60}$ Values	Undrained Shear Strength (Cu) [kPa]
Very Soft	0 - 2	0 - 12.5
Soft	2 - 5	12.5 - 25
Medium Stiff	5 - 10	25 - 50
Stiff	10 - 20	50 - 100
Very Stiff	20 - 30	100 - 200
Hard	>30	>200

Table 7-3: Additional Parameters used for Representative Soil Profile

Layer	Soil Type	Elevation [m]		SPT $N1_{60}$ Value		SPT Correlated Effective Unit Weight [kN/m^3]		SPT Correlated Friction [degrees]		SPT Correlated Cu [kPa]	
		Top	Bottom	Top	Bottom	Top	Bottom	Top	Bottom	Top	Bottom
1	Clay w/ free	17.5	21.5	6.4	7.2	7.2	7.3	31.0	31.5	37.1	43.1
2	API Sand	21.5	26.5	98.7	99.3	13.8	13.8	45.0	45.0	-	-
3	API Sand	26.5	31.5	85.5	45.5	12.2	10.1	42.5	40.0	-	-
4	Silt	31.5	36.5	16.2	26.7	8.1	8.9	34.5	37.0	98.2	160.4
5	Clay w/o free	36.5	40.5	8.2	25.1	9.0	10.6	32.0	36.5	47.9	149.6
6	Rock	40.5	50.0	-	-	12.8	12.8	-	-	-	-

7.2 STEP 2 – Predict the Amount of Lateral Spreading

For this analysis, the magnitude of the soil movement from lateral spreading was measured to be as low as 1.5 and as high as 3.0 meters (Brunet et al., 2012). The value of 2.25 meters was used for this study. This value comes from taking the average magnitudes of all the pile displacements in the "Liquefied" zone of the pier. This is the maximum soil movement that would be anticipated in the layer susceptible to liquefaction. It is assumed that the soil above the layer of liquefaction also experienced the same magnitude of movement, and that the magnitude of movement decreased linearly through the liquefiable layer until reaching zero at the bottom of the layer.

7.3 STEP 3 – Create a Two-Dimensional Geotechnical Base Model

After analyzing the data collected by Tyron (2014), the pier was subsequently divided into two sections according to the soil profiles along the pier and the zones where lateral spreading was observed. The two sections that resulted were labeled as the "Liquefied" section and the "Non-Liquefied" section. This division of the two sections corresponds with the lateral spread damages that were observed in the piles as shown in Figure 6-8. Once again, the CAD drawing is shown (Figure 7-5) to identify the division that was made.

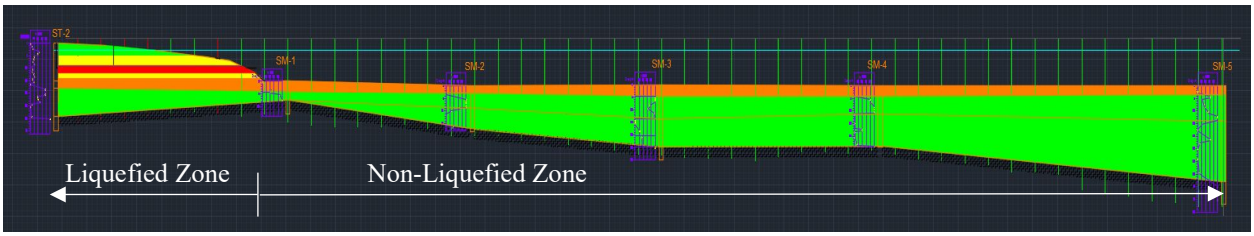

Figure 7-5: AutoCAD Soil Profile Depiction (Tryon, 2014) (with Divisions)

The "Liquefied Zone" is considered to be the section of the pier nearest to shore that experienced liquefaction. This zone is also known as the approach zone. This section was observed to have had pile deflections and damages caused by lateral spreading that occurred during the 2010 earthquake. The remaining section of the pier, known as the berthing zone, was observed to have very minimal or no damage or deflection and is considered the "Non-Liquefied Zone". Brunet et al. (2012) showed there were some damages observed in this zone, however, the locations and details of the different types of damages that occurred in this section were undocumented. However, later in the analysis, a way to account for the 46 damaged piles mentioned in the berthing zone will be explained.

The liquefied zone (approach zone) covers the first 8 rows of piles and also corresponds with the sea floor shelf slope nearest to the shore. The soil profile in this section of piles gradually sloped downward until reaching the non-liquefied zone which is relatively flat. The liquefied zone is where the lateral spreading was observed to have occurred during the earthquake. The non-liquefied zone reflects the remaining 47 rows of piles were lateral spreading was not observed.

It was observed that the non-liquefied zone had relatively the same soil profile throughout the entire section and therefore, the data collected on this section was used to create a

single soil profile that would represent the average of all the boring data in this section. Each individual pile that falls within this section will ultimately use the same modeled soil profile for analysis.

7.4 STEP 4 – Establish "Super Pile" Parameters

7.4.1 "Super Pile" Moduli

For this analysis, it was not practical to analyze all 308 piles along the pier. So instead, it was determined that each of the 47 rows of piles in the non-liquefied zone of the pier had a relatively similar and consistent soil profile and could be grouped together into a single "Super Pile". The only significant difference in each of the rows in the non-liquefied zone is the lengths of the piles; therefore, the average length was used. While the non-liquefied zone all had a consistent soil profile along each row, the liquefied zone did not. Instead, 8 separate "Super Piles" had to be developed to represent each individual row due to the variation in the soil profile.

The number of piles supporting the span of the pier deck was determined for each row to be used for developing the "Super Piles". For the single non-liquefied zone "Super Pile", the average number of piles within the 47 rows was used. The number of piles (or average) within the respective row is then multiplied by the elastic modulus of one single pile (200,000,000 kPa) to create a modified elastic modulus values used when evaluating and creating the respective "Super Piles" for the rows. Table 7-4 shows the number of rows each "Super Pile" represents, the number of piles within each row, and the subsequent "Super Pile" elastic modulus that was used for this study.

Table 7-4: Number of Piles and Respective Elastic Modulus for each "Super Pile"

"Super Pile" Row	Number of Rows Represented	Piles within Row	"Super Pile" Elastic Modulus [kPa]
1	1	3	600,000,000
2	1	2	400,000,000
3	1	2	400,000,000
4	1	3	600,000,000
5	1	4	800,000,000
6	1	2	400,000,000
7	1	3	600,000,000
8	1	4	800,000,000
Non-Liquefied Zone	47	6 (Average)	1,200,000,000

It was determined that the distance between each separate row was greater than 5.65 times the pile diameter, and therefore, shadowing effects from one row to the next was not taken into account for this study.

7.4.2 Other "Super Pile" Parameters

Most of the parameters of the piles were determined from the details that were collected during the reconnaissance efforts. The piles consisted of round, hollow, pipe piles with a diameter of approximately 500 mm (19.7 in.) and a wall thickness of 14 mm (0.6 in). Additionally, it was assumed that the piles used for the North Pier consisted of standard grade steel which has an elastic modulus of 200,000,000 kPa (29,000 ksi). The parameters used for the individual "Super Piles" are shown in Table 7-5.

Table 7-5: Pile Parameters used for the Respective "Super Piles"

"Super Pile" Row	Pile Diameter [mm]	Pile Wall Thickness [mm]	Length of Pile [m]
1	500	14	31.69
2	500	14	30.5
3	500	14	30.32
4	500	14	29.23
5	500	14	28.59
6	500	14	27.5
7	500	14	28.32
8	500	14	29.58
Non-Liquefied Zone	500	14	44.5

The most difficult parameter to establish is the rotational stiffness of the piles because it is not a standard industry parameter and instead must be calculated. These calculations were discussed in Section 5.4.4. For the North Pier, it was observed that the individual support beams experienced differential yielding across the whole span of the beam due to where the connection points to the supporting piles were located. Only the section that was directly connected to the piles was considered in the calculations due to this section experiencing the most observed yielding. It was also assumed that a portion of the support beam adjacent to the connection of the piles also yielded. To account for the adjacent section also yielding, a conservative length, equivalent to the depth of the beam, was used for the effective length (L') of each yielded section along the beam.

After applying all the parameters to the appropriate equations, the resulting rotational stiffness of the support beams was determined to be 45 kN*m/Rad. Such a low value is negligible. It was therefore assumed that the piles were not affected by rotational stiffness because the support beams yielded so easily during the lateral spreading.

7.5 STEP 5 – Generate "Super Pile" Model(s) in LPILE

7.5.1 Configure LPILE for the Model

7.5.1.1 Allow Soil Loads to be Applied

The option to use *loading by single soil movement* was toggled on in the program options dialog box so that the analysis can apply soil movement from lateral spreading.

7.5.1.2 Other Options and Settings

This study and analysis consisted of running a conventional analysis with static loading. The conventional analysis mode allows the program to utilize the additional options for distributed lateral loadings by soil movement, pile head stiffness, push-over analysis, and pile buckling. For this research, not all the additional options were required; however, several were used to complete the analysis. For example, the effect of lateral spreading can only be applied by selecting to use the option of *loading by a single soil movement profile.* Additionally, to simplify and accelerate the analysis, a *push-over analysis* was selected.

All other options were left as the default values.

7.5.1.3 Select Section Type

For this procedure, the Elastic Section (Non-Yielding) was selected to model the "Super Piles". The reason for this approach was to allow the selected piles to become non-yielding so as to allow unlimited deflections to be analyzed and used. This is important to be able to run the full Simplified Modeling Procedure. Although this might neglect important pile performance issues (i.e. yielding limit), LPILE will not complete the proper analysis and will result in an error if an

elastic section is not selected. With a larger span of possible deflections, it allows the user to run the needed analyses and eventually target the point of equilibrium, which is ultimately the focus of the procedure.

7.5.1.4 Input Model Parameters

7.5.1.4.1 Pile Parameters

The individual "Super Pile" parameters established in Step 4 are entered for the models in LPILE.

Table 7-6: Non-Liquefied Section Soil Layers

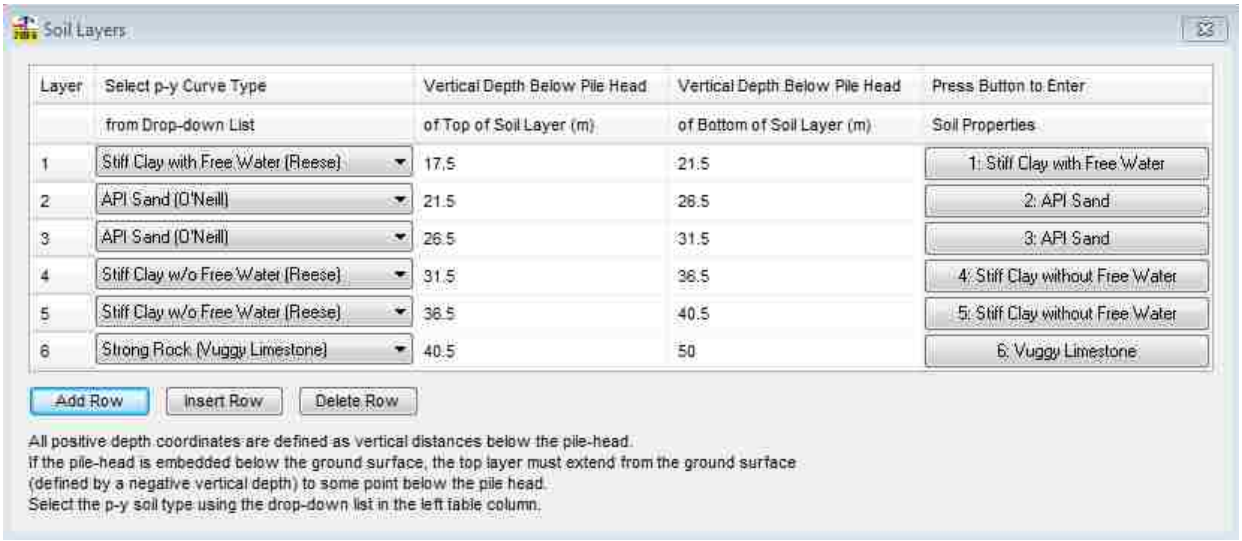

7.5.1.4.1 Soil Profiles

The respective soil layer parameters that were determined during Step 1 for each "Super Piles" soil profile were inputted into LPILE using the Soil Layers dialog box. Each separate "Super Pile" had to be individually created. Table 7-6 shows an example of the completed soil

layer dialog box within LPILE that was used for the "Super Pile" that represented the entire non-liquefied zone. Additionally, the soil parameter values used in the parameter dialog box for Layer 3 (API Sand) are shown in Table 7-7. Not all of the "Super Pile" soil profile sections that were used for this study will be shown in the body of this thesis, but instead can be viewed in Appendix B for reference.

Table 7-7: Non-Liquefied Section Layer 3 Parameters

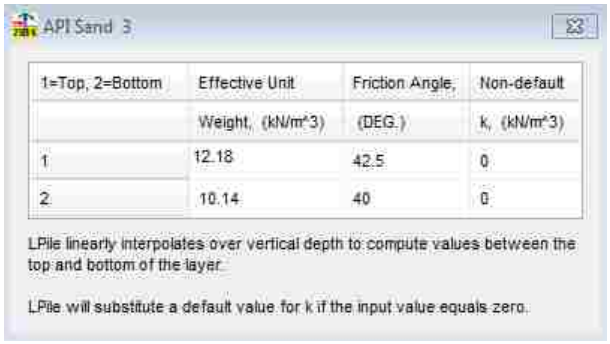

API Sand 3

1=Top, 2=Bottom	Effective Unit Weight, (kN/m^3)	Friction Angle, (DEG.)	Non-default k, (kN/m^3)
1	12.18	42.5	0
2	10.14	40	0

LPile linearly interpolates over vertical depth to compute values between the top and bottom of the layer.

LPile will substitute a default value for k if the input value equals zero.

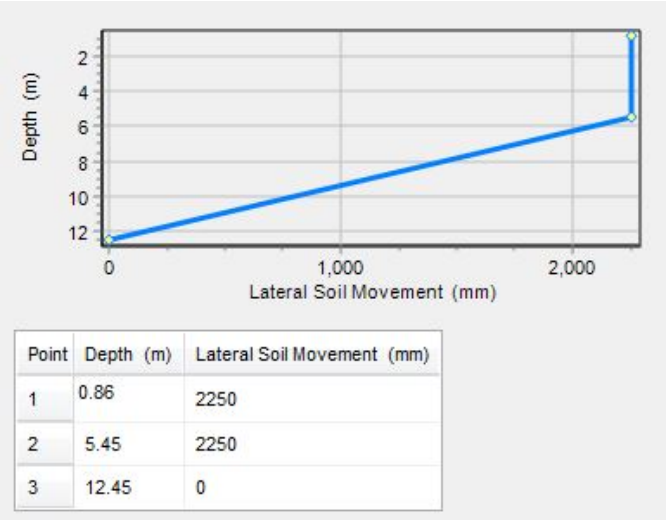

Point	Depth (m)	Lateral Soil Movement (mm)
1	0.86	2250
2	5.45	2250
3	12.45	0

Figure 7-6: Soil Movement Profile for Pile Row 1

7.5.1.5 Soil Movement (Lateral Spreading)

Using the determined lateral spreading magnitude of 2.25 meters in Step 2, the lateral spreading forces to act on the piles was created. It was assumed that the soil layer above the layer of liquefaction also experienced the same magnitude of movement, and that the magnitude of movement decreased linearly through the liquefiable layer until reaching zero at the bottom of the layer. The soil movement profile that was created for pile row 1 of this analysis is shown in Figure 7-6.

See Appendix B for the respective tables showing the soil movement profiles used for each of the other "Super Piles" in this study.

7.5.2 Resulting Model(s)

A total of nine "Super Piles" were created as part of this study to account for the 55 different rows in the system. Eight "Super Piles" were created to represent the 8 rows in the liquefied zone while a single "Super Pile" was used to represent the remaining 47 rows in the non-liquefied zone. Once all the "Super Piles" had been created using their respective parameters, the final profiles were compared side-by-side to confirm that the established models were consistent to the original AutoCAD model (Figure 7-1). The final side-by-side profile of all the "Super Piles" can be seen in Figure 7-7.

7.6 Part B - Run the Analysis

7.6.1 STEP 6 – Perform Push-Over Analysis on each "Super Pile"

For this analysis, a range of pile head deflections between 0 and 1.5 m (4.9 ft) was selected. It was assumed that 1.5 m (4.9 ft) was past the expected yield point of all the piles,

which is required for the analysis to work properly. Additionally, a relatively small interval of 0.05 m (0.2 ft) was used between each deflection tested. The interval could have been smaller, but for this procedure it was sufficient.

Table 7-8 shows an example of the results tab that resulted from the non-liquefied zone analysis. The results from the other rows can be found in Appendix C.

7.6.2 STEP 7 - Record the Individual Analysis Results

The push-over analysis results from each individual "Super Pile" were all recorded in a simple spreadsheet that listed the respective magnitudes of shear force that were required to deflect the various "Super Piles" to the specified deflections. For this study, it was assumed the entire pier deck and the piles performed as expected (i.e no failures). This means that the piles would still be free to rotate from lateral spreading effects but they would never completely yield or shear away from the pier deck.

To account for the other 46 rows in the non-liquefied zone, the push-over shear results were multiplied by the number of rows in the in that zone. This section was also considered to have had no failures and therefore all 47 rows in the non-liquefied zone were used. This analysis of assuming everything performed perfectly with no defects is considered to be the "No Failures" condition. Chapter 8 discusses how the analysis can be applied to the pier with considering failures.

Each "Super Pile" result was added to the spreadsheet until all "Super Piles" were recorded. After running the analyses and recording the results, it was easy to observe that each row performed differently. It was observed that several of the rows contributed to the movement of the pier deck while some of the rows contributed to the bracing of the pier. This is indicated

by the direction or sign convention (i.e. right/left or +/-) of the resulting shear forces. The spreadsheet used for this study is shown in Table 7-9.

Table 7-8: Push-Over Results for the Non-Liquefied Section (Red Box Shows Applicable Results)

Pushover Point Number	Pile-head Fixity Condition	Pile-head Deflection meters	Pile-head Shear kN	Max Moment in Pile kN-m (abs)	Max Shear in Pile kN (abs)	Depth to Max Moment meters	Depth to Max Shear meters
1	Free-head	0.00	0.00	0.00	0.00	0.00	0.00
2	Free-head	0.05000	12.7631	229.1679	65.6135	0.00	0.00
3	Free-head	0.10000	24.3712	439.4757	118.2260	0.00	0.00
4	Free-head	0.1500	35.3300	638.9530	165.5987	0.00	0.00
5	Free-head	0.2000	45.7448	832.4590	212.0461	0.00	0.00
6	Free-head	0.2500	55.6884	1019.	265.6570	0.00	0.00
7	Free-head	0.3000	65.2919	1200.	317.5911	0.00	0.00
8	Free-head	0.3500	74.5825	1375.	378.5046	0.00	0.00
9	Free-head	0.4000	83.5626	1550.	439.9142	0.00	0.00
10	Free-head	0.4500	92.2508	1720.	498.8431	0.00	0.00
11	Free-head	0.5000	100.6123	1885.	554.0119	0.00	0.00
12	Free-head	0.5500	108.6586	2046.	621.1860	0.00	0.00
13	Free-head	0.6000	116.4833	2208.	685.5460	0.00	0.00
14	Free-head	0.6500	124.0928	2365.	745.9357	0.00	0.00
15	Free-head	0.7000	131.4474	2520.	801.4177	0.00	0.00
16	Free-head	0.7500	138.5407	2677.	864.4748	0.00	0.00
17	Free-head	0.8000	145.4888	2830.	933.1514	0.00	0.00
18	Free-head	0.8500	152.4331	2988.	997.0637	0.00	0.00
19	Free-head	0.9000	159.1793	3144.	1057.	0.00	0.00
20	Free-head	0.9500	165.7864	3303.	1112.	0.00	0.00
21	Free-head	1.0000	172.5503	3462.	1166.	0.00	0.00
22	Free-head	1.0500	179.1794	3622.	1235.	0.00	0.00
23	Free-head	1.1000	185.8621	3785.	1300.	0.00	0.00
24	Free-head	1.1500	192.6295	3945.	1361.	0.00	0.00
25	Free-head	1.2000	199.2946	4110.	1419.	0.00	0.00
26	Free-head	1.2500	206.0714	4275.	1472.	0.00	0.00
27	Free-head	1.3000	212.8769	4436.	1522.	0.00	0.00
28	Free-head	1.3500	219.6156	4597.	1568.	0.00	0.00
29	Free-head	1.4000	226.3457	4756.	1622.	0.00	0.00
30	Free-head	1.4500	233.1903	4913.	1684.	0.00	0.00
31	Free-head	1.5000	239.9842	5068.	1744.	0.00	0.00

7.6.3 STEP 8 - Determine the Displacement where all Shear Forces Reach Equilibrium

The red line shown on Table 7-9 indicates approximately where the system is in equilibrium. This line was determined by summing the results of the shear forces. Where the forces cancel each other out and result in zero shear forces is where the pier reaches equilibrium. Because the intervals between each deflection were not smaller, a linear interpolation is made between the two rows that the line falls between to obtain the true point of equilibrium and the corresponding deflection. The deflections that have shear forces less than the equilibrium deflection (above the equilibrium deflection line) are perceived to be deflections that the pile undergoes before equilibrium is reached. The piles undergo these deflections fairly quickly during the earthquake and the resulting lateral spreading. The deflections greater than the equilibrium deflection (below the equilibrium deflection line) are deflections that are either briefly reached and then return back to the equilibrium or are never achieved due to the piles resisting further deflection. If the pier had failed and/or the piles had yielded, these higher deflections could have been achieved as the pier collapsed into the port.

The results of the analysis indicate that the pier in the "No Failures" condition would be expected to experience approximately 0.31 meters (1.01 feet) of deflection in the pier deck. Additionally, from the equilibrium spreadsheet created, it was also determined that between rows 5, 6, and 7 is where the shear forces approach zero at that deflection. This is understood to indicate that the majority of the deflections in the pier occurred in the first 5-6 rows and then reduced with each additional row. This would cause the pier deck within the first 6-7 rows to be in compression compared to the rest of the pier. These results help give reasoning to some of the cracks and buckling observed in the deck after the earthquake.

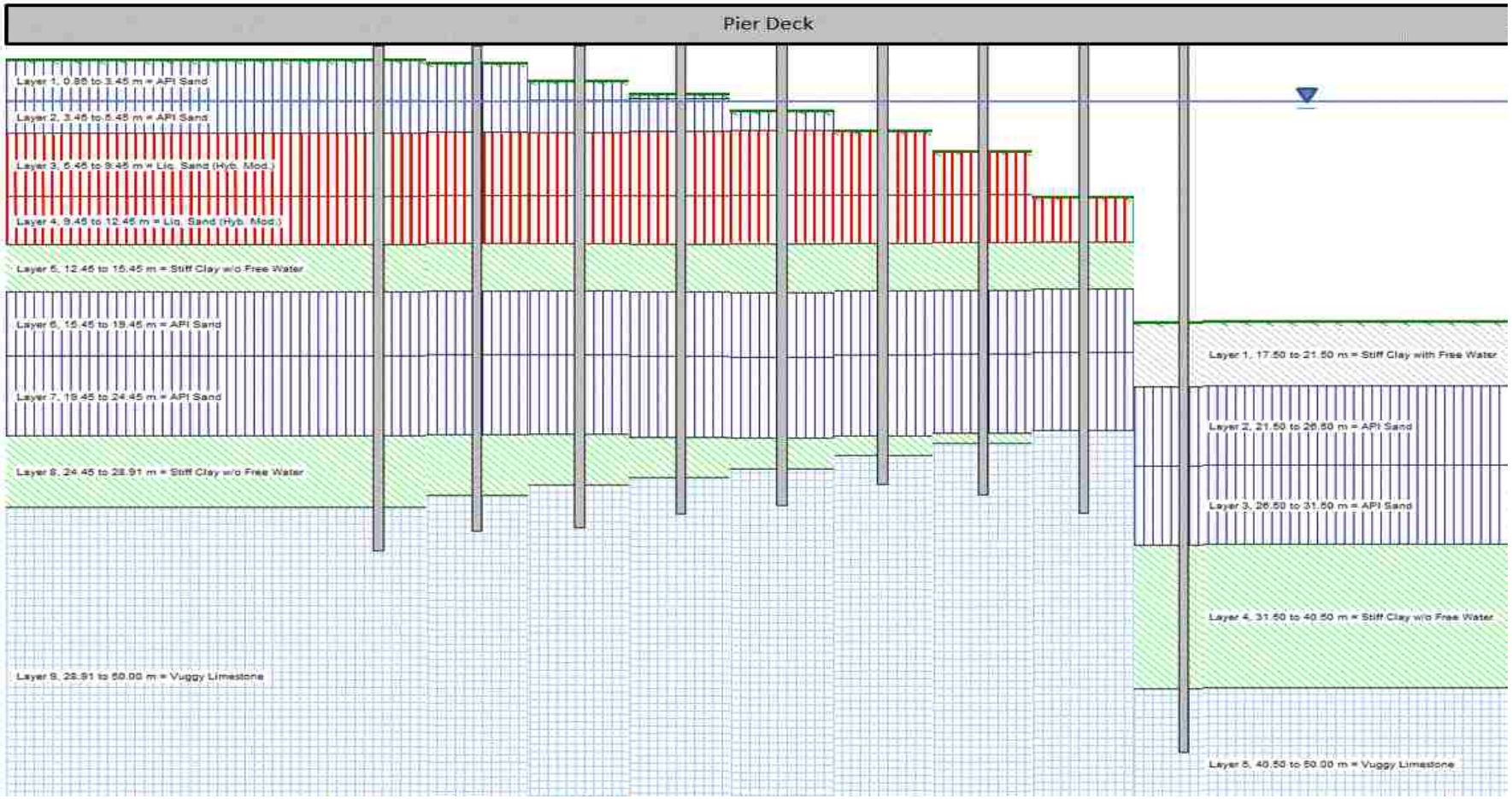

Figure 7-7: LPILE Combined Pile Profile

Table 7-9: Analysis Results – "No Failures" Condition

# Rows	1	1	1	1	1	1	1	1	47	
# Piles	3	2	2	3	4	2	3	4	6	
Deflection [m]	Row 1	Row 2	Row 3	Row 4	Row 5	Row 6	Row 7	Row 8	Non-Liquefied	Shear Total
0.00	-1561.00	-1278.00	-522.09	-211.06	-81.52	-53.36	-30.23	-8.36	0.00	-3745.63
0.05	-1550.00	-1270.00	-513.56	-197.57	-62.48	-43.26	-14.45	10.21	599.87	-3041.24
0.10	-1538.00	-1262.00	-505.07	-184.44	-44.62	-33.54	0.47	26.89	1145.45	-2394.86
0.15	-1527.00	-1254.00	-496.64	-171.56	-27.58	-24.04	14.76	42.61	1660.51	-1782.94
0.20	-1515.00	-1246.00	-488.25	-158.89	-11.09	-14.86	28.41	57.81	2150.01	-1197.85
0.25	-1504.00	-1238.00	-479.90	-146.37	5.03	-5.91	41.61	72.67	2617.35	-637.51
0.30	-1493.00	-1230.00	-471.60	-133.99	20.85	2.89	54.51	87.30	3068.72	-94.33
0.35	-1482.00	-1222.00	-463.33	-121.73	36.46	11.54	67.21	101.72	3505.38	433.24
0.40	-1470.00	-1214.00	-455.10	-109.56	51.87	20.07	79.71	115.98	3927.44	946.42
0.45	-1459.00	-1206.00	-446.90	-97.48	67.13	28.55	92.04	130.09	4335.79	1444.23
0.50	-1448.00	-1198.00	-438.74	-85.47	82.26	36.99	104.23	144.11	4728.78	1926.16
0.55	-1437.00	-1190.00	-430.60	-73.54	97.27	45.35	116.30	158.12	5106.95	2392.85
0.60	-1426.00	-1183.00	-422.50	-61.67	112.17	53.65	128.26	171.98	5474.72	2847.61
0.65	-1415.00	-1175.00	-414.42	-49.84	127.06	61.88	140.13	185.69	5832.36	3292.87
0.70	-1404.00	-1167.00	-406.37	-37.98	141.91	70.06	151.91	199.26	6178.03	3725.81
0.75	-1393.00	-1159.00	-398.23	-26.18	156.65	78.19	163.60	212.67	6511.41	4146.10
0.80	-1383.00	-1152.00	-390.11	-14.44	171.30	86.26	175.22	225.92	6837.97	4557.12
0.85	-1372.00	-1144.00	-382.02	-2.76	185.85	94.30	186.76	239.03	7164.36	4969.51
0.90	-1361.00	-1136.00	-373.96	-8.86	200.32	102.29	198.24	252.02	7481.43	5354.48
0.95	-1351.00	-1129.00	-365.94	20.41	214.70	110.25	209.70	265.01	7791.96	5766.09
1.00	-1340.00	-1121.00	-357.94	31.91	228.99	118.16	221.17	277.90	8109.86	6169.07
1.05	-1330.00	-1114.00	-349.97	43.36	243.19	126.06	232.57	290.58	8421.43	6563.22
1.10	-1319.00	-1106.00	-342.03	54.74	257.30	134.04	243.90	303.12	8735.52	6961.58
1.15	-1309.00	-1098.00	-334.12	66.07	271.38	141.97	255.15	315.52	9053.59	7362.56
1.20	-1298.00	-1091.00	-326.24	77.34	285.51	149.87	266.33	327.79	9366.85	7758.45
1.25	-1288.00	-1083.00	-318.38	88.72	299.54	157.73	277.45	339.88	9685.36	8159.29
1.30	-1278.00	-1076.00	-310.48	100.05	313.47	165.56	288.49	351.77	10005.21	8560.07
1.35	-1267.00	-1069.00	-302.67	111.30	327.29	173.35	299.46	363.81	10321.93	8958.47
1.40	-1257.00	-1061.00	-294.90	122.49	340.90	181.10	310.36	375.74	10638.25	9355.94
1.45	-1247.00	-1054.00	-287.16	133.51	354.42	188.83	321.27	387.58	10959.94	9757.39
1.50	-1237.00	-1046.00	-279.47	144.47	367.80	196.52	322.10	399.27	11279.26	10146.95

Another interesting observation in the LPILE results is that the first three rows of the Liquefied Zone experienced rotations of the piles where the determined pier deck equilibrium deflection was met. These rotations are a result of the lateral spreading, as well as, the restraint of the pier deck on the piles. These effects resulted in larger negative shear stresses acting on the piles. Rotation of the piles was something that was also observed during the post-earthquake observations and the results of this research indicate that several of the piles would have experienced rotations. Figure 7-8 shows the general shape that resulted in rows 1-3 as well as 4-8, respectively. Additionally, it was interesting that at row 5 and 6, the shear forces determined were very relatively small. Referring back to elevation view shown in Figure 6-8, it can be seen that Rows 5 and 6 didn't have any major observed damages and remained relatively the same pre and post-earthquake. The results of the Simplified Modeling Procedure are consistent to what was observed.

The general shape of rows 1-3 indicates that these rows would likely experience some rotation. The actual magnitudes of the rotations was not evaluated during this study, however, it is anticipated that the predicted results would be reduced and smaller than the physically measured results. The predicted values are affected from several assumptions and unknowns made throughout the analysis. Assumptions like lateral spread magnitudes, SPT to soil parameter correlations, and pile material properties are only a couple things that could have led to reduced rotational results.

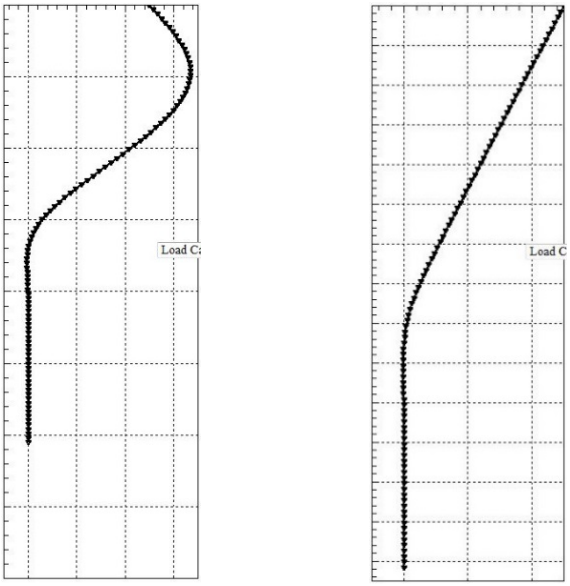

Figure 7-8: General Resulting Shape of Pile Rows 1-3 (Left) and Rows 4-8 (Right)

This concludes the steps of the procedure. The convenience of this procedure is that you can reevaluate the analysis as many times as needed and change different parameters to refine the results or evaluate different scenarios. The next chapter explains one of the directions that the analysis was taken to evaluate the situation differently and how it expanded the understanding of the North Pier.

8 ADDITIONAL EVALUATIONS AND APPLICATIONS

8.1 "With Failures" Condition

The previous condition ("No Failures") was analyzed to determine how much movement would be anticipated if the entire pier performed as expected and had no pile failures during the earthquake. The "with failures" condition represents what was observed after the earthquake and considers all the piles that failed. Analyzing both conditions allows for a comparison of the two different conditions to be made and the effects of the failures to be evaluated. Both conditions are important for analysis in order to see the difference in the pier performance. See Table 8-1 for the number of piles that were considered for each analysis condition.

Table 8-1: Number of Piles Considered for Analysis for Both Failure Conditions

Row	# of piles (No Failures)	# of piles (with Failures)
1	3	3
2	2	2
3	2	1
4	3	1
5	4	0
6	2	2
7	3	2
8	4	4
Non-Liquefied Zone	6	6

This condition ("with Failures") takes into effect all the shearing and yielding damages that were identified in both the liquefied zone and the non-liquefied zone. Brunet, et al. (2012) identified that in addition to the damaged piles identified in the liquefied zone, that a total of 46 piles were damaged in the non-liquefied zone. The locations and the extent of the damages were not specifically identified. Therefore, to conservatively account for the 46 damaged piles, it was simply assumed that the damaged piles would not contribute at all to the overall strength of the pier (i.e. the piles sheared off from the pier deck similar to what was observed in the liquefied zone). The damaged piles were treated as if they were in consecutive rows along this section. The number of rows that the damaged piles would represent was equivalent to 7.7 rows (46 damaged piles/6 piles per row = 7.7 equivalent rows). The 7.7 rows that account for the damaged piles were taken out of the 47 total rows of the non-liquefied zone of the pier to give a reduced contributing number of rows to the system. Instead of 47 rows contributing, only 39.3 were considered contributing. Table 8-3 shows the spreadsheet of this analysis.

The point of equilibrium for the "no failures" and "with failures" conditions resulted in values of 0.31 meters (1.01 ft) and 0.38 meters (1.26 ft), respectively. This is a difference of approximately 0.07 meters (0.23 ft) between the two conditions evaluated. Sensitivity analyses also indicate that the predicted pier deflection was not significantly affected by variations of plus or minus 50% in the ground displacement (lateral spreading) for this case. As anticipated, these two analyses show that the more failed piles in the system, the more deflection is expected in the pier deck. This also correlates to more anticipated damages. The more the pier deck deflects the more stress each pile will experience and increased damages, such as stiffener buckling, sheet pile welding ruptures, and natural torsion (horizontal rotation) will be expected to occur. The whole pier system performs in a snowball effect as more piles fail. If desired, the user could

continue running additional analysis to determine how many piles could fail in the system and at which locations before the pier would be deemed failed/collapsed.

8.2 Predicted vs. Measured Evaluation

Since actual measured values were collected during the reconnaissance efforts, the relative accuracy of the Simplified Modeling Procedure in predicting the values for displacements and pile rotations on the North Pier could be determined. The presented accuracy results in Table 8-2 and Table 8-4 are only based on this one case history alone.

Table 8-2: Simplified Modeling Procedure Predicted vs. Measured Values of Displacement

	Displacements			
	Predicted [m]	Measured [m]	Predicted/Measured	Over/Under
Pile Row 1	0.41	0.27	151.9%	51.9%
Pile Row 2	0.43	0.30	142.3%	42.3%
Pile Row 3	0.44	0.48	91.3%	-8.7%
Average	0.38	0.35	109.5%	9.5%

Table 8-2 shows the pile displacements (predicted and measured) measured at the ground level. To obtain the predicted measurements at the ground level, the Simplified Modeling Procedure is first performed to determine the magnitude of pier deck deflection. Once the pier deck deflection and respective shear forces are determined, the shear forces required to achieve equilibrium in the procedure are then used to perform a conventional analysis on each row. Running a conventional analysis allows for the displacements along the entire length of the pile

(i.e. at the ground surface) to be determined. Figure 8-1 shows the shape and the displacement results of the conventional analysis for row 2.

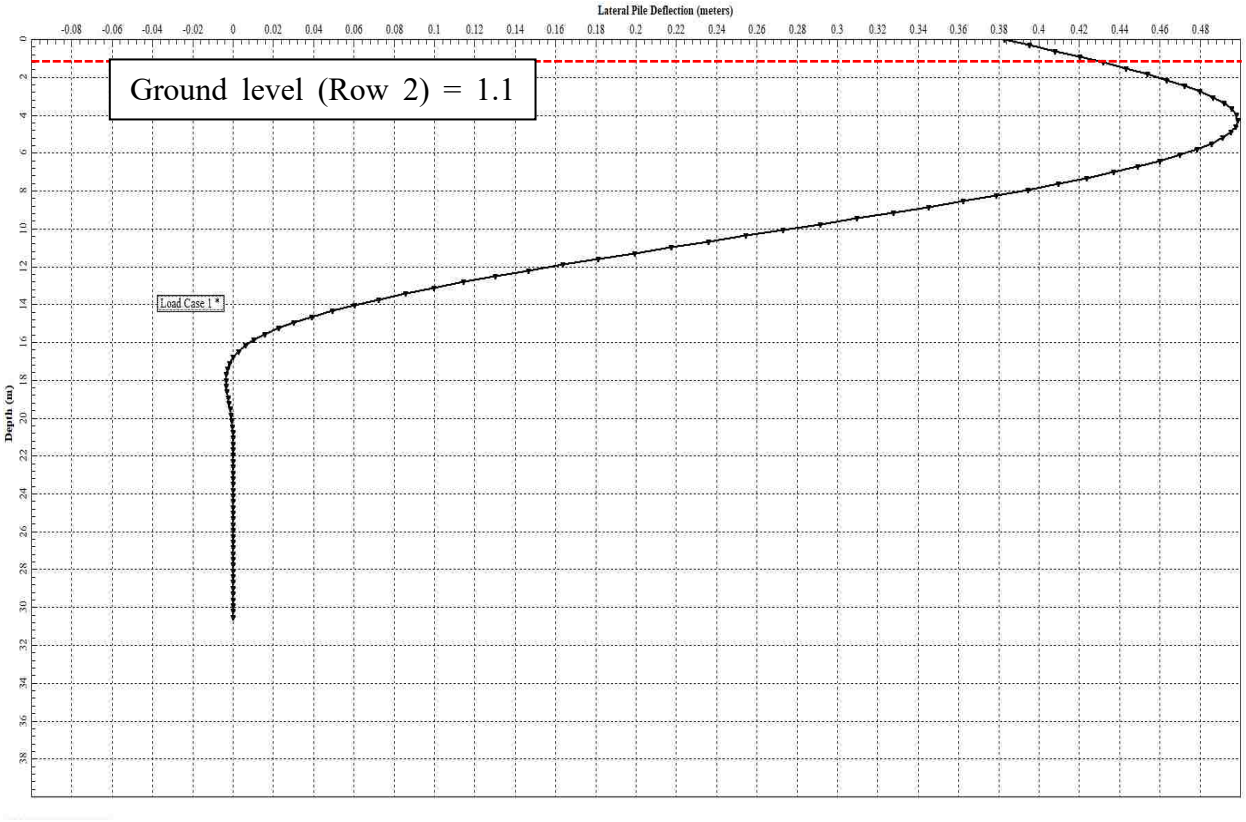

Figure 8-1: Row 2 Shape and Deflection Results from Conventional Analysis

It can be seen in Figure 8-1 that the top of the pile matches the predicted pier deck displacement of approximately 0.38 m, but because of the shape of the pile, the displacement at the ground level is slightly larger (approximately 0.43 m). This approach and analysis was performed for rows 1 to 3 since only measured displacement values were collected for these rows.

Table 8-3: Analysis Results - "With Failures" Condition

# Rows	1	1	1	1	1	1	1	1	39.3	
# Piles	3	2	1	1	0	2	2	4	6	
Deflection [m]	Row 1	Row 2	Row 3	Row 4	Row 5	Row 6	Row 7	Row 8	Non-Liquefied	Shear Total
0.00	-1561.00	-1278.00	-515.70	-205.91	0.00	-53.36	-29.55	-8.36	0.00	-3651.88
0.05	-1550.00	-1270.00	-511.22	-200.97	0.00	-43.26	-18.58	10.21	501.59	-3082.23
0.10	-1538.00	-1262.00	-506.75	-196.10	0.00	-33.54	-8.13	26.89	957.79	-2559.85
0.15	-1527.00	-1254.00	-502.31	-191.27	0.00	-24.04	2.05	42.61	1388.47	-2065.49
0.20	-1515.00	-1246.00	-497.88	-186.49	0.00	-14.86	11.82	57.81	1797.77	-1592.83
0.25	-1504.00	-1238.00	-493.46	-181.75	0.00	-5.91	21.46	72.67	2188.55	-1140.42
0.30	-1493.00	-1230.00	-489.06	-177.05	0.00	2.89	30.78	87.30	2565.97	-702.17
0.35	-1482.00	-1222.00	-484.67	-172.39	0.00	11.54	39.95	101.72	2931.09	-276.75
0.40	-1470.00	-1214.00	-480.29	-167.75	0.00	20.07	48.96	115.98	3284.01	136.98
0.45	-1459.00	-1206.00	-475.83	-163.15	0.00	28.55	57.82	130.09	3625.46	537.95
0.50	-1448.00	-1198.00	-471.37	-158.57	0.00	36.99	66.57	144.11	3954.06	925.79
0.55	-1437.00	-1190.00	-466.94	-154.02	0.00	45.35	75.22	158.12	4270.28	1301.01
0.60	-1426.00	-1183.00	-462.51	-149.45	0.00	53.65	83.78	171.98	4577.79	1666.24
0.65	-1415.00	-1175.00	-458.11	-144.86	0.00	61.88	92.25	185.69	4876.85	2023.71
0.70	-1404.00	-1167.00	-453.72	-140.30	0.00	70.06	100.67	199.26	5165.88	2370.85
0.75	-1393.00	-1159.00	-449.34	-135.76	0.00	78.19	109.01	212.67	5444.65	2707.42
0.80	-1383.00	-1152.00	-444.97	-131.24	0.00	86.26	117.30	225.92	5717.71	3035.98
0.85	-1372.00	-1144.00	-440.62	-126.74	0.00	94.30	125.53	239.03	5990.62	3366.12
0.90	-1361.00	-1136.00	-436.27	-122.26	0.00	102.29	133.72	252.02	6255.75	3688.24
0.95	-1351.00	-1129.00	-431.94	-117.80	0.00	110.25	141.86	265.01	6515.41	4002.78
1.00	-1340.00	-1121.00	-427.61	-113.36	0.00	118.16	149.95	277.90	6781.23	4325.28
1.05	-1330.00	-1114.00	-423.17	-108.93	0.00	126.06	158.11	290.58	7041.75	4640.41
1.10	-1319.00	-1106.00	-418.78	-104.52	0.00	134.04	166.24	303.12	7304.38	4959.48
1.15	-1309.00	-1098.00	-414.43	-100.12	0.00	141.97	175.32	315.52	7570.34	5281.60
1.20	-1298.00	-1091.00	-410.15	-95.74	0.00	149.87	182.36	327.79	7832.28	5597.41
1.25	-1288.00	-1083.00	-405.88	-91.34	0.00	157.73	190.35	339.88	8098.61	5918.35
1.30	-1278.00	-1076.00	-401.63	-86.88	0.00	165.56	198.31	351.77	8366.06	6239.19
1.35	-1267.00	-1069.00	-397.39	-82.43	0.00	173.35	206.22	363.81	8630.89	6558.45
1.40	-1257.00	-1061.00	-393.17	-78.00	0.00	181.10	214.10	375.74	8895.39	6877.16
1.45	-1247.00	-1054.00	-388.96	-73.59	0.00	188.83	221.94	387.58	9164.38	7199.17
1.50	-1237.00	-1046.00	-384.69	-69.19	0.00	196.52	229.74	399.27	9431.38	7520.03

The results indicate the Simplified Modeling Procedure over-predicts the deflection for Rows 1 and 2 by 42.3 and 51.9%, respectively. The procedure, however, under-predicts the deflection of Row 3 by 8.7%. It is believed that the assumptions made in regards to lateral spreading, soil profiles, soil parameters, pile parameters, etc. affect the overall predicted values for the deflections of the rows. Several of the assumptions used average values for the analysis, therefore, the averages of both the measured values as well as the predicted values were compared with that in mind. The resulting values of the averages are much closer to one another and indicate only approximately 9.5% over prediction.

Table 8-4: Simplified Modeling Procedure Predicted vs. Measured Values of Pile Rotation

	Pile Rotation			
	Predicted [°]	Measured [°]	Predicted/Measured	Over/Under
Pile Row 1	16.43	11.7	140.4%	40.4%
Pile Row 2	19.2	15.3	125.5%	25.5%
Pile Row 3	9.9	12.3	80.5%	-19.5%
Average	15.2	13.1	115.9%	15.9%

Table 8-4 shows the predicted pile rotations using the determined pile deflections of the Simplified Modeling Procedure. Once again, a comparison of predicted verses measured values indicate that the Simplified Modeling Procedure over-predicts the pile rotations by 25.5 to 40.4% for Rows 1 and 2 while it under-predicts rotation by 19.5% on Row 3. A comparison of the averages indicates over-prediction by 15.9%. The resulting predictions are once again believed to have been affected by some of the assumptions that were made and used in the procedure.

8.3 Bending Moment Evaluation

Another evaluation that can be performed to determine the performance of the individual piles is to evaluate the bending moments along the entire length of the pile. The Simplified Modeling Procedure utilizes a non-yielding pile approach to perform the necessary push-over analysis. When evaluating the developed bending moments in the "Super Piles", the pile needs to be allowed to yield to identify the allowable bending moment. To determine the allowable bending moment, an individual pile within the respective "Super Pile" can be analyzed using a conventional analysis that uses a pile type allowed to yield. Figure 8-2 show the lateral pile deflection, bending moment, and shear forces vs. depth for an individual pile found in the "Super Pile" representing row 3.

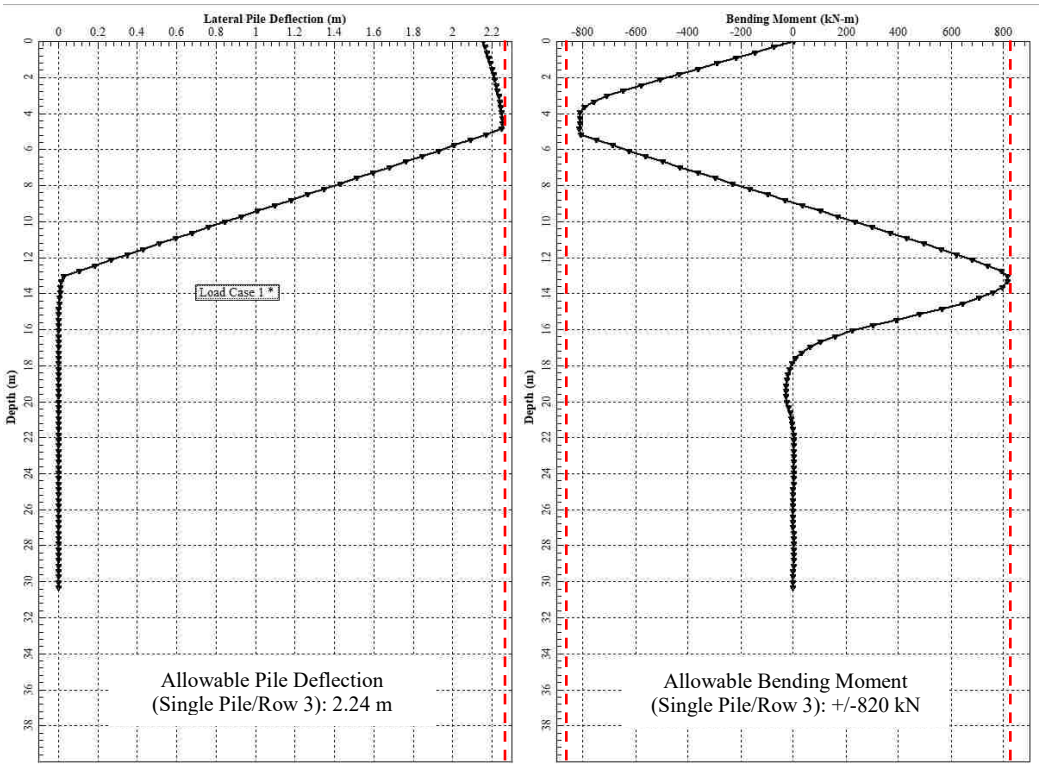

Figure 8-2: Pile Deflection, and Bending Moment vs. Depth (Single Pile/Row 3)

To obtain the charts above, the shear force required to reach the point of yielding was manually increased until the results indicated that the pile had yielded. The direction (i.e. sign) of the applied shear force at the head of the pile is the same as the direction that was determined during the Simplified Modeling Procedure. It was determined that the single pile would yield once a shear force greater than -238 kN was applied at the head of the pile. The results indicate that a pile in row 3 will likely yield once a deflection of approximately 2.24 meters or a bending moment of +/- 820 kN is exceeded.

After the allowable deflection and bending moments of a single pile is determined, the same charts can be produced for the "Super Pile". The "Super Pile" results can be determined using a conventional analysis and applying the shear force that was determined during Step 8 of the procedure to the pile head. For this analysis, the "Super Pile" representing the "no failures" condition was evaluated. This condition was evaluated to determine if the specific row would actually be expected to experience some type of failure as was observed. The shear force that was used for the conventional analysis of the "Super Pile" was determined from step 8 of the analysis to be approximately -471 kN. This value of shear force is the value that was predicted to be needed at Row 3 in order for the pier to be in equilibrium and deflect to the resulting deflection of 0.31 m. The results of running a conventional analysis on the "Super Pile" (Row 3) are presented in Figure 8-3 with the allowable values from the single pile evaluation overlaying the charts.

The evaluation of both the deflection vs. depth and bending moment vs. depth is a way to identify possible yielding within individual piles as well as the probable depth of possible yielding. As can be seen, the resulting deflection of the "Super Pile" representing Row 3 never reaches the allowable threshold (2.24 m) determined for a single pile and, therefore, would not

be expected to yield if looking at deflection alone. The pile only deflects 0.31 m. However, the resulting bending moments along the length of the "Super Pile" does exceed the allowable bending moment at certain locations along the depth of the pile. This indicates that there would be some form of yielding anticipated to happen along Row 3 due to the exceedance of bending of the pile due to shear forces at certain depths. The yielding would most likely be observed to happen at approximately 12 to 17 feet down from the top of the pile. If the "Super Pile" bending moments did not exceed the allowable bending moment, than yielding would not be anticipated to be observed.

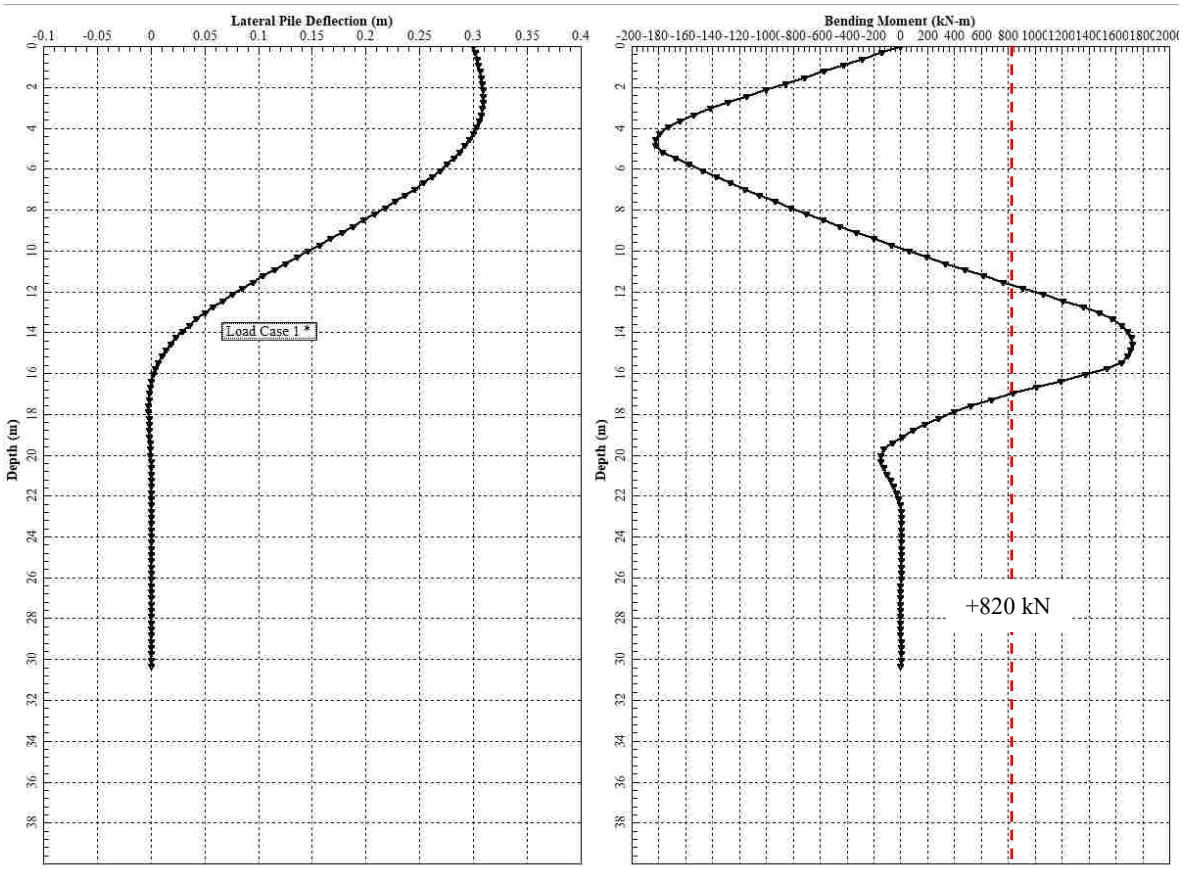

Figure 8-3: Pile Deflection and Bending Moment vs. Depth ("Super Pile"/Row 3)

As mentioned, this evaluation indicated that there could be piles in this row that could experience yielding if the allowable bending moment of a single pile is exceeded. However, because the "Super pile" is representing the entire row as one pile, it is unknown exactly what deflections, shear forces, and bending moments are specifically applied to each individual pile in that row. Therefore, it is important to understand that the results do not guarantee yielding or failures but simply give an indication of the possibility.

This evaluation is not necessary to complete the Simplified Modeling Procedure but is an additional evaluation that can be performed. Therefore, not every "Super Pile" row was evaluated or presented as part of this research.

8.4 Forward Design Application

This procedure is unique and powerful because it not only can be used to evaluate the performance of a pier after an earthquake but can also be used during forward design to mitigate damages before an earthquake. By utilizing site specific anticipated parameters and having a known tolerance in parameters, such as the pier deck deflection, a pier design could be performed by utilizing this procedure in an iterative process. This procedure can help a designer determine pile parameters that would support the pier in certain earthquake conditions. This procedure allows for a variety of parameters to be evaluated and altered during the design process. For example, different magnitudes of lateral spreading could be evaluated to determine the extent of the rows of piles in resisting deflections along the pier. This would help the in the design to determine if additional piles, stiffer pile material, different pile types, etc., would be required. Although many iterations of the procedure would be required, these varieties in the parameters can be easily utilized in the design process.

9 CONCLUSIONS

A case study of the North Pier, located in the Port of Coronel (Maule, Chile), was used to show how the Simplified Modeling Procedure is performed. The Simplified Modeling Procedure was able to evaluate the approximate amount of pier deck displacement that resulted from the M_w 8.8 earthquake in 2010. The North Pier was observed and evaluated after the earthquake by different research teams. The data from the reconnaissance efforts was later published and used as the foundation to create a representative model of the pier. The Simplified Model Procedure can be performed by following these steps:

STEP 1: Characterize the soils at the site;

Using a variety of in-situ field tests (e.g. SPT, CPT, vane shear, etc.) and the corresponding laboratory testing results from reconnaissance efforts, the soil parameters for the soil stratum can be identified. The respective parameters (i.e. cohesion, friction angle, liquefaction potential, etc.) for each respective layer should be identified and recorded.

STEP 2: Predict the amount of lateral spreading;

If liquefiable layers are identified in the soil profile, then the "anticipated" or "measured" values of lateral spread should be determined. Anticipated values can be predicted using attenuation relationship methods. Ideally, measured values are to be gathered during the reconnaissance efforts.

STEP 3: Create a two-dimensional geotechnical base model;

By combining the geometric design of the pier, the site topography, and the two-dimensional representative soil profile along with the corresponding geotechnical properties, a geotechnical base model can be developed. The user should identify areas in the soil profile that are uniform from one pile location to the next. If there are variations in soil profiles between separate pile rows, determine if an average soil profile could still be made that would still result in a representative profile of the area.

STEP 4: Determine "Super Pile" Parameters;

Analyzing a large number of piles along a pier is a challenging task. To simplify the process, individual rows of piles can be grouped together into "Super Piles" for analysis. To simplify the process, identify what the required "Super Pile" modulus will be. In addition, determine as many pile parameters as possible that will be associated with each "Super Pile". Some of these parameters include: pile material, thickness, length, diameter, stiffness, shadowing effects, etc.

STEP 5: Generate "Super Pile" models in LPILE;

Within LPILE, input as much of the gathered info of the pile and pier as possible. Each determined "Super Pile" used in the analysis needs a separate model. Make sure each model uses the correct parameters.

STEP 6: Perform push-over analysis on each "Super Pile";

Set up LPILE to perform a push-over analysis using a non-yielding approach. Perform the analysis over a range of deflections that evaluates the pile past the anticipated possible deflection. This will allow for a complete comparison of the results.

STEP 7: Record the individual push-over analysis results;

Use a spreadsheet to compare the individual analysis results side-by-side. Make sure each analysis is accounted for on the spreadsheet.

STEP 8: Determine the displacements where all shear forces reach equilibrium.

Summate the shear forces of each respective deflection evaluated for the push-over analyses. Where the sum is equal to zero is where the shear forces are in equilibrium. Where equilibrium is achieved is also considered the resulting deflection magnitude of the pier as a result of the induced lateral spreading.

It was determined that the Simplified Modeling Procedure predicted that the pier deck would experience a deflection of approximately 0.31 meters (1.01 feet) if the pier would have had no failures while it predicated the pier to experience 0.38 meters (1.26 feet) of deflection if failures along the pier were accounted for. This is a difference of 0.07 meters (0.23 feet). This is evidence that the procedure is properly accounting for piles that fail. The more the piles fail, the more deflection is anticipated. This procedure relatively shows how each row along the length of the pier is generally performing. Some rows will be adding stress to the pier while others are resisting the stresses. Additionally, evaluating the probability of an individual pile experiencing yielding within the rows using deflection vs. depth and bending moment vs. depth charts from a conventional analysis was also presented.

The Simplified Modeling Procedure is unique and powerful because it utilizes a commonly used and well-known software package (LPILE) to predict pier deck deflections when a pier has been impacted from lateral spreading. The predicted values of pile deflections and rotations of the procedure in comparison to the measured values determined during

reconnaissance efforts of the North Pier indicate that the procedure over-predicts the measured respective average values by approximately 9.5 – 15.9%. These values indicate that the predicted values produced from the procedure are relatively accurate especially taking into account all the assumptions that are used for the creation of the models and the analysis. The accuracy values are based on the North Pier case history only.

The procedure is not only useful for predictions after a seismic event, but also useful and powerful if used in a forward design approach to determine the necessary parameters to mitigate damages if a pier were to be affected by lateral spread during an earthquake. It can help identify problem locations along the pier so that mitigation can be performed to prevent failures. The procedure can easily be duplicated on other similar events and structures by following the steps provided throughout this thesis.

REFERENCES

Andrus, R.D., Piratheepan, P., Ellis, B.S., Zhang, J., Hsein Juang, C. (2004). Comparison of liquefaction evaluation methods using penetration-VS relationships. *Soil Dynamics and Earthquake Engineering*, 24(9-10), 713-721.

Arduino, S.A., Ilankatharan, M., Kramer, S.L., Kutter, B.L., Shin, H.S. (2006), Experimental and numerical analysis of seismic soil-pile-structure interaction of a two-span bridge. *Proceedings, 8th U.S. National Conference on Earthquake Engineering, Paper No. 504.* San Francisco, CA. 126.

Ashford, S. A., & Rollins, K. M. (2002). TILT: Treasure Island liquefaction test final report. Report No. SSRP-2001/17. Department of Structural Engineering, University of California, San Diego.

Astroza, M, Ruiz, S., Astroza, R. (2012). Damage Assessment and Seismic Intensity Analysis of the 2010 (Mw 8.8) Maule Earthquake. *Earthquake Spectra,* Vol. 28, No. S1, S145-S164.

Bardet, J.P., Tobita, T., Mace, N., Hu, J. (2002). Regional modeling of liquefaction-induced ground deformation. *Earthquake Spectra*, 18(1), 19-46.

Bartlett, S.F., and Youd, T.L. (1992). Empirical analysis of horizontal ground displacement generated by liquefaction-induced lateral spread. *Report No. NCEER-92-0021*, NCEER, State University of New York, Buffalo, 114 pp.

Bartlett, S.F., and Youd, T.L. (1995). Empirical prediction of liquefaction-induced lateral spread. *Journal of Geotechnial Engineering,* 121(4), 316-329.

Baska, D. (2002). An analytical model for prediction of lateral spread displacement. *Ph.D. Dissertation,* Univ. of Washington, Seattle, WA.

Boulanger, R. W., Mejia, L. H., & Idriss, I. M. (1997). Liquefaction at Moss Landing during Loma Prieta earthquake. *Journal of Geotechnical and Geoenvironmental Engineering, 123*(5), 453-467.

Boulanger, R. W., Kutter, B. L., Brandenberg, S. J., Singh, P., & Chang, D. (2003). Pile foundations in liquefied and laterally spreading ground during earthquakes: centrifuge experiments and analysis. Report No. UCD/CGM-03/01. University of California at Davis.

Boulanger, R.W., and Idriss, I.M. (2014). CPT and SPT Based Liquefaction Triggering Procedures. Report No. UCD/CGM-14/01, Davis, CA.

Bowles, J. E., 1977, Foundation Analysis and Design, McGraw-Hill, Inc., New York

Bowles, S. I. (2005). Statnamic load testing and analysis of a drilled shaft in liquefied sand. MS Thesis. Provo, Utah: Department of Civil and Environmental Engineering, Brigham Young University.

Brandenberg, S. J. (2005). Behavior of pile foundations in liquefied and laterally spreading ground. PhD Dissertation. Davis, California: University of California, Davis.

Brandenberg, S. J., Boulanger, R. W., Kutter, B. L., & Chang, D. (2007). Static pushover analyses of pile groups in liquefied and laterally spreading ground in centrifuge tests. Journal of Geotechnical and Geoenvironmental Engineering, 133, 9, 1055-1066. ASCE.

Bray, J.D. and Travasarou, T. (2007). Simplified procedure for estimating earthquake-induced deviatoric slope displacements. *Journal of Geotechnical and Geoenvironmental Engineering,* 133(4), 381-392.

Bray, J.., and Frost, D. (2010). Geo-Engineering Reconnaissance of the 2010 Maule, Chile Earthquake. *Geotechnical Extreme Events Reconnaissance (GEER) Association,* http://www.geerassociation.org/GEER_Post%20EQ%20Reports/Maule_Chile_2010/Maule_Chile_2010index.html.

Bray, J., et al. (2012). Effects of Ground Failure on Buildings, Ports, and Industrial Facilities. *Earthquake Spectra*, Vol. 28, No. S1, S97-S118.

Brunet, S., De la Llera, J.C., Jacobsen, A., Miranda, E., Meza, C. (2012). Performance of Port Facilities in Southern Chile during the 27 February 2010 Maule Earthquake. *Earthquake Spectra,* Vol. 28, No. S1, S553-S579.

Bryne, P.M. (1991). A model for predicting liquefaction-induced displacements. *Proceedings, 2nd International Conference on recent Advances in Geotechnical Earthquake and Engineering and Soil Dynamics*, 2, 1027-1035. St. Louis, Missouri.

Bryne, P.M., Jitno, H., Salgado, R. (1992). Earthquake-induced displacements of soil-structure systems. *Proceedings, 10th World Conference on Earthquake Engineering*, 3, 1407-1412. Madrid, Spain.

California Department of Transportation. (2011, February). Guidelines on foundation loading and deformation due to liquefaction induced lateral spreading. Retrieved from http://dap3.dot.ca.gov/shake_stable/references/Guidelines%20on%20Foundation%20Loading-Feb%202011.pdf

Carraro, J.A., Bandini, P., Salgado, R. (2003). Liquefaction resistance of clean and non-plastic silty sand based on cone penetrometer resistance. *Journal of Geotechnical and Geoenvironmental Engineering*, 129(11), 965-976.

Casagrande, A. (1936). Characteristics of cohesionless soil affecting the stability of slopes and earth fills. *Journal of the Boston Society of Civil Engineers*, 257-276.

Castro, G. (1969). Liquefaction of sands. *PhD Dissertation*, Cambridge, Massachusetts: Harvard University.

Castro, G., Poulos, S.J. (1977). Factors affecting liquefaction and cyclic mobility. *Journal of the Geotechnical Engineering Division*, 106(GT6), 501-506.

Cetin, K.O., Seed, R.B., Der Kiureghian, A., Tokimatsu, K., Harder Jr., L.F., Kayen, R.E. (2004). Standard penetration-based probabilistic and deterministic assessment of seismic soil liquefaction potential. *Journal of Geotechnical and Geoenvironmental Engineering.*

Chen, L., Yuan, X., Zhenzhong, C., Sun, R., Dong,L. (2009). Liquefaction macrophenomena in the great Wenchauan earthquake. *Earthquake Engineering and Engineering Vibration*, 8(2), 219-229.

Cheng, Z., & Jeremic, B. (2009, March 15-19). Numerical modeling and simulation of soil lateral spreading against piles. Proceedings, International Foundation Congress and Equipment Expo, 1, 183-189. Orlando, FL.

Coulter, M., & Migliaccio, L. (1966). Effects of the earthquake of March 27, 1964 at Valdez, Alaska. *Professional Paper 542-C*, Washington, D.C.:U.S. Geological Survey, U.S. Department of the Interior.

Dobry, R., Ladd, R.S. (1980). Discussion to "Soil liquefaction and cyclic mobility evaluation for level ground during earthquakes," by H.B. Seed and "Liquefaction potential: science versus practice," by R.B. Peck. *Journal of Geotechnical Engineering*, 106 (GT6), 720-724.

Dobry, R., Ladd, R.S., Yokel, F.Y., Chang, R.M., Powell, D. (1982). Predictions of pore water pressure buildup and liquefaction of sands during earthquake by the cyclic strain method. *NBS Building Science Series 138,* Gaithersburg, Maryland, National Bureau of Standards, 150 pp., 129

Dobry, R., Mohamad, R., Dakoulas, P., Gazetas, G. (1984). Liquefaction evaluation of earth dams – a new approach. *Proceedings, 8th World Conference on Earthquake Engineering*, 3, 333-340.

Dobry, R., Baziar, M.H. (1991) Evaluation of ground deformation caused by lateral spreading. *Proceedings, 3rd- Japan-U.S. Workshop on Earthquake Resistant Design of Lifeline Facilities and Countermeasures for Soil Liquefaction, Technical Report NCEER-91-0001*, 209-223.

Douglas, B.J., Olsen, R.S., Martin, G.R. (1981). Evaluation of the cone penetrometer test for SPT liquefaction assessment. *Proceedings, In Situ Testing to Evaluate Liquefaction Susceptibility*, New York, New York: ASCE.

ENSOFT, LPILE (Version 2016) [Computer software]. Authored by Isenhower, W. M., Ph.D., P.E., Wang, S., Ph.D., P.E., & Vasquez, L. G., Ph.D., P.E. (n.d.).

Esrig, M. E., & Kirby, R. C. (1979). Advances in general effective stress method for the prediction of axial capacity for driven piles in clay. Proceedings, 11th Annual Offshore Technology Conference, 437-449. Houston, Texas.

Faris, A. T., Seed, R. B., Kayen, R. E., & Wu, J. (2006). A semi-empirical model for the estimation of maximum horizontal displacement due to liquefaction-induced lateral spreading. Proceedings, 8th U.S. National Conference on Earthquake Engineering, Paper No. 1323, 10 pp. San Francisco, California.

Finn, W.D., Yogendrakumar, M., Yoshida, M., Yoshida, N. (1986). TARA-3: A program to compute the response of 2-D embankments and soil-structure interaction systems to seismic loadings. Vancouver, British Columbia: Department of Civil Engineering, University of British Columbia.

Finn, W.D., Ledbetter, R.H., Fleming, R.L., Jr., Templeton, A.E., Forrest, T.W., and Stacy, S.T. (1991). Dam on liquefiable foundation: Safety assessment and remediation. *Proceedings, 17th International conference on Large Dams,* 531-553. Vienna.

Franke, Kevin W. (2011). "A Performance-Based Model for the Computation of Kinematic Pile Response Due to Lateral Spreading and Its Application on Select Bridges Damaged During the M7.6 Earthquake in the Limon Province, Costa Rica" (2011). All Theses and Dissertations. 2748.

Franke, Kevin & Rollins, Kyle. (2013). Simplified Hybrid Spring Model for Liquefied Soils. Journal of Geotechnical and Geoenvironmental Engineering. 139. 564-576. 10.1061/(ASCE)GT.1943-5606.0000750.

GEER. "Geo-Engineering Reconnaissance of the February 27, 2010 Maule Chile Earthquake." GEER Association. May 25, 2010. http://www.geerassociation.org/GEER_Post %20EQ%20Reports/Maule_Chile_2010/Ver2_Maule_Chile_2010_index.html

Gillins, D.T, and Bartlett, S.F., (2014). Multilinear Regression Equations for Predicting Lateral Spread Displacement from Soil Type and Cone Penetration Test Data, Journal of Geotechnical and Geoenvironmental Engineering, 140(4).

Gonzalez, L., Abdoun, T., & Dobry, R. (2005, March 16-19). Effect of soil permeability on centrifuge modeling of pile response to lateral spreading. Seismic Performance and 421 Simulation of Pile Foundations in Liquefied and Laterally Spreading Ground, Proceedings. Davis, California: University of California, Davis.

Gu, W.H., Morgenstern, N.R., Robertson, P.K. (1994). Post-earthquake deformation analysis of wildlife sites. *Journal of Geotechnical Engineering*, 120(2), 274-289.

Hales, L. J. (2003). Cyclic lateral load testing and analysis of a CISS pile in liquefied sand. MS Thesis. Provo, Utah: Department of Civil and Environmental Engineering, Brigham Young University.

Hamada, M., Yasuda, S., Isoyama, R., Emoto, K. (1986). Study on liquefaction induced permanent ground displacements. *Association for the Development of Earthquake Prediction in Japan*, 87.

Hamada, M., Towhata, I., Yasuda, S., and Isoyama, R. (1987). Study of permanent ground displacement induced by seismic liquefaction. *Computers and Geotechnics,* 4, 197-220.

Hanzawa, H., Itoh, Y., Suzuki, K. (1979). Shear characteristics of a quick sand in the Arabian Gulf. *Soils and Foundations*, 14(3), 1-5.

He, L., Elgamal, A., Abdoun, T., Abe, A., Dobry, R., Hamada, M., et al. (2009). Liquefactioninduced lateral load on pile in a medium Dr sand layer. Journal of Earthquake Engineering, 13, 7, 916-938.

Idriss, I.M. and Boulanger, R.W. (2008). *Soil Liquefaction During Earthquakes,* EERI Monograph MNO-12. Oakland, CA.

Ishihara, K. (1984). Post-earthquake failure of a tailings dam due to liquefaction of the pond deposit. *Proceedings, International Conference on Case Histories in Geotechnical Engineering*, Vol 3, 1129-1143.

Ishihara, K. (1985). Stability of natural deposits during earthquakes. *Proceedings, 11th International Conference on Soil Mechanics and Foundation Engineering*, Vol. 1, 321-376.

Ishihara, K. (1993). Liquefaction and flow failure during earthquakes. *Geotechnique, 43(3),351-415.*

Juirnarongrit, T., & Ashford, S. A. (2006). Soil-pile response of blast-induced lateral spreading II: Analysis and assessment of the p-y method. Journal of Geotechnical Engineering, 132(2), 163-172. ASCE.

Kayen, R.E., Mitchell, J.K., Seed, R.B., Lodge, A., Nishio, S., Cotinho, R. (1992). Evaluation of SPT-, CPT-, and shear wave-based methods for liquefaction potential assessment using Loma Prieta data. *Proceedings, 4th U.S.-Japan Workshop on Earthquake Resistant Design of Lifeline Facilities and Countermeasures for Soil Liquefaction*, 1, 177-204.

Kishida, H., & Meyerhof, G. G. (1965). Bearing capacity of pile groups under eccentric load in sand. Proceedings, 6th International Conference on Soil Mechanics and Foundation Engineering, 2, 270-274.

Kramer, S.L. (1996). *Geotechnical Earthquake Engineering*, Prentice Hall, Inc., Upper Saddle River, NJ, 653 pp.

Ku, C.S., Lee, D.H., Wu, J.H. (2004) Evaluation of soil liquefaction in the Chi-Chi, Taiwan earthquake using CPT. *Soil Dynamics and Earthquake Engineering*, 24(9-10), 659-673.

Kulhawy, F. H., & Phoon, K. K. (1993). Drilled shaft side resistance in clay soil to rock. Design and Performance of Deep Foundations: Piles and Piers in Soil and Rock, GSP No. 38, 172-183. ASCE.

Lam, I. P., Arduino, P., & Mackenzie-Helnwein, P. (2009, March 15-19). OPENSEES soil-pile interaction study under lateral spread loading. Proceedings, International Foundation Congress and Equipment Expo, 1, 206-213. Orlando, FL.

Ledezma, C., & Bray, J. D. (2010). Probabilistic performance-based procedure to evaluate pile foundations at sites with liquefaction-induced lateral displaement. Journal of Geotechnical and Geoenvironmental Engineering, 136(3), 464-476.

Ledezma, Christian & Tiznado, Juan Carlos. (2017). *Liquefaction Effects On The Northern Coronel Pier During The 2010 Maule Chile Earthquake.*

Marchetti, S. (1982). Detection of liquefiable sand layers by means of quasi-static penetration tests. *Proceedings, Stability and Performance of Slopes and Embankments*, 1, 116-142. Geotechnical Special Publication No. 31, ASCE.

Martin, G.R. (1992). Evaluation of soil parameters for seismic stability of slopes. *Proceedings, Stability and Performance of Slopes and Embankments*, 1, 116-142. Geotechnical Special Publication No. 31, ASCE.

Matlock, H. (1970). Correlations for design of laterally loaded piles in soft clay. Proceedings, 2nd Offshore Technology Conference, Paper No. OTC 1204, 1, 577-594. Houston, Texas.

"Maule, 2010 Chile Earthquake and Tsunami." (n.d.). The most destructive Tsunamis, <http://www.sms-tsunami-warning.com/pages/tsunami-chile-2010#.v5j2s_krkuk>

Middlebrooks, T.A. (1942). Fort Peck Slide. *Transactions of the American Society of Civil Engineers*, 107, 723-764.

Mitchell, J.K., Tseng, D.J. (1990). Assessment of liquefaction potential by cone penetration resistance. *Proceedings, H. Bolton Seed Memorial Symposium*, 2, 335-350. Berkeley, California

Miyajima, Kitaura, Ando. (1991). Experiments on liquefaction-induced large ground deformation. *Proceedings, 3rd Japan-U.S. Workshop on Earthquake Resistant Design of Lifeline Facilities and Countermeasures for Soil Liquefaction, Technical Report NCEER-91-0001,* 269-292. (O'Rourke & Hamada, Eds.).

Mogami, T., and K. Kubo. (1953). "The behavior of soil during vibration. *Proceedings of the Third International Conference of Soil Mechanics and Foundation Engineering*. Vol.1, 152-155.

Mohamad, R., Dobry, R. (1986). Undrained monotonic and cyclic triaxial strength of sand. *Journal of Geotechnical Engineering*, 112(10), 941-958.

Mokwa, R. L. (1999). Investigation of the resistance of pile caps to lateral spreading. PhD Thesis. Blacksburg, Virginia: Department of Civil Engineering, Virginia Polytechnic Institute and State University.

Mokwa, R. L., & Duncan, J. M. (2003). Rotational restraint of pile caps during lateral loading. Journal of Geotechnical and Geoenvironmental Engineering, 129, 9, 829-837. ASCE.

Moss, R.E., Seed, R.B., Kayen, R.E., Steward, J.P., Der Kiureghian, A., Cetin, K.O. (2006). CPT-based probabilistic and deterministic assessment of in situ seismic soil liquefaction potential. *Journal of Geotechnical and Geoenvironmental Engineering*, 132(8), 1032-1051.

Nakase, H., Hiro-oka, A., Yanagihata, T. (1997). Deformation characteristics of liquefied loose sand by triaxial compression tests. *Proceedings, IS-Nagoya 97, Deformation and Progressive Failure in Geomechanics*, 559-564. (A. Asaoka, T. Adachi, F. Oka, Eds.) Pegamon, Elsevier Science.

National Research Council (US). (1985). *Liquefaction of soil during earthquakes*. Vol 1., National Academies.

Newmark, N. (1965). Effects of earthquakes on dams and embankments. *Geotechnics*, 152(2), 139-160.

Obermeier, S.F., & Pond, E.C. (1999) Issues in using liquefaction features for paleoseismic analysis. *Seismological Research Letters*, 70(1), 34-58.

Olson, S.M., and Johnson, C.I. (2008). Analyzing liquefaction-induced lateral spreads using strength ratios. *Journal of Geotechnical and Geoenvironmental Engineering.* 134(8), 1035-1049.

Pallardy, R. (n.d.). Chile earthquake of 2010. *Encyclopedia Britannica Online, Encyclopedia Britannica*, <https://www.britannica.com/event/chile-earthquake-of-2010>

Poulos, S.J. (1981). The steady state of deformation. *Journal of Geotechnical and Geoenvironmental Engineering*, 107, ASCE 16241 Proceedings.

Reese, L. C., Cox, W. R., & Koop, F. D. (1974). Analysis of laterally loaded piles in sand. Proceedings, 6th Offshore Technology Conference, Paper No. OTC 2090, 2, 473-483. Houston, Texas.

Reese, L. C., Cox, W. R., & Koop, F. D. (1975). Field testing and analysis of laterally loaded piles in stiff clay. Proceedings, 7th Offshore Technology Conference, Paper No. OTC 2312, 671-690. Houston, Texas.

Reese, L. C., Wang, S. T., Isenhower, W. M., & Arrellaga, J. A. ((2000)). Computer program LPILE plus version 4.0 technical manual. Ensoft, Inc., Austin, Texas.

Reyna, F., Chameau, J.L. (1991) Dilatometer-based liquefaction potential of sites in the Imperial Valley. *Proceedings, 2nd International Conference on Recent Advances in Geotechnical Earthquake Engineering and Soil* Dynamic, 1, 385-392. St. Louis, Missouri.

Robertson, P.K., Campanella, R.G. (1985). Liquefaction potential of sands using the CPT. *Journal of Geotechnical Engineering*, 111(3), 384-403.

Robertson, P.K., Campanella, R.G. (1986). Estimating liquefaction potential of sands using the flat dilatometer. *Geotechnical Testing Journal*, 9(1), 38-40.

Rollins, K. M., Gerber, T. M., Lane, J. D., & Ashford, S. (2005). Lateral resistance of a full-scale pile group in liquefied sand. Journal of Geotechnical and Geoenvironmental Engineering, 131, 1, 115-125. ASCE.

Rollins, K.M., Olsen, R., Egbert, J., Jensen, D., Olsen, K., Garrett, B. (2006). Pile Spacing Effects on Lateral Pile Group Behavior: Load Test. *Journal of Geotechnical and Geoenvironmental Engineering, 132.10.1061/* (ASCE)1090-0241(2006)132:10(1262)

Sasaki, Tokaida, Matsumoto, Saya. (1991). Shake table tests on lateral ground flow induced by soil liquefaction. *Proceedings, 3rd Japan-U.S. Workshop on Earthquake Resistant Design of Lifeline Facilities and Countermeasures for Soil Liquefaction, Technical Report NCEER-91-0001*, 371-385. (O'Rourke & Hamada, Eds.).

Saygili, G. and Rathje, E.M. (2008). Empirical predictive models for earthquake-induced sliding displacements of slopes. *Journal of Geotechnical and Geoenvironmental Engineering,* 134(6), 790-803.

Seed, H.B. (1980). Closure to soil liquefaction and cyclic mobility evaluation for level ground during earthquakes. *Journal of Geotechnical Engineering*, 106(GT6), 724.

Seed, H. B., and Idriss, I.M. (1982). Ground motions and soil liquefaction during earthquakes. *Earthquake Engineering Research Institute*, Monograph, Oakland, California.

Seed, H.B., Idriss, I.M., Arango, I. (1983). Evaluation of liquefaction potential using field performance data. *Journal of Geotechnical Engineering*, 109(3), 458-482.

Seed, H.B., Tokimatsu, K., Harder, L.F., and Chung, R.M. (1985), Influence of SPT procedures in soil liquefaction resistance evaluations. *Journal of Geotechnical Engineering,* 111(12), 1425-1445.

Seed, H.B., De Alba, P. (1986). Use of SPT and CPT test for evaluating soil liquefaction potential. *Proceedings, In Situ '86*, ASCE.

Seed, H. B., and Idriss, I.M. (1971). Simplified procedure for evaluating soil liquefaction potential. *Journal of Geotechnical Engineering.* 97(9), 1249–1273.

Shamoto, Y., Zhang, J.M., Goto, S. (1997). Mechanism of large post-liquefaction deformation in saturated sands. *Soils and Foundations*, 37(2), 71-80.

Shiomi, T., Tsukuni, S., Hatanaka, M., Tanaka, Y., Suzuki, Y., Hirose, T. (1987). Simulation analysis of ground liquefaction induced by earthquake. *Computers and Geotechnics*, 4(4), 221-245.

Silver, N.L., and Seed, H.B. (1971). Volume changes in sands during cyclic loading. *Journal of the Soil Mechanics and Foundations Division*, 97(SM9), 1171-.

Stokoe, K.H., Roesset, J.M., Bierschwale, J.G., Aouad, M. (1988). Liquefaction potential of sands from shear wave velocity. *Proceedings, 9th World Conference of Earthquake Engineering*, 3, 213-218. Tokyo, Japan.

Suzuki, Y., Tokimatsu, K., Koyamada, K. (2004). Correlation between soil liquefaction during earthquake and shear wave velocity. *Journal of Structural and Construction Engineering*, (578), 67-74.

Terzaghi, K., Peck, R., B., 1967, "Soil Mechanics in Engineering Practice", John Wiley & Sons, USA.

Toboadao, V.M., Andoun, T., Dobry, R. (1996). Prediction of liquefaction-induced lateral spreading by bilateral sliding block model calibrated by centrifuge tests. *Proceedings, 11th World Conference on Earthquake Engineering*, Paper No. 1037. Acapulco, Mexico.

Toboadao, V.M., Dobry, R. (1998). Centrifuge modeling of earthquake-induced lateral spreading in sand. *Journal of Geotechnical and Geoenvironmental Engineering*, 124(12), 1195-1206.

Tokimatsu, K., Kuwayama, S., Tamura, S. (1991). Liquefaction potential evaluation based on Rayleigh Wave investigation and its comparison with field behavior. *Proceedings, 2nd Internationals Conference on Recent Advances in Geotechnical Earthquake Engineering and Soil Dynamics*, 1, 357-364. St Louis, Missouri.

Tokimatsu, K., Suzuki, H., & Suzuki, Y. (2001). Backcalculated p-y relation of liquefied soils from large shaking table tests. Proceedings, 4th International Conference on Recent Advances in Geotechnical Earthquake Engineering and Soil Dynamics, Paper No. 6.24. (S. Prakash, Ed.) Rolla, Missouri: University of Missouri-Rolla.

Tokimatsu, K., & Suzuki, H. (2004). Pore water pressure response around pile and its effects on p-y behavior duing soil liquefaction. Soils and Foundations, 43, 6, 101-110.

Tomlinson, M. J. (1994). Pile design and construction practice, 4th edition. London, U.K.: E&FN Spon.

Towhata, I., Tokida, K., Tamari, H., Matsumoto, H., Yamada, L. (1991). Prediction of permanent lateral displacement of liquefied ground by means of variational principle. *Proceedings, 3rd Japan U.S. Workshop on Earthquake Resistant Design of Lifeline Facilities and Countermeasures for Soil Liquefaction*, Technical Report NCEER-91-0001, 237-251. (O'Rourke & Hamada, Eds.).

Towhata, I., Sasaki, K., Tokida, K., Matsumoto, H., Tamari, Y., Yamuda, K. (1992). Prediction of permanent displacements of liquefied ground by means of minimum energy principle. *Soils and Foundations*, 32(2), 97-116.

Tryon, G.E. (2014). Evaluation of Current Empirical Methods for Predicting Lateral Spread-Induced Ground Deformations for Large Magnitude Earthquakes Using Maule Chile 2010 Case Histories. *All Theses and Dissertations (BYU)*. 5852.

Vaid, Y.P., and Chern, J.C. (1983). Effects of static shear on resistance of liquefaction. *Soils and Foundations,* Vol. 23, No. 1, pp. 47-60.

Valsamis, A.I., Bouckovalas, G.D., Papadimitrou, A.G. (2010). Parametric investigation of lateral spreading of gently sloping liquefied ground. *Soil Dynamics and Earthquake Engineering*, 30(6), 490-508.

Vasquez-Herrera, A., Dobry, R. (1988). The behavior of undrained contractive sand and its effect of seismic liquefaction flow failures of earth structures. *Report to the U.S. Army Core of Engineers*, 510 pp., Troy, New York: Rennsalaer Polytechnic Institute.

Wang, S. T., & Reese, L. C. (1998). Design of pile foundations in liquefied soils. Geotechnical Earthquake Engineering and Soil Dynamics III, Geotechnical Special Pub. No. 75, 2, 1331-1343. (P. Dakoulas, M. Yegian, & R. Holtz, Eds.) ASCE.

Weaver, T. J., Ashford, S. A., & Rollins, K. M. (2005). Response of 0.6 m cast-in-steel-shell pile in liquefied soil under lateral loading. Journal of Geotechnical and Geoenvironmental Engineering, 131, 1, 94-102. ASCE.

Wilson, D. W., Boulanger, R. W., & Kutter, M. L. (2000). Observed seismic lateral resistance of liquefying sand. Journal of Geotechnical and Geoenvironmental Engineering, 126, 10, 898-906. ASCE.

Wong, R.T., Seed, H.B., Chan, C.K. (1975). Liquefaction of gravelly soil under cyclic loading conditions. *Journal of the Geotechnical Engineering Division*, 101(GT6), 571-583.

Wu, J. (2002). Liquefaction triggering and post-liquefaction deformations of Monterey 0/30 sand under uni-directional cyclic simple shear loading. *PhD Dissertation*, Berkeley, California: University of California.

Yang, Z. (2000). "Numerical modeling of earthquake site response including dilation and liquefaction." *Ph.D. Dissertation*, Columbia Univ., New York.

Yang, Z., Elgamal, A., Parra, E. (2003). A computational model for liquefaction and associated shear deformation. *Journal of Geotechnical and Geoenvironmental Engineering*, 129(12), 1119-1127.

Yasuada, S., Nagase, H., Kiku, H., Uchida, Y. (1991). A simplified procedure for the analysis of the permanent ground displacement. *Proceedings, 3rd Japan-U.S. Workshop on Earthquake Resistant Design of Lifeline Facilities and Countermeasures against Soil Liquefaction*, NCEER-91-0001, 225-236. (O'Rourke & Hamada, Eds.).

Yasuada, S., Masuda, T., Yoshida, N., Kiku, H., Itafuji, S., Mine, K. (1994). Torsional shear and triaxial compression tests on deformation characteristics of sands before and after liquefaction. *Proceedings, 5th U.S.-Japan Workshop on Earthquake Resistant Design of Lifeline Facilities and Countermeasures against Soil Liquefaction*, NCEER-94-0026, 249-266, Salt Lake City, UT.

Youd, T.L. (1972). Compaction of sands by repeated shear straining. *Journal of the Soil Mechanics and Foundations Division,* 98(SM7), 709-725.

Youd, L.T., Hoose S.N. (1978). *Historic ground failures in northern California triggered by earthquakes*. Vol. 993, U.S. Govt. Print Off., Washington D.C.

Youd, T.L. (1984). Recurrence of liquefaction at the same site. *Proceedings, 8th World Conference on Earthquake Engineering*, Vol. 3, 231-238.

Youd, T.L., Idriss, I.M., Andrus, R.D., Arango, I., Castro, G., Christian, J.T. (2001). Liquefaction resistance of soils; summary report from the 1996 NCEER and 1998 NCEER/NSF Workshops on evaluation of liquefaction resistance of soils. *Journal of Geotechnical and Geoenvironmental Engineering*, 127(10), 817-833.

Youd, T.L., Hansen, C.M., and Bartlett, S.F. (2002). Revised multilinear regression equations for prediction of lateral spread displacement. *Journal of Geotechnical and Geoenvironmental Engineering,* ASCE, 128(12), 1007-1017.

Youd, T.L., DeDan, D.W., Bray, J.D., Sancio, R.B., Cetin, K.O., Gerber, T.M. (2009). Zero displacement lateral spreads, 1999 Kocaeli, Turkey, earthquake. *Journal of Geotechnical and Geoenvironmental Engineering*, 135(1), 46-61.

Zhang, G., Robertson, P. K., & Brachman, R. W. (2004). Estimating liquefaction-induced lateral displacements using the standard penetration test or cone penetration test. Journal of Geotechnical and Geoenvironmental Engineering, 130(8), 861-871.

Zhang, J., Wang, G. (2012). Large post liquefaction deformation of sand, part I: physical mechanism, constitutive description, and numerical algorithm. *Acta Geotechnica*, 7, 69-113.

Zhang, J., Chagwei, Y., Zhao, J.X., and McVerry, G.H. (2012). Empirical models for predicting Lateral Spreading Considering the Effects of Regional Seismicity. *Earthquake Engineering and Engineering Vibration*, 2012: 121-131.

Zienkiewicz, O.C., Chang, C.T., Hinton, E. (1978). Non-linear seismic response and liquefaction. *International Journal for Numerical and Analytical Methods in Geomechanics*, 2, 381-404.

Zienkiewicz, O.C., Shiomi, T. (1984). Dynamic behavior of saturated porous media: the generalized Biot formulation and its numerical solution. *International Journal for Numerical and Analytical Methods in Geomechanics*, 8, 71-96.

APPENDIX A RECONNAISSANCE DATA – NORTH PIER

Table A-1: Boring Data from ST-2

Sample Depth (ft.)	N_{field}	Unit Weight (pcf)	σ_v (tsf)	σ_v' (tsf)	C_N	C_E	C_B	C_R	C_{SS}	N_{60}	$(N_1)_{60}$	C_{SO}	$(N_1)_{60}$	Soil Type	Soil behaves cohesionless	Rel. Density (granular)	Consistency (cohesive)	LL (From Lab Test)	PI (From Lab Test)
1.6404	5	120	0.10	0.10	1.70	1.0	1	0.75	1	4	6	1.0	6	Poorly Graded SAND With Silt (SP-SM)	No		soft		
4.9212	10	120	0.30	0.30	1.70	1.0	1	0.80	1	8	14	1.0	14	Poorly Graded SAND With Silt (SP-SM)	No		medium stiff		
8.202	30	120	0.49	0.49	1.43	1.0	1	0.85	1	26	36	1.0	36	Poorly Graded SAND With Silt (SP-SM)	No		very stiff		
11.4828	40	120	0.69	0.64	1.25	1.0	1	0.85	1	34	43	1.0	43	Poorly Graded SAND With Silt (SP-SM)	No		hard		
14.7636	30	120	0.89	0.73	1.17	1.0	1	0.95	1	28	33	1.0	33	Poorly Graded SAND With Silt (SP-SM)	Yes	medium			
18.0444	20	120	1.08	0.83	1.10	1.0	1	0.95	1	19	21	1.0	21	Poorly Graded SAND With Silt (SP-SM)	Yes	medium			
21.3252	16	120	1.28	0.92	1.04	1.0	1	0.95	1	15	16	1.0	16	Poorly Graded SAND With Silt (SP-SM)	Yes	medium			
24.606	17.5	120	1.48	1.02	0.99	1.0	1	0.95	1	17	16	1.0	16	Poorly Graded SAND (SP)	Yes	medium			
27.8868	16	120	1.67	1.11	0.95	1.0	1	1.00	1	16	15	1.0	15	Poorly Graded SAND (SP)	Yes	medium			
31.1676	11	120	1.87	1.20	0.91	1.0	1	1.00	1	11	10	1.0	10	Poorly Graded SAND (SP)	Yes	loose-medium			
34.4484	11	120	2.07	1.30	0.88	1.0	1	1.00	1	11	10	1.0	10	Poorly Graded SAND (SP)	Yes	loose-medium			
37.7292	12.5	120	2.26	1.39	0.85	1.0	1	1.00	1	13	11	1.0	11	Sandy SILT (ML)	Yes	loose-medium			
41.01	17.5	120	2.46	1.49	0.82	1.0	1	1.00	1	18	14	1.0	14	SILT (ML)	Yes	medium			
44.2908	17.5	120	2.66	1.58	0.79	1.0	1	1.00	1	18	14	1.0	14	SILT (ML)	Yes	medium			
47.5716	14	120	2.85	1.68	0.77	1.0	1	1.00	1	14	11	1.0	11	SILT (ML)	Yes	loose-medium			
50.8524	11.5	120	3.05	1.77	0.75	1.0	1	1.00	1	12	9	1.0	9	Silty CLAY (CL-ML)	Yes	loose-medium			
54.1332	7.5	120	3.25	1.87	0.73	1.0	1	1.00	1	8	5	1.0	5	Clayey SAND (SC)	Yes	loose		36	12
57.414	7.5	120	3.44	1.96	0.71	1.0	1	1.00	1	8	5	1.0	5	Clayey SAND (SC)	Yes	loose		36	12
60.6948	7.5	120	3.64	2.06	0.70	1.0	1	1.00	1	8	5	1.0	5	Clayey SAND (SC)	Yes	loose		36	12
63.9756	75	120	3.84	2.15	0.68	1.0	1	1.00	1	75	51	1.0	51	Silty SAND (SM)	No		hard		
67.2564	75	120	4.04	2.24	0.67	1.0	1	1.00	1	75	50	1.0	50	Silty SAND (SM)	No		hard		
70.5372	40	120	4.23	2.34	0.65	1.0	1	1.00	1	40	26	1.0	26	Silty SAND (SM)	No		hard		
73.818	40	120	4.43	2.43	0.64	1.0	1	1.00	1	40	26	1.0	26	Silty SAND (SM)	No		hard		
77.0988	50	120	4.63	2.53	0.63	1.0	1	1.00	1	50	31	1.0	31	Silty SAND (SM)	No		hard		
80.3796	7.5	120	4.82	2.62	0.62	1.0	1	1.00	1	8	5	1.0	5	SILT With Sand (ML)	Yes	loose		30	5
83.6604	7.5	120	5.02	2.72	0.61	1.0	1	1.00	1	8	5	1.0	5	SILT With Sand (ML)	Yes	loose		30	5
86.9412	7.5	120	5.22	2.81	0.60	1.0	1	1.00	1	8	4	1.0	4	SILT With Sand (ML)	Yes	loose		30	5
90.222	7.5	120	5.41	2.91	0.59	1.0	1	1.00	1	8	4	1.0	4	Lean CLAY (CL)	No		medium stiff	40	16
93.5028	7.5	120	5.61	3.00	0.58	1.0	1	1.00	1	8	4	1.0	4	Lean CLAY (CL)	No		medium stiff	40	16

Table A-2: Boring Data from SM-1

Sample Depth (ft.)	N_{field}	Unit Weight (pcf)	σ_v (tsf)	σ_v' (tsf)	C_N	C_E	C_B	C_R	C_{SS}	N_{60}	$(N_1)_{60}$	C_{SO}	$(N_1)_{60}$	Soil Type	Soil behaves cohesionless	Rel. Density (granular)	Consistency (cohesive)	LL (From Lab Test)	PI (From Lab Test)
1.6404	5	112	0.09	0.04	1.70	1.0	1	0.75	1	4	6	1.0	6	Lean CLAY (CL)	No		soft		
4.9212	5	112	0.28	0.12	1.70	1.0	1	0.80	1	4	7	1.0	7	Lean CLAY (CL)	No		soft		
8.202	5	112	0.46	0.20	1.70	1.0	1	0.85	1	4	7	1.0	7	Lean CLAY (CL)	No		medium stiff		
11.4828	5	112	0.64	0.28	1.70	1.0	1	0.85	1	4	7	1.0	7	Lean CLAY (CL)	No		medium stiff		
14.7636	40	112	0.83	0.37	1.65	1.0	1	0.95	1	38	63	1.0	63	Silty SAND (SM)	0.0				
15.0444	60	112	1.01	0.45	1.49	1.0	1	0.95	1	57	86	1.0	85	Silty SAND (SM)	0.0				
21.3252	80	112	1.19	0.53	1.38	1.0	1	0.96	1	86	118	1.0	118	Silty SAND (SM)	0.0				
24.606	100	112	1.38	0.61	1.28	1.0	1	0.95	1	95	122	1.0	122	Silty SAND (SM)	0.0				
27.8868	100	112	1.56	0.69	1.20	1.0	1	1.00	1	100	120	1.0	120	Elastic SILT (MH)	0.0			34	40
31.1676	100	112	1.75	0.77	1.14	1.0	1	1.00	1	100	114	1.0	114	SILT (ML)	0.0			32	16
34.4484	100	112	1.93	0.85	1.08	1.0	1	1.00	1	100	108	1.0	108	SILT (ML)	0.0			32	16
37.7292	100	112	2.11	0.94	1.03	1.0	1	1.00	1	100	103	1.0	103	Elastic SILT (MH)	0.0				
41.01	100	112	2.30	1.02	0.99	1.0	1	1.00	1	100	99	1.0	99	SILT (ML)	0.0			35	6

Table A-3: Boring Data from SM-2

Sample Depth (ft.)	N_{field}	Unit Weight (pcf)	σ_v (tsf)	σ_v' (tsf)	C_N	C_E	C_B	C_R	C_{SS}	N_{60}	$(N_1)_{60}$	C_{SO}	$(N_1)_{60}$	Soil Type	Soil behaves cohesionless	Rel. Density (granular)	Consistency (cohesive)	LL (From Lab Test)	PI (From Lab Test)
1.6404	5	112	0.09	0.04	1.70	1.0	1	0.75	1	4	6	1.0	6	Lean CLAY (CL)	No		soft		
4.9212	5	112	0.28	0.12	1.70	1.0	1	0.80	1	4	7	1.0	7	Lean CLAY (CL)	No		soft		
8.202	5	112	0.46	0.20	1.70	1.0	1	0.85	1	4	7	1.0	7	Lean CLAY (CL)	No		medium stiff		
11.4828	5	112	0.64	0.28	1.70	1.0	1	0.85	1	4	7	1.0	7	Lean CLAY (CL)	No		medium stiff		
14.7636	50	112	0.83	0.37	1.65	1.0	1	0.95	1	48	79	1.0	79	Lean CLAY (CL)	No		hard		
18.0444	100	112	1.01	0.45	1.49	1.0	1	0.95	1	95	142	1.0	142	Poorly Graded SAND With Silt (SP-SM)	No		hard		
21.3252	100	112	1.19	0.53	1.38	1.0	1	0.96	1	95	131	1.0	131	Poorly Graded SAND With Silt (SP-SM)	No		hard		
24.606	100	112	1.38	0.61	1.28	1.0	1	0.95	1	95	122	1.0	122	Poorly Graded SAND With Silt (SP-SM)	No		hard		
27.8868	100	112	1.56	0.69	1.20	1.0	1	1.00	1	100	120	1.0	120	Poorly Graded SAND With Silt (SP-SM)	No		hard		
31.1676	70	112	1.75	0.77	1.14	1.0	1	1.00	1	70	80	1.0	80	Poorly Graded SAND With Silt (SP-SM)	No		hard		
34.4484	22	112	1.93	0.85	1.08	1.0	1	1.00	1	22	24	1.0	24	Elastic SILT (MH)	Yes	medium		35	15
37.7292	5	112	2.11	0.94	1.03	1.0	1	1.00	1	5	5	1.0	5	Elastic SILT (MH)	Yes	loose		35	15
41.01	5	112	2.30	1.02	0.99	1.0	1	1.00	1	5	5	1.0	5	Elastic SILT (MH)	Yes	loose		35	15
44.2908	5	112	2.48	1.10	0.95	1.0	1	1.00	1	5	5	1.0	5	Elastic SILT (MH)	Yes	loose		35	15
47.5716	5	112	2.66	1.18	0.92	1.0	1	1.00	1	5	5	1.0	5	Elastic SILT (MH)	Yes	loose		35	15
50.8524	5	112	2.85	1.26	0.89	1.0	1	1.00	1	5	4	1.0	4	Elastic SILT (MH)	Yes	loose		35	15
54.1332	30	112	3.03	1.34	0.86	1.0	1	1.00	1	30	26	1.0	26	Silty CLAY (CL-ML)	No		very stiff	25	20
57.414	65	112	3.22	1.42	0.84	1.0	1	1.00	1	65	54	1.0	54	Silty CLAY (CL-ML)	No		hard	30	20
60.6948	100	112	3.40	1.51	0.82	1.0	1	1.00	1	100	82	1.0	82	Silty CLAY (CL-ML)	No		hard	30	20

Table A-4: Boring Data from SM-3

Sample Depth (ft.)	N_{field}	Unit Weight (pcf)	σ_v (tsf)	σ_v' (tsf)	C_N	C_E	C_B	C_R	C_{SS}	N_{60}	$(N_1)_{60}$	C_{SS}	$(N_1)_{60}$	Soil Type	Soil behaves cohesionless	Rel. Density (granular)	Consistency (cohesive)	LL (From Lab Test)	PI (From Lab Test)
1.6404	5	120	0.10	0.05	1.70	1.0	1	0.75	1	4	6	1.0	6	Clayey SAND (SC)	No		soft	23	10
4.9212	5	120	0.30	0.14	1.70	1.0	1	0.80	1	4	7	1.0	7	Clayey SAND (SC)	No		soft	23	10
8.202	5	120	0.49	0.24	1.70	1.0	1	0.85	1	4	7	1.0	7	Clayey SAND (SC)	No		medium stiff	23	10
11.4828	5	120	0.69	0.33	1.70	1.0	1	0.85	1	4	7	1.0	7	Clayey SAND (SC)	0.0			23	10
14.7636	100	120	0.89	0.43	1.53	1.0	1	0.95	1	95	146	1.0	145	Poorly Graded SAND With Silt (SP-SM)	0.0				
18.0444	100	120	1.08	0.52	1.39	1.0	1	0.95	1	95	132	1.0	132	Poorly Graded SAND With Silt (SP-SM)	0.0				
21.3252	95	120	1.28	0.61	1.28	1.0	1	0.95	1	90	115	1.0	115	Poorly Graded SAND With Silt (SP-SM)	0.0				
24.606	85	120	1.48	0.71	1.18	1.0	1	0.95	1	81	96	1.0	96	Poorly Graded SAND With Silt (SP-SM)	0.0				
27.8868	78	120	1.67	0.80	1.12	1.0	1	1.00	1	78	87	1.0	87	SILT (ML)	0.0				
31.1676	65	120	1.87	0.90	1.06	1.0	1	1.00	1	65	69	1.0	69	Silty SAND (SM)	0.0				
34.4484	95	120	2.07	0.99	1.00	1.0	1	1.00	1	95	95	1.0	95	Silty SAND (SM)	0.0				
37.7292	95	120	2.26	1.09	0.96	1.0	1	1.00	1	95	91	1.0	91	Silty SAND (SM)	0.0				
41.01	95	120	2.46	1.18	0.92	1.0	1	1.00	1	95	87	1.0	87	Silty SAND (SM)	0.0				
44.2908	95	120	2.66	1.28	0.89	1.0	1	1.00	1	95	84	1.0	84	Silty SAND (SM)	0.0				
47.5716	5	120	2.85	1.37	0.85	1.0	1	1.00	1	5	4	1.0	4	SILT (ML)	No		medium stiff	31	14
50.8524	5	120	3.05	1.46	0.83	1.0	1	1.00	1	5	4	1.0	4	Elastic SILT With Sand (MH)	No		medium stiff	34	16
54.1332	15	120	3.25	1.56	0.80	1.0	1	1.00	1	15	12	1.0	12	Elastic SILT With Sand (MH)	No		stiff	34	16
57.414	23	120	3.44	1.65	0.78	1.0	1	1.00	1	23	18	1.0	18	SILT (ML)	No		very stiff	26	15
60.6948	23	120	3.64	1.75	0.76	1.0	1	1.00	1	23	17	1.0	17	SILT (ML)	No		very stiff		
63.9756	23	120	3.84	1.84	0.74	1.0	1	1.00	1	23	17	1.0	17	Elastic SILT (MH)	No		very stiff	37	13
67.2564	33	120	4.04	1.94	0.72	1.0	1	1.00	1	33	24	1.0	24	Lean CLAY (CL)	No		hard		
70.5372	33	120	4.23	2.03	0.70	1.0	1	1.00	1	33	23	1.0	23	Lean CLAY (CL)	No		hard	22	18
73.818	33	120	4.43	2.13	0.69	1.0	1	1.00	1	33	23	1.0	23	Lean CLAY (CL)	No		hard		
77.0988	33	120	4.63	2.22	0.67	1.0	1	1.00	1	33	22	1.0	22	Lean CLAY (CL)	No		hard	23	20
80.3796	33	120	4.82	2.31	0.66	1.0	1	1.00	1	33	22	1.0	22	Lean CLAY (CL)	No		hard		
83.6604	100	120	5.02	2.41	0.64	1.0	1	1.00	1	100	64	1.0	64	Elastic SILT With Sand (MH)	No		hard		
86.9412	100	120	5.22	2.50	0.63	1.0	1	1.00	1	100	63	1.0	63	Elastic SILT With Sand (MH)	No		hard	35	15
90.222	100	120	5.41	2.60	0.62	1.0	1	1.00	1	100	62	1.0	62	Elastic SILT With Sand (MH)	No		hard		

Table A-5: Boring Data from SM-4

Sample Depth (ft.)	N_{field}	Unit Weight (pcf)	σ_v (tsf)	σ_v' (tsf)	C_N	C_E	C_B	C_R	C_{SS}	N_{60}	$(N_1)_{60}$	C_{SZ}	$(N_1)_{60}$	Soil Type	Soil behaves cohesionless	Rel. Density (granular)	Consistency (cohesive)	LL (From Lab Test)	PI (From Lab Test)
1.6404	5	120	0.10	0.05	1.70	1.0	1	0.75	1	4	6	1.0	6	Lean CLAY (CL)	0.0				
4.9212	5	120	0.30	0.14	1.70	1.0	1	0.80	1	4	7	1.0	7	Lean CLAY (CL)	0.0				
8.202	5	120	0.49	0.24	1.70	1.0	1	0.85	1	4	7	1.0	7	Lean CLAY (CL)	0.0				
11.4828	5	120	0.69	0.33	1.70	1.0	1	0.85	1	4	7	1.0	7	Lean CLAY (CL)	0.0				
14.7636	40	120	0.89	0.43	1.53	1.0	1	0.95	1	38	58	1.0	58	Silty SAND (SM)	0.0				
18.0444	80	120	1.08	0.52	1.39	1.0	1	0.95	1	76	105	1.0	105	Silty SAND (SM)	0.0				
21.3252	85	120	1.28	0.61	1.28	1.0	1	0.95	1	81	103	1.0	103	Silty SAND (SM)	0.0				
24.606	100	120	1.48	0.71	1.19	1.0	1	0.95	1	95	113	1.0	113	Silty SAND (SM)	0.0				
27.8868	100	12	1.50	0.83	1.28	1.0	1	1.00	1	100	126	1.0	126	Silty SAND (SM)	0.0				
31.1676	100	120	1.69	0.72	1.18	1.0	1	1.00	1	100	118	1.0	118	Silty SAND (SM)	0.0				
34.4484	100	120	1.89	0.81	1.11	1.0	1	1.00	1	100	111	1.0	111	Silty SAND (SM)	0.0				
37.7292	5	120	2.09	0.91	1.05	1.0	1	1.00	1	5	5	1.0	5	Elastic SILT (MH)	0.0				
41.01	5	120	2.28	1.00	1.00	1.0	1	1.00	1	5	5	1.0	5	Elastic SILT (MH)	0.0				
44.2908	5	120	2.48	1.10	0.95	1.0	1	1.00	1	5	5	1.0	5	Elastic SILT (MH)	0.0				
47.5716	5	120	2.68	1.19	0.92	1.0	1	1.00	1	5	5	1.0	5	Elastic SILT (MH)	0.0				
50.8524	5	120	2.87	1.29	0.88	1.0	1	1.00	1	5	4	1.0	4	Elastic SILT (MH)	0.0				
54.1332	35	120	3.07	1.38	0.85	1.0	1	1.00	1	35	30	1.0	30	Elastic SILT (MH)	0.0				
57.414	5	120	3.27	1.48	0.82	1.0	1	1.00	1	5	4	1.0	4	Elastic SILT (MH)	0.0				
60.6948	5	120	3.46	1.57	0.80	1.0	1	1.00	1	5	4	1.0	4	Elastic SILT (MH)	0.0				
63.9756	5	120	3.66	1.67	0.77	1.0	1	1.00	1	5	4	1.0	4	Elastic SILT (MH)	0.0				
67.2564	5	120	3.86	1.76	0.75	1.0	1	1.00	1	5	4	1.0	4	Elastic SILT (MH)	0.0				
70.5372	10	120	4.06	1.85	0.73	1.0	1	1.00	1	10	7	1.0	7	Elastic SILT (MH)	0.0				
73.818	10	120	4.25	1.95	0.72	1.0	1	1.00	1	10	7	1.0	7	Lean CLAY (CL)	0.0			18	22
77.0988	15	120	4.45	2.04	0.70	1.0	1	1.00	1	15	10	1.0	10	Lean CLAY (CL)	0.0				
80.3796	100	120	4.65	2.14	0.68	1.0	1	1.00	1	100	68	1.0	68	Lean CLAY (CL)	0.0			25	10

Table A-6: Boring Data from SM-5

Sample Depth (ft.)	N_{field}	Unit Weight (pcf)	σ_v (tsf)	σ_v' (tsf)	C_N	C_E	C_B	C_R	C_{S1}	N_{60}	$(N_1)_{60}^*$	C_{S2}	$(N_1)_{60}$	Soil Type	Soil behaves cohesionless	Rel. Density (granular)	Consistency (cohesive)	LL (From Lab Test)	PI (From Lab Test)
1.6404	5	120	0.10	0.05	1.70	1.0	1	0.75	1	4	6	1.0	6	Silty SAND (SM)	Yes	very loose			
4.9212	5	120	0.30	0.14	1.70	1.0	1	0.80	1	4	7	1.0	7	Silty SAND (SM)	Yes	very loose			
8.202	5	120	0.49	0.24	1.70	1.0	1	0.85	1	4	7	1.0	7	SILT (ML)	No		medium stiff	25	10
11.4828	5	120	0.69	0.33	1.70	1.0	1	0.85	1	4	7	1.0	7	SILT (ML)	No		medium stiff	25	10
14.7636	64	120	0.89	0.43	1.53	1.0	1	0.95	1	61	93	1.0	93	0	0.0				
18.0444	22	120	1.08	0.52	1.39	1.0	1	0.95	1	21	29	1.0	29	0	0.0				
21.3252	24	120	1.28	0.61	1.28	1.0	1	0.95	1	23	29	1.0	29	0	0.0				
24.606	26	120	1.48	0.71	1.19	1.0	1	0.95	1	25	29	1.0	29	0	0.0				
27.8868	38	120	1.67	0.80	1.12	1.0	1	1.00	1	38	42	1.0	42	0	0.0				
31.1676	45	120	1.87	0.90	1.06	1.0	1	1.00	1	45	47	1.0	47	0	0.0				
34.4484	50	120	2.07	0.99	1.00	1.0	1	1.00	1	50	50	1.0	50	0	0.0				
37.7292	75	120	2.26	1.09	0.96	1.0	1	1.00	1	75	72	1.0	72	0	0.0				
41.01	100	120	2.46	1.18	0.92	1.0	1	1.00	1	100	92	1.0	92	0	0.0				
44.2908	100	120	2.66	1.28	0.89	1.0	1	1.00	1	100	89	1.0	89	0	0.0				
47.5716	60	120	2.85	1.37	0.85	1.0	1	1.00	1	60	51	1.0	51	0	0.0				
50.8524	20	120	3.05	1.46	0.83	1.0	1	1.00	1	20	17	1.0	17	0	0.0				
54.1332	10	120	3.25	1.56	0.80	1.0	1	1.00	1	10	8	1.0	8	0	0.0				
57.414	5	120	3.44	1.65	0.78	1.0	1	1.00	1	5	4	1.0	4	0	0.0			35	15
60.6948	5	120	3.64	1.75	0.76	1.0	1	1.00	1	5	4	1.0	4	0	0.0			35	15
63.9756	5	120	3.84	1.84	0.74	1.0	1	1.00	1	5	4	1.0	4	0	0.0			29	21
67.2564	5	120	4.04	1.94	0.72	1.0	1	1.00	1	5	4	1.0	4	0	0.0				
70.5372	64	120	4.23	2.03	0.70	1.0	1	1.00	1	64	45	1.0	45	0	0.0				
73.818	10	120	4.43	2.13	0.69	1.0	1	1.00	1	10	7	1.0	7	0	0.0			35	4
77.0988	5	120	4.63	2.22	0.67	1.0	1	1.00	1	5	3	1.0	3	0	0.0				
80.3796	5	120	4.82	2.31	0.66	1.0	1	1.00	1	5	3	1.0	3	0	0.0				
83.6604	5	120	5.02	2.41	0.64	1.0	1	1.00	1	5	3	1.0	3	0	0.0				
86.9412	5	120	5.22	2.50	0.63	1.0	1	1.00	1	5	3	1.0	3	0	0.0				
90.222	5	120	5.41	2.60	0.62	1.0	1	1.00	1	5	3	1.0	3	0	0.0				
93.5028	5	120	5.61	2.69	0.61	1.0	1	1.00	1	5	3	1.0	3	0	0.0				

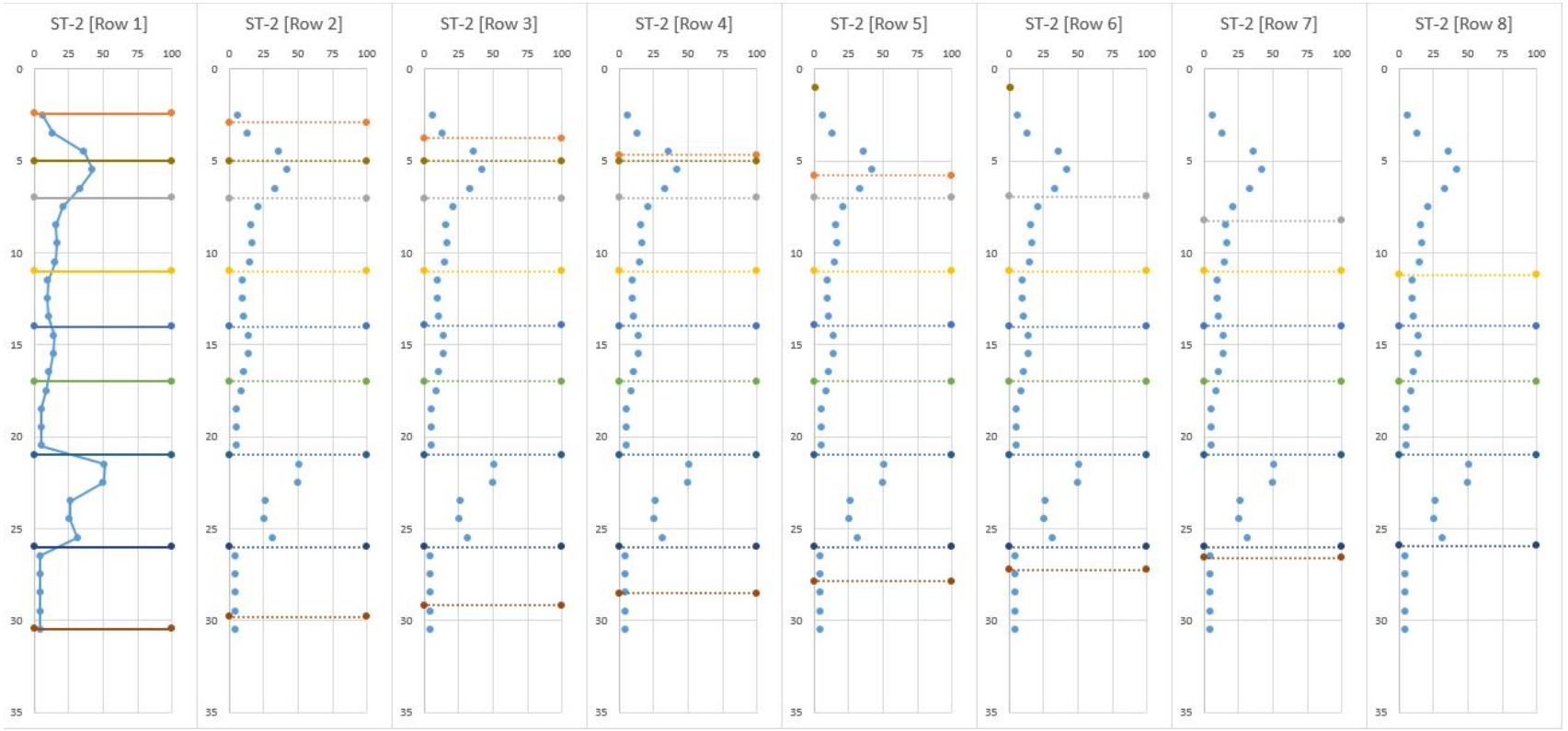

Figure A-1: "Liquefied" Zone Soil Profile over ST-2 Data

APPENDIX B INDIVIDUAL PILE ROW TABLES AND FIGURES

Row 1 Tables and Figures

Table B-1a: Caltrans Parameters used for Row 1 Soil Profile

Row 1	SI [m] Elevation		SPT		SI [Kn/m^3] Caltrans Unit Weight		SI [m] Caltrans Friction		SI [kPA] Caltrans Cohesion		Uniaxial Compressive Strength [kN/m^2]	Soil Type
	Top	Bottom	Top	Bottom	Top	Bottom	Top	Bottom	Top	Bottom		
Layer 1	1.30	3.45	-	-	17.6	20.9	31	38.5	-	-	-	API SAND
Layer 2	3.45	5.45	-	-	11.7	10	39.5	38	-	-	-	API SAND
Layer 3	5.45	9.45	20.9	15.2	10	9.5	-	-	-	-	-	LIQUIFIED SAND
Layer 4	9.45	12.45	10	10.6	9	9.2	-	-	-	-	-	LIQUIFIED SAND
Layer 5	12.45	15.45	-	-	10.5	9.8	-	-	86.18	64.64	-	STIFF CLAY
Layer 6	15.45	19.45	-	-	7.2	5.1	30	27.5	-	-	-	API SAND
Layer 7	19.45	24.45	-	-	10.8	8.6	40.5	36.5	-	-	-	API SAND
Layer 8	24.45	28.91	-	-	8.4	8.3	-	-	28.73	26.33	-	STIFF CLAY
Layer 9	28.91	50	-	-	12.75	12.75	-	-	-	-	7000	ROCK

Table B-1b: Pile Parameters used for Row 1

	Pile Diameter [mm]	Pile Wall Thickness [mm]	Length of Pile [m]
Row 1	500	14	31.69

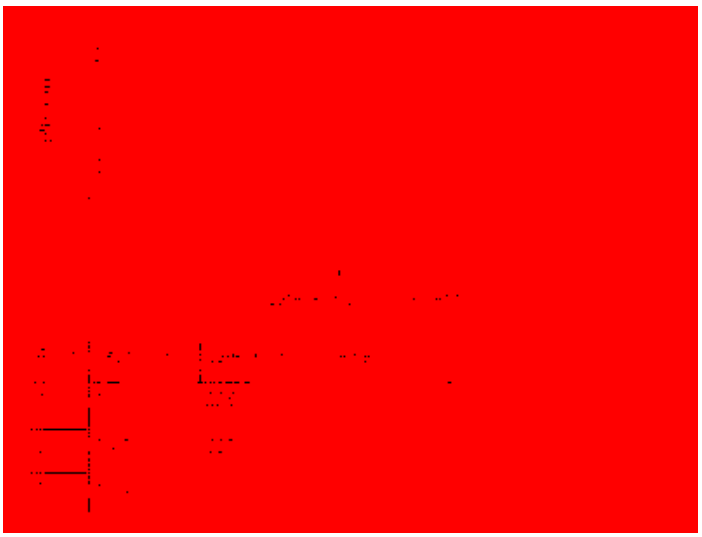

Figure B-1: Soil Movement Profile for Row 1

Row 2 Tables and Figures

Table B-2a: Caltrans Parameters used for Row 2 Soil Profile

Row 2	SI [m] Elevation		SPT		SI [Kn/m^3] Caltrans Unit Weight		SI [m] Caltrans Friction		SI [kPA] Caltrans Cohesion		Uniaxial Compressive Strength [kN/m^2]	Soil Type
	Top	Bottom	Top	Bottom	Top	Bottom	Top	Bottom	Top	Bottom		
Layer 1	1.10	3.45	-	-	19.3	20.9	33.5	38.5	-	-	-	API SAND
Layer 2	3.45	5.45	-	-	11.7	10	39.5	38	-	-	-	API SAND
Layer 3	5.45	9.45	20.9	15.2	10	9.5	-	-	-	-	-	LIQUIFIED SAND
Layer 4	9.45	12.45	10	10.6	9	9.2	-	-	-	-	-	LIQUIFIED SAND
Layer 5	12.45	15.45	-	-	10.5	9.8	-	-	86.18	64.64	-	STIFF CLAY
Layer 6	15.45	19.45	-	-	7.2	5.1	30	27.5	-	-	-	API SAND
Layer 7	19.45	24.45	-	-	10.8	8.6	40.5	36.5	-	-	-	API SAND
Layer 8	24.45	28.26	-	-	8.4	8.3	-	-	28.73	26.33	-	STIFF CLAY
Layer 9	28.26	50	-	-	12.75	12.75	-	-	-	-	7000	ROCK

Table B-2b: Pile Parameters used for Row 2

	Pile Diameter [mm]	Pile Wall Thickness [mm]	Length of Pile [m]
Row 2	500	14	30.5

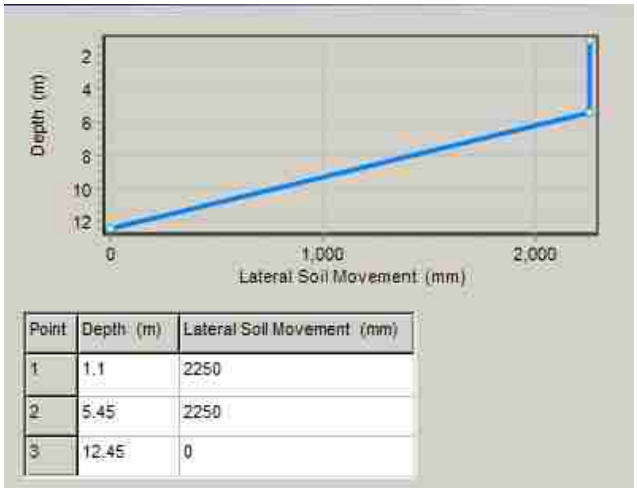

Figure B-2: Soil Movement Profile for Row 2

Row 3 Tables and Figures

Table B-3a: Caltrans Parameters used for Row 3 Soil Profile

Row 3	SI [m] Elevation		SPT		SI [Kn/m^3] Caltrans Unit Weight		SI [m] Caltrans Friction		SI [kPA] Caltrans Cohesion		Uniaxial Compressive Strength [kN/m^2]	Soil Type
	Top	Bottom	Top	Bottom	Top	Bottom	Top	Bottom	Top	Bottom		
Layer 1	2.2	3.45	-	-	19.3	20.9	33.5	38.5	-	-	-	API SAND
Layer 2	3.45	5.45	-	-	11.7	10	39.5	38	-	-	-	API SAND
Layer 3	5.45	9.45	20.9	15.2	10	9.5	-	-	-	-	-	LIQUIFIED SAND
Layer 4	9.45	12.45	10	10.6	9	9.2	-	-	-	-	-	LIQUIFIED SAND
Layer 5	12.45	15.45	-	-	10.5	9.8	-	-	86.18	64.64	-	STIFF CLAY
Layer 6	15.45	19.45	-	-	7.2	5.1	30	27.5	-	-	-	API SAND
Layer 7	19.45	24.45	-	-	10.8	8.6	40.5	36.5	-	-	-	API SAND
Layer 8	24.45	27.62	-	-	8.4	8.3	-	-	28.73	26.33	-	STIFF CLAY
Layer 9	27.62	50	-	-	12.75	12.75	-	-	-	-	7000	ROCK

Table B-3b: Pile Parameters used for Row 3

	Pile Diameter [mm]	Pile Wall Thickness [mm]	Length of Pile [m]
Row 3	500	14	30.32

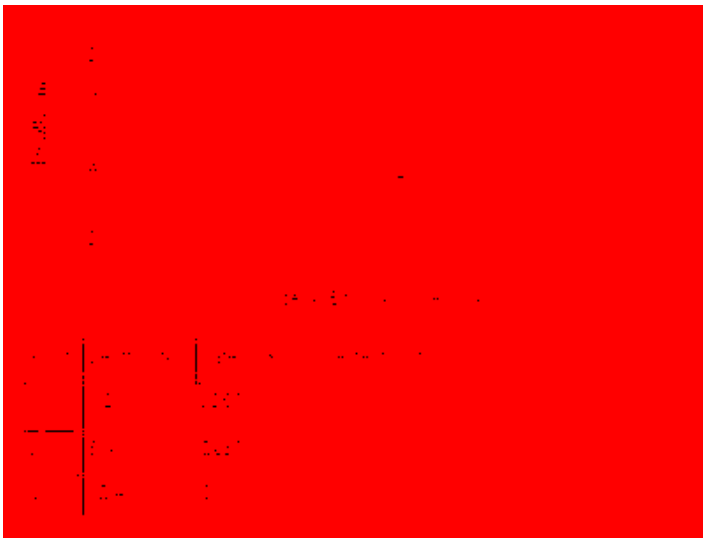

Figure B-3: Soil Movement Profile for Row 3

Row 4 Tables and Figures

Table B-4a: Caltrans Parameters used for Row 4 Soil Profile

Row 4	SI [m] Elevation		SPT		SI [Kn/m^3] Caltrans Unit Weight		SI [m] Caltrans Friction		SI [kPA] Caltrans Cohesion		Uniaxial Compressive Strength [kN/m^2]	Soil Type
	Top	Bottom	Top	Bottom	Top	Bottom	Top	Bottom	Top	Bottom		
Layer 1	3.14	3.45	-	-	20.9	20.9	38.5	38.5	-	-	-	API SAND
Layer 2	3.45	5.45	-	-	11.7	10	39.5	38	-	-	-	API SAND
Layer 3	5.45	9.45	20.9	15.2	10	9.5	-	-	-	-	-	LIQUIFIED SAND
Layer 4	9.45	12.45	10	10.6	9	9.2	-	-	-	-	-	LIQUIFIED SAND
Layer 5	12.45	15.45	-	-	10.5	9.8	-	-	86.18	64.64	-	STIFF CLAY
Layer 6	15.45	19.45	-	-	7.2	5.1	30	27.5	-	-	-	API SAND
Layer 7	19.45	24.45	-	-	10.8	8.6	40.5	36.5	-	-	-	API SAND
Layer 8	24.45	26.97	-	-	8.4	8.4	-	-	28.73	28.73	-	STIFF CLAY
Layer 9	26.97	50	-	-	12.75	12.75	-	-	-	-	7000	ROCK

Table B-4b: Pile Parameters used for Row 4

	Pile Diameter [mm]	Pile Wall Thickness [mm]	Length of Pile [m]
Row 4	500	14	29.23

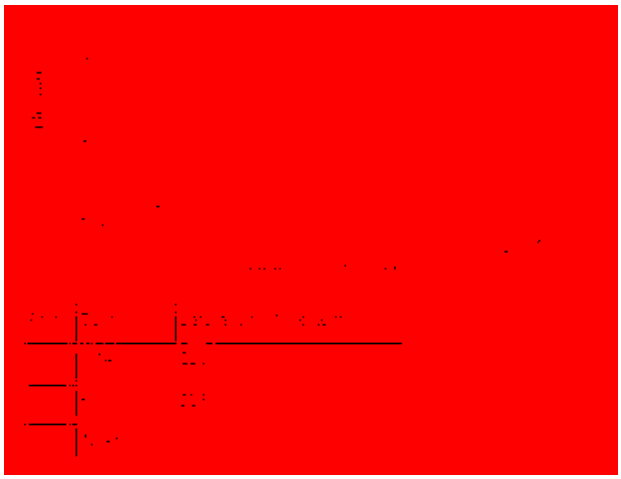

Figure B-4: Soil Movement Profile for Row 4

Row 5 Tables and Figures

Table B-5a: Caltrans Parameters used for Row 5 Soil Profile

Row 5	SI [m] Elevation		SPT		SI [Kn/m^3] Caltrans Unit Weight		SI [m] Caltrans Friction		SI [kPA] Caltrans Cohesion		Uniaxial Compressive Strength [kN/m^2]	Soil Type
	Top	Bottom	Top	Bottom	Top	Bottom	Top	Bottom	Top	Bottom		
Layer 1	4.23	5.45	-	-	11.7	10	39.5	38	-	-	-	API SAND
Layer 2	5.45	9.45	20.9	15.2	10	9.5	-	-	-	-	-	LIQUIFIED SAND
Layer 3	9.45	12.45	10	10.6	9	9.2	-	-	-	-	-	LIQUIFIED SAND
Layer 4	12.45	15.45	-	-	10.5	9.8	-	-	86.18	64.64	-	STIFF CLAY
Layer 5	15.45	19.45	-	-	7.2	5.1	30	27.5	-	-	-	API SAND
Layer 6	19.45	24.45	-	-	10.8	8.6	40.5	36.5	-	-	-	API SAND
Layer 7	24.45	26.33	-	-	8.4	8.4	-	-	28.73	28.73	-	STIFF CLAY
Layer 8	26.33	50	-	-	12.75	12.75	-	-	-	-	7000	ROCK

Table B-5b: Pile Parameters used for Row 5

	Pile Diameter [mm]	Pile Wall Thickness [mm]	Length of Pile [m]
Row 5	500	14	28.59

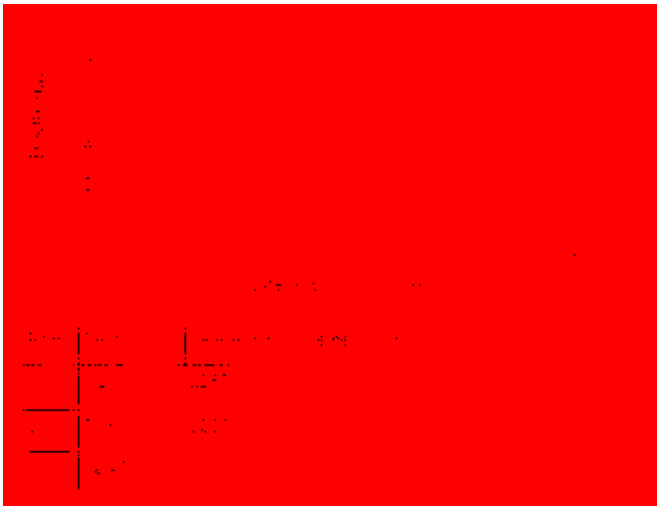

Figure B-5: Soil Movement Profile for Row 5

Row 6 Tables and Figures

Table B-6a: Caltrans Parameters used for Row 6 Soil Profile

Row 6	SI [m] Elevation		SPT		SI [Kn/m^3] Caltrans Unit Weight		SI [m] Caltrans Friction		SI [kPA] Caltrans Cohesion		Uniaxial Compressive Strength [kN/m^2]	Soil Type
	Top	Bottom	Top	Bottom	Top	Bottom	Top	Bottom	Top	Bottom		
Layer 1	5.45	9.45	20.9	15.2	10	9.5	-	-	-	-	-	LIQUIFIED SAND
Layer 2	9.45	12.45	10	10.6	9	9.2	-	-	-	-	-	LIQUIFIED SAND
Layer 3	12.45	15.45	-	-	10.5	9.8	-	-	86.18	64.64	-	STIFF CLAY
Layer 4	15.45	19.45	-	-	7.2	5.1	30	27.5	-	-	-	API SAND
Layer 5	19.45	24.45	-	-	10.8	8.6	40.5	36.5	-	-	-	API SAND
Layer 6	24.45	25.68	-	-	8.4	8.4	-	-	28.73	28.73	-	STIFF CLAY
Layer 7	25.68	50	-	-	12.75	12.75	-	-	-	-	7000	ROCK

Table B-6b: Pile Parameters used for Row 6

	Pile Diameter [mm]	Pile Wall Thickness [mm]	Length of Pile [m]
Row 6	500	14	27.5

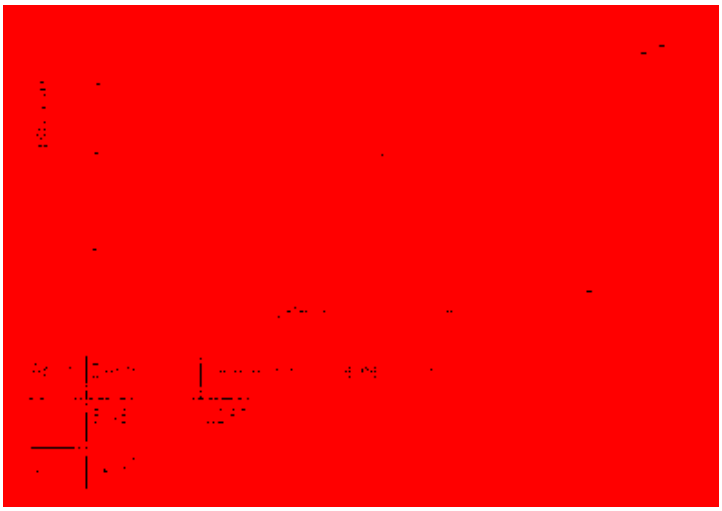

Figure B-6: Soil Movement Profile for Row 6

Row 7 Tables and Figures

Table B-7a: Caltrans Parameters used for Row 7 Soil Profile

Row 7	SI [m] Elevation		SPT		SI [Kn/m^3] Caltrans Unit Weight		SI [m] Caltrans Friction		SI [kPA] Caltrans Cohesion		Uniaxial Compressive Strength [kN/m^2]	Soil Type
	Top	Bottom	Top	Bottom	Top	Bottom	Top	Bottom	Top	Bottom		
Layer 1	6.7	9.45	15.8	15.2	9.7	9.5	-	-	-	-	-	LIQUIFIED SAND
Layer 2	9.45	12.45	10	10.6	9	9.2	-	-	-	-	-	LIQUIFIED SAND
Layer 3	12.45	15.45	-	-	10.5	9.8	-	-	86.18	64.64	-	STIFF CLAY
Layer 4	15.45	19.45	-	-	7.2	5.1	30	27.5	-	-	-	API SAND
Layer 5	19.45	24.45	-	-	10.8	8.6	40.5	36.5	-	-	-	API SAND
Layer 6	24.45	25.04	-	-	8.4	8.4	-	-	28.73	28.73	-	STIFF CLAY
Layer 7	25.04	50	-	-	12.75	12.75	-	-	-	-	7000	ROCK

Table B-7b: Pile Parameters used for Row 7

	Pile Diameter [mm]	Pile Wall Thickness [mm]	Length of Pile [m]
Row 7	500	14	28.32

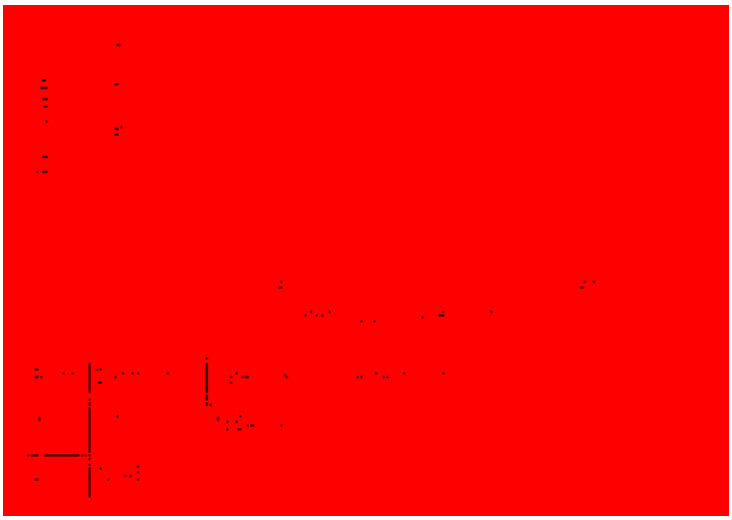

Figure B-7: Soil Movement Profile for Row 7

Row 8 Tables and Figures

Table B-7a: Caltrans Parameters used for Row 7 Soil Profile

Row 8	SI [m] Elevation		SPT		SI [Kn/m^3] Caltrans Unit Weight		SI [m] Caltrans Friction		SI [kPA] Caltrans Cohesion		Uniaxial Compressive Strength [kN/m^2]	Soil Type
	Top	Bottom	Top	Bottom	Top	Bottom	Top	Bottom	Top	Bottom		
Layer 1	9.64	12.45	10	10.6	9	9.2	-	-	-	-	-	LIQUIFIED SAND
Layer 2	12.45	15.45	-	-	10.5	9.8	-	-	86.18	64.64	-	STIFF CLAY
Layer 3	15.45	19.45	-	-	7.2	5.1	30	27.5	-	-	-	API SAND
Layer 4	19.45	24.39	-	-	10.8	8.6	40.5	36.5	-	-	-	API SAND
Layer 5	24.39	50	-	-	12.75	12.75	-	-	-	-	7000	ROCK

Table B-8b: Pile Parameters used for Row 8

	Pile Diameter [mm]	Pile Wall Thickness [mm]	Length of Pile [m]
Row 8	500	14	29.58

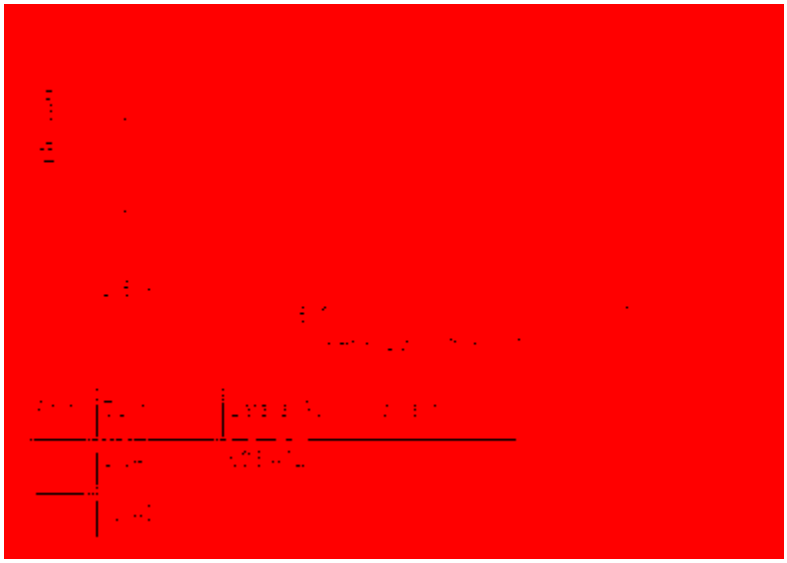

Figure B-8: Soil Movement Profile for Row 8

APPENDIX C PUSH-OVER ANALYSIS RESULTS

Table C-1: Analysis Results for Row 1 "No Failures" Condition

Pushover Point Number	Pile-head Fixity Condition	Pile-head Deflection meters	Pile-head Shear kN	Max Moment in Pile kN-m (abs)	Max Shear in Pile kN (abs)	Depth to Max Moment meters	Depth to Max Shear meters
1	Free-head	0.00	-1561.	5932.	1570.	15.5281	17.7464
2	Free-head	0.05000	-1550.	5877.	1559.	15.5281	17.7464
3	Free-head	0.10000	-1538.	5823.	1547.	15.5281	17.7464
4	Free-head	0.1500	-1527.	5768.	1536.	15.5281	17.7464
5	Free-head	0.2000	-1515.	5715.	1524.	15.5281	17.7464
6	Free-head	0.2500	-1504.	5661.	1513.	15.5281	17.7464
7	Free-head	0.3000	-1493.	5607.	1502.	15.5281	17.7464
8	Free-head	0.3500	-1482.	5554.	1491.	15.5281	17.7464
9	Free-head	0.4000	-1470.	5501.	1479.	15.5281	17.7464
10	Free-head	0.4500	-1459.	5447.	1468.	15.5281	17.7464
11	Free-head	0.5000	-1448.	5394.	1482.	15.5281	17.7464
12	Free-head	0.5500	-1437.	5341.	1530.	15.5281	17.7464
13	Free-head	0.6000	-1426.	5288.	1578.	15.5281	17.7464
14	Free-head	0.6500	-1415.	5236.	1625.	15.5281	17.7464
15	Free-head	0.7000	-1404.	5211.	1672.	15.5281	17.7464
16	Free-head	0.7500	-1393.	5364.	1719.	15.5281	17.7464
17	Free-head	0.8000	-1383.	5519.	1766.	15.5281	17.7464
18	Free-head	0.8500	-1372.	5672.	1812.	15.5281	17.7464
19	Free-head	0.9000	-1361.	5824.	1857.	15.5281	17.7464
20	Free-head	0.9500	-1351.	5974.	1902.	15.5281	17.7464
21	Free-head	1.0000	-1340.	6125.	1946.	15.5281	17.7464
22	Free-head	1.0500	-1330.	6276.	1989.	15.5281	17.7464
23	Free-head	1.1000	-1319.	6426.	2034.	15.5281	17.7464
24	Free-head	1.1500	-1309.	6575.	2081.	15.5281	17.7464
25	Free-head	1.2000	-1298.	6724.	2128.	15.5281	17.7464
26	Free-head	1.2500	-1288.	6872.	2174.	15.5281	17.7464
27	Free-head	1.3000	-1278.	7018.	2219.	15.5281	17.7464
28	Free-head	1.3500	-1267.	7164.	2264.	15.5281	17.7464
29	Free-head	1.4000	-1257.	7310.	2309.	15.5281	17.7464
30	Free-head	1.4500	-1247.	7456.	2354.	15.5281	17.7464
31	Free-head	1.5000	-1237.	7602.	2398.	15.5281	17.7464

Table C-2: Analysis Results for Row 2 "No Failures" Condition

Pushover Point Number	Pile-head Fixity Condition	Pile-head Deflection meters	Pile-head Shear kN	Max Moment in Pile kN-m (abs)	Max Shear in Pile kN (abs)	Depth to Max Moment meters	Depth to Max Shear meters
1	Free-head	0.00	-1278.	4689.	1278.	15.2500	17.0800
2	Free-head	0.05000	-1270.	4652.	1270.	15.2500	17.0800
3	Free-head	0.10000	-1262.	4614.	1262.	15.2500	17.0800
4	Free-head	0.1500	-1254.	4577.	1254.	15.2500	17.0800
5	Free-head	0.2000	-1246.	4540.	1246.	15.2500	17.0800
6	Free-head	0.2500	-1238.	4504.	1238.	15.2500	17.0800
7	Free-head	0.3000	-1230.	4467.	1230.	15.2500	17.0800
8	Free-head	0.3500	-1222.	4431.	1222.	15.2500	17.0800
9	Free-head	0.4000	-1214.	4394.	1214.	15.2500	17.0800
10	Free-head	0.4500	-1206.	4358.	1206.	15.2500	17.0800
11	Free-head	0.5000	-1198.	4322.	1198.	15.2500	17.0800
12	Free-head	0.5500	-1190.	4287.	1235.	15.2500	17.0800
13	Free-head	0.6000	-1183.	4251.	1271.	15.2500	17.0800
14	Free-head	0.6500	-1175.	4215.	1307.	15.2500	17.0800
15	Free-head	0.7000	-1167.	4179.	1343.	15.2500	17.0800
16	Free-head	0.7500	-1159.	4144.	1379.	15.2500	17.0800
17	Free-head	0.8000	-1152.	4109.	1414.	15.2500	17.0800
18	Free-head	0.8500	-1144.	4093.	1449.	15.2500	17.0800
19	Free-head	0.9000	-1136.	4199.	1484.	15.2500	17.0800
20	Free-head	0.9500	-1129.	4305.	1519.	15.2500	17.0800
21	Free-head	1.0000	-1121.	4411.	1553.	15.2500	17.0800
22	Free-head	1.0500	-1114.	4515.	1586.	15.2500	17.0800
23	Free-head	1.1000	-1106.	4619.	1620.	15.2500	17.0800
24	Free-head	1.1500	-1098.	4723.	1652.	15.2500	17.0800
25	Free-head	1.2000	-1091.	4827.	1687.	15.2500	17.0800
26	Free-head	1.2500	-1083.	4932.	1723.	15.2500	17.0800
27	Free-head	1.3000	-1076.	5037.	1759.	15.2500	17.0800
28	Free-head	1.3500	-1069.	5142.	1794.	15.2500	17.0800
29	Free-head	1.4000	-1061.	5245.	1829.	15.2500	17.0800
30	Free-head	1.4500	-1054.	5347.	1863.	15.2500	17.0800
31	Free-head	1.5000	-1046.	5449.	1897.	15.2500	17.0800

Table C-3: Analysis Results for Row 3 "No Failures" Condition

Pushover Point Number	Pile-head Fixity Condition	Pile-head Deflection meters	Pile-head Shear kN	Max Moment in Pile kN-m (abs)	Max Shear in Pile kN (abs)	Depth to Max Moment meters	Depth to Max Shear meters
1	Free-head	0.00	-522.0948	2067.	522.0948	14.8568	16.9792
2	Free-head	0.05000	-513.5567	2026.	513.5567	14.8568	16.9792
3	Free-head	0.10000	-505.0712	1984.	505.0712	14.8568	16.9792
4	Free-head	0.1500	-496.6371	1944.	496.6371	14.8568	16.9792
5	Free-head	0.2000	-488.2491	1903.	522.1773	14.8568	16.9792
6	Free-head	0.2500	-479.9035	1864.	559.7868	14.8568	16.9792
7	Free-head	0.3000	-471.5989	1826.	597.3219	14.8568	16.9792
8	Free-head	0.3500	-463.3319	1832.	634.7555	14.8568	16.9792
9	Free-head	0.4000	-455.1004	1942.	672.0617	14.8568	16.9792
10	Free-head	0.4500	-446.9026	2051.	709.2150	14.8568	16.9792
11	Free-head	0.5000	-438.7369	2161.	747.4295	14.8568	16.9792
12	Free-head	0.5500	-430.6020	2270.	785.7080	14.8568	16.9792
13	Free-head	0.6000	-422.4967	2379.	823.9173	14.8568	16.9792
14	Free-head	0.6500	-414.4195	2488.	862.0361	14.8568	16.9792
15	Free-head	0.7000	-406.3693	2597.	900.0445	14.8568	16.9792
16	Free-head	0.7500	-398.2331	2705.	937.5079	14.8568	16.9792
17	Free-head	0.8000	-390.1095	2813.	974.7880	14.8568	16.9792
18	Free-head	0.8500	-382.0193	2920.	1012.	14.8568	16.9792
19	Free-head	0.9000	-373.9616	3028.	1049.	14.8568	16.9792
20	Free-head	0.9500	-365.9353	3135.	1086.	14.8568	16.9792
21	Free-head	1.0000	-357.9393	3242.	1122.	14.8568	16.9792
22	Free-head	1.0500	-349.9727	3349.	1159.	14.8568	16.9792
23	Free-head	1.1000	-342.0342	3455.	1195.	14.8568	16.9792
24	Free-head	1.1500	-334.1226	3562.	1231.	14.8568	16.9792
25	Free-head	1.2000	-326.2372	3668.	1267.	14.8568	16.9792
26	Free-head	1.2500	-318.3814	3774.	1302.	14.8568	16.9792
27	Free-head	1.3000	-310.4755	3879.	1337.	14.8568	16.9792
28	Free-head	1.3500	-302.6660	3984.	1372.	14.8568	16.9792
29	Free-head	1.4000	-294.8959	4089.	1407.	14.8568	16.9792
30	Free-head	1.4500	-287.1643	4194.	1441.	14.8568	16.9792
31	Free-head	1.5000	-279.4695	4299.	1475.	14.8568	16.9792

Table C-4: Analysis Results for Row 4 "No Failures" Condition

Pushover Point Number	Pile-head Fixity Condition	Pile-head Deflection meters	Pile-head Shear kN	Max Moment in Pile kN-m (abs)	Max Shear in Pile kN (abs)	Depth to Max Moment meters	Depth to Max Shear meters
1	Free-head	0.00	-211.0612	914.9001	262.9347	14.0304	16.6611
2	Free-head	0.05000	-197.5729	847.8751	275.8078	14.0304	16.6611
3	Free-head	0.10000	-184.4359	883.3395	288.3497	14.0304	16.6611
4	Free-head	0.1500	-171.5606	1049.	302.2475	14.0304	16.6611
5	Free-head	0.2000	-158.8856	1214.	350.1039	14.0304	16.6611
6	Free-head	0.2500	-146.3740	1377.	397.8956	14.0304	16.6611
7	Free-head	0.3000	-133.9938	1539.	445.5887	14.0304	16.6611
8	Free-head	0.3500	-121.7280	1700.	493.1422	14.0304	16.6611
9	Free-head	0.4000	-109.5594	1860.	540.5148	14.0304	16.6611
10	Free-head	0.4500	-97.4761	2019.	588.1301	14.0304	16.6611
11	Free-head	0.5000	-85.4722	2178.	637.9172	14.0304	16.6611
12	Free-head	0.5500	-73.5395	2337.	687.6217	14.0304	16.6611
13	Free-head	0.6000	-61.6729	2495.	737.1939	14.0304	16.6611
14	Free-head	0.6500	-49.8448	2653.	786.5199	14.0304	16.6611
15	Free-head	0.7000	-37.9791	2810.	835.3562	14.0304	16.6611
16	Free-head	0.7500	-26.1779	2967.	883.9532	14.0304	16.6611
17	Free-head	0.8000	-14.4391	3124.	932.2651	14.0304	16.6611
18	Free-head	0.8500	-2.7621	3280.	980.2448	14.0304	16.6611
19	Free-head	0.9000	8.8550	3435.	1028.	14.0304	16.6611
20	Free-head	0.9500	20.4130	3590.	1075.	14.0304	16.6611
21	Free-head	1.0000	31.9130	3745.	1122.	14.0304	16.6611
22	Free-head	1.0500	43.3552	3899.	1168.	14.0304	16.6611
23	Free-head	1.1000	54.7401	4052.	1214.	14.0304	16.6611
24	Free-head	1.1500	66.0703	4205.	1259.	14.0304	16.6611
25	Free-head	1.2000	77.3440	4357.	1307.	14.0304	16.6611
26	Free-head	1.2500	88.7240	4509.	1354.	14.0304	16.6611
27	Free-head	1.3000	100.0451	4659.	1401.	14.0304	16.6611
28	Free-head	1.3500	111.3014	4809.	1447.	14.0304	16.6611
29	Free-head	1.4000	122.4860	4959.	1493.	14.0304	16.6611
30	Free-head	1.4500	133.5075	5108.	1538.	14.0304	16.6611
31	Free-head	1.5000	144.4693	5257.	1583.	14.0304	16.6611

Table C-5: Analysis Results for Row 5 "No Failures" Condition

Pushover Point Number	Pile-head Fixity Condition	Pile-head Deflection meters	Pile-head Shear kN	Max Moment in Pile kN-m (abs)	Max Shear in Pile kN (abs)	Depth to Max Moment meters	Depth to Max Shear meters
1	Free-head	0.00	-81.5225	414.8708	173.7311	13.7232	16.2963
2	Free-head	0.05000	-62.4762	560.7596	192.2421	13.7232	16.2963
3	Free-head	0.10000	-44.6233	787.7095	219.5520	13.7232	16.2963
4	Free-head	0.1500	-27.5839	1007.	265.4777	13.7232	16.2963
5	Free-head	0.2000	-11.0859	1220.	313.1770	13.7232	16.2963
6	Free-head	0.2500	5.0293	1430.	362.3874	13.7232	16.2963
7	Free-head	0.3000	20.8549	1637.	414.5168	13.7232	16.2963
8	Free-head	0.3500	36.4552	1843.	467.8936	13.7232	16.2963
9	Free-head	0.4000	51.8713	2046.	520.8632	13.7232	16.2963
10	Free-head	0.4500	67.1323	2248.	575.3090	13.7232	16.2963
11	Free-head	0.5000	82.2589	2449.	631.7657	13.7232	16.2963
12	Free-head	0.5500	97.2673	2648.	688.0081	13.7232	16.2963
13	Free-head	0.6000	112.1686	2847.	743.9607	13.7232	16.2963
14	Free-head	0.6500	127.0639	3044.	799.3700	13.7232	16.2963
15	Free-head	0.7000	141.9054	3241.	854.2734	13.7232	16.2963
16	Free-head	0.7500	156.6491	3437.	908.7279	13.7232	16.2963
17	Free-head	0.8000	171.2979	3631.	965.8284	13.7232	16.2963
18	Free-head	0.8500	185.8544	3825.	1023.	13.7232	16.2963
19	Free-head	0.9000	200.3202	4020.	1079.	13.7232	16.2963
20	Free-head	0.9500	214.6968	4213.	1135.	13.7232	16.2963
21	Free-head	1.0000	228.9850	4406.	1190.	13.7232	16.2963
22	Free-head	1.0500	243.1859	4598.	1245.	13.7232	16.2963
23	Free-head	1.1000	257.3004	4790.	1299.	13.7232	16.2963
24	Free-head	1.1500	271.3796	4980.	1352.	13.7232	16.2963
25	Free-head	1.2000	285.5090	5169.	1404.	13.7232	16.2963
26	Free-head	1.2500	299.5387	5356.	1456.	13.7232	16.2963
27	Free-head	1.3000	313.4729	5543.	1510.	13.7232	16.2963
28	Free-head	1.3500	327.2876	5729.	1564.	13.7232	16.2963
29	Free-head	1.4000	340.8970	5914.	1617.	13.7232	16.2963
30	Free-head	1.4500	354.4162	6098.	1670.	13.7232	16.2963
31	Free-head	1.5000	367.8046	6282.	1722.	13.7232	16.2963

Table C-6: Analysis Results for Row 6 "No Failures" Condition

Pushover Point Number	Pile-head Fixity Condition	Pile-head Deflection meters	Pile-head Shear kN	Max Moment in Pile kN-m (abs)	Max Shear in Pile kN (abs)	Depth to Max Moment meters	Depth to Max Shear meters
1	Free-head	0.00	-53.3604	339.2546	171.2480	13.4750	15.9500
2	Free-head	0.05000	-43.2551	430.5646	181.0998	13.4750	15.9500
3	Free-head	0.10000	-33.5410	554.2463	190.5542	13.4750	15.9500
4	Free-head	0.1500	-24.0388	676.1899	220.4187	13.4750	15.9500
5	Free-head	0.2000	-14.8642	794.0675	249.1082	13.4750	15.9500
6	Free-head	0.2500	-5.9053	909.5741	273.8581	13.4750	15.9500
7	Free-head	0.3000	2.8850	1023.	301.0115	13.4750	15.9500
8	Free-head	0.3500	11.5356	1135.	328.2250	13.4750	15.9500
9	Free-head	0.4000	20.0705	1246.	354.4632	13.4750	15.9500
10	Free-head	0.4500	28.5515	1356.	384.8596	13.4750	15.9500
11	Free-head	0.5000	36.9909	1465.	414.9136	13.4750	15.9500
12	Free-head	0.5500	45.3540	1574.	444.6916	13.4750	15.9500
13	Free-head	0.6000	53.6491	1681.	474.2056	13.4750	15.9500
14	Free-head	0.6500	61.8822	1788.	503.8016	13.4750	15.9500
15	Free-head	0.7000	70.0593	1895.	536.3429	13.4750	15.9500
16	Free-head	0.7500	78.1852	2001.	568.7974	13.4750	15.9500
17	Free-head	0.8000	86.2642	2107.	601.1428	13.4750	15.9500
18	Free-head	0.8500	94.2983	2212.	633.3541	13.4750	15.9500
19	Free-head	0.9000	102.2913	2316.	665.4069	13.4750	15.9500
20	Free-head	0.9500	110.2456	2421.	697.2749	13.4750	15.9500
21	Free-head	1.0000	118.1634	2525.	728.9316	13.4750	15.9500
22	Free-head	1.0500	126.0628	2628.	760.3148	13.4750	15.9500
23	Free-head	1.1000	134.0390	2732.	791.2175	13.4750	15.9500
24	Free-head	1.1500	141.9745	2835.	822.7559	13.4750	15.9500
25	Free-head	1.2000	149.8714	2939.	855.7915	13.4750	15.9500
26	Free-head	1.2500	157.7312	3042.	888.6714	13.4750	15.9500
27	Free-head	1.3000	165.5553	3144.	921.3703	13.4750	15.9500
28	Free-head	1.3500	173.3450	3247.	953.8631	13.4750	15.9500
29	Free-head	1.4000	181.1016	3349.	986.1245	13.4750	15.9500
30	Free-head	1.4500	188.8259	3451.	1018.	13.4750	15.9500
31	Free-head	1.5000	196.5205	3552.	1050.	13.4750	15.9500

Table C-7: Analysis Results for Row 7 "No Failures" Condition

Pushover Point Number	Pile-head Fixity Condition	Pile-head Deflection meters	Pile-head Shear kN	Max Moment in Pile kN-m (abs)	Max Shear in Pile kN (abs)	Depth to Max Moment meters	Depth to Max Shear meters
1	Free-head	0.00	-30.2274	219.3556	137.9300	13.3104	15.2928
2	Free-head	0.05000	-14.4510	409.1224	153.6313	13.3104	15.2928
3	Free-head	0.10000	0.4739	597.5451	184.9250	13.3104	15.2928
4	Free-head	0.1500	14.7587	779.2572	229.0572	13.3104	15.2928
5	Free-head	0.2000	28.4144	953.4601	268.7535	13.3104	15.2928
6	Free-head	0.2500	41.6095	1122.	301.3145	13.3104	15.2928
7	Free-head	0.3000	54.5124	1288.	336.6267	13.3104	15.2928
8	Free-head	0.3500	67.2109	1450.	372.2398	13.3104	15.2928
9	Free-head	0.4000	79.7101	1611.	410.6627	13.3104	15.2928
10	Free-head	0.4500	92.0416	1770.	448.2985	13.3104	15.2928
11	Free-head	0.5000	104.2327	1927.	488.3870	13.3104	15.2928
12	Free-head	0.5500	116.3027	2083.	529.8656	13.3104	15.2928
13	Free-head	0.6000	128.2644	2238.	571.0243	13.3104	15.2928
14	Free-head	0.6500	140.1296	2392.	611.8297	13.3104	15.2928
15	Free-head	0.7000	151.9064	2545.	652.2385	13.3104	15.2928
16	Free-head	0.7500	163.6008	2697.	695.7320	13.3104	15.2928
17	Free-head	0.8000	175.2189	2848.	739.0999	13.3104	15.2928
18	Free-head	0.8500	186.7626	2999.	782.1559	13.3104	15.2928
19	Free-head	0.9000	198.2359	3150.	824.8446	13.3104	15.2928
20	Free-head	0.9500	209.7005	3301.	867.0033	13.3104	15.2928
21	Free-head	1.0000	221.1740	3451.	908.5639	13.3104	15.2928
22	Free-head	1.0500	232.5733	3600.	949.6247	13.3104	15.2928
23	Free-head	1.1000	243.8995	3749.	990.1275	13.3104	15.2928
24	Free-head	1.1500	255.1528	3896.	1033.	13.3104	15.2928
25	Free-head	1.2000	266.3346	4043.	1076.	13.3104	15.2928
26	Free-head	1.2500	277.4457	4190.	1118.	13.3104	15.2928
27	Free-head	1.3000	288.4869	4335.	1160.	13.3104	15.2928
28	Free-head	1.3500	299.4579	4480.	1201.	13.3104	15.2928
29	Free-head	1.4000	310.3619	4624.	1242.	13.3104	15.2928
30	Free-head	1.4500	321.2746	4767.	1281.	13.3104	15.2928
31	Free-head	1.5000	332.0967	4909.	1321.	13.3104	15.2928

Table C-8: Analysis Results for Row 8 "No Failures" Condition

Pushover Point Number	Pile-head Fixity Condition	Pile-head Deflection meters	Pile-head Shear kN	Max Moment in Pile kN-m (abs)	Max Shear in Pile kN (abs)	Depth to Max Moment meters	Depth to Max Shear meters
1	Free-head	0.00	-8.3595	92.5118	80.8193	13.9026	12.4236
2	Free-head	0.05000	10.2064	327.3178	98.6526	13.9026	12.4236
3	Free-head	0.10000	26.8879	544.8637	137.6153	13.9026	12.4236
4	Free-head	0.1500	42.6098	752.2704	182.4279	13.9026	12.4236
5	Free-head	0.2000	57.8106	954.2160	229.0278	13.9026	12.4236
6	Free-head	0.2500	72.6742	1153.	277.4924	13.9026	12.4236
7	Free-head	0.3000	87.2959	1348.	326.8990	13.9026	12.4236
8	Free-head	0.3500	101.7236	1542.	377.0472	13.9026	12.4236
9	Free-head	0.4000	115.9846	1734.	426.6179	13.9026	12.4236
10	Free-head	0.4500	130.0926	1926.	477.3078	13.9026	12.4236
11	Free-head	0.5000	144.1086	2116.	527.7862	13.9026	12.4236
12	Free-head	0.5500	158.1170	2304.	577.3408	13.9026	12.4236
13	Free-head	0.6000	171.9795	2491.	626.1084	13.9026	12.4236
14	Free-head	0.6500	185.6940	2676.	675.2702	13.9026	12.4236
15	Free-head	0.7000	199.2578	2859.	724.5605	13.9026	12.4236
16	Free-head	0.7500	212.6675	3040.	773.0577	13.9026	12.4236
17	Free-head	0.8000	225.9172	3220.	820.6672	13.9026	12.4236
18	Free-head	0.8500	239.0253	3399.	867.2517	13.9026	12.4236
19	Free-head	0.9000	252.0174	3577.	914.8726	13.9026	12.4236
20	Free-head	0.9500	265.0109	3752.	961.7005	13.9026	12.4236
21	Free-head	1.0000	277.9048	3925.	1008.	13.9026	12.4236
22	Free-head	1.0500	290.5819	4097.	1053.	13.9026	12.4236
23	Free-head	1.1000	303.1212	4267.	1097.	13.9026	12.4236
24	Free-head	1.1500	315.5224	4436.	1142.	13.9026	12.4236
25	Free-head	1.2000	327.7857	4602.	1187.	13.9026	12.4236
26	Free-head	1.2500	339.8796	4767.	1230.	13.9026	12.4236
27	Free-head	1.3000	351.7692	4931.	1273.	13.9026	12.4236
28	Free-head	1.3500	363.8089	5093.	1315.	13.9026	12.4236
29	Free-head	1.4000	375.7433	5254.	1358.	13.9026	12.4236
30	Free-head	1.4500	387.5813	5414.	1399.	13.9026	12.4236
31	Free-head	1.5000	399.2740	5573.	1439.	13.9026	12.4236

Table C-9: Analysis Results for Row 1 "With Failures" Condition

Pushover Point Number	Pile-head Fixity Condition	Pile-head Deflection meters	Pile-head Shear kN	Max Moment in Pile kN-m (abs)	Max Shear in Pile kN (abs)	Depth to Max Moment meters	Depth to Max Shear meters
1	Free-head	0.00	-1561.	5932.	1570.	15.5281	17.7464
2	Free-head	0.05000	-1550.	5877.	1559.	15.5281	17.7464
3	Free-head	0.10000	-1538.	5823.	1547.	15.5281	17.7464
4	Free-head	0.1500	-1527.	5768.	1536.	15.5281	17.7464
5	Free-head	0.2000	-1515.	5715.	1524.	15.5281	17.7464
6	Free-head	0.2500	-1504.	5661.	1513.	15.5281	17.7464
7	Free-head	0.3000	-1493.	5607.	1502.	15.5281	17.7464
8	Free-head	0.3500	-1482.	5554.	1491.	15.5281	17.7464
9	Free-head	0.4000	-1470.	5501.	1479.	15.5281	17.7464
10	Free-head	0.4500	-1459.	5447.	1468.	15.5281	17.7464
11	Free-head	0.5000	-1448.	5394.	1482.	15.5281	17.7464
12	Free-head	0.5500	-1437.	5341.	1530.	15.5281	17.7464
13	Free-head	0.6000	-1426.	5288.	1578.	15.5281	17.7464
14	Free-head	0.6500	-1415.	5236.	1625.	15.5281	17.7464
15	Free-head	0.7000	-1404.	5211.	1672.	15.5281	17.7464
16	Free-head	0.7500	-1393.	5364.	1719.	15.5281	17.7464
17	Free-head	0.8000	-1383.	5519.	1766.	15.5281	17.7464
18	Free-head	0.8500	-1372.	5672.	1812.	15.5281	17.7464
19	Free-head	0.9000	-1361.	5824.	1857.	15.5281	17.7464
20	Free-head	0.9500	-1351.	5974.	1902.	15.5281	17.7464
21	Free-head	1.0000	-1340.	6125.	1946.	15.5281	17.7464
22	Free-head	1.0500	-1330.	6276.	1989.	15.5281	17.7464
23	Free-head	1.1000	-1319.	6426.	2034.	15.5281	17.7464
24	Free-head	1.1500	-1309.	6575.	2081.	15.5281	17.7464
25	Free-head	1.2000	-1298.	6724.	2128.	15.5281	17.7464
26	Free-head	1.2500	-1288.	6872.	2174.	15.5281	17.7464
27	Free-head	1.3000	-1278.	7018.	2219.	15.5281	17.7464
28	Free-head	1.3500	-1267.	7164.	2264.	15.5281	17.7464
29	Free-head	1.4000	-1257.	7310.	2309.	15.5281	17.7464
30	Free-head	1.4500	-1247.	7456.	2354.	15.5281	17.7464
31	Free-head	1.5000	-1237.	7602.	2398.	15.5281	17.7464

Table C-10: Analysis Results for Row 2 "With Failures" Condition

Pushover Point Number	Pile-head Fixity Condition	Pile-head Deflection meters	Pile-head Shear kN	Max Moment in Pile kN-m (abs)	Max Shear in Pile kN (abs)	Depth to Max Moment meters	Depth to Max Shear meters
1	Free-head	0.00	-1278.	4689.	1278.	15.2500	17.0800
2	Free-head	0.05000	-1270.	4652.	1270.	15.2500	17.0800
3	Free-head	0.10000	-1262.	4614.	1262.	15.2500	17.0800
4	Free-head	0.1500	-1254.	4577.	1254.	15.2500	17.0800
5	Free-head	0.2000	-1246.	4540.	1246.	15.2500	17.0800
6	Free-head	0.2500	-1238.	4504.	1238.	15.2500	17.0800
7	Free-head	0.3000	-1230.	4467.	1230.	15.2500	17.0800
8	Free-head	0.3500	-1222.	4431.	1222.	15.2500	17.0800
9	Free-head	0.4000	-1214.	4394.	1214.	15.2500	17.0800
10	Free-head	0.4500	-1206.	4358.	1206.	15.2500	17.0800
11	Free-head	0.5000	-1198.	4322.	1198.	15.2500	17.0800
12	Free-head	0.5500	-1190.	4287.	1235.	15.2500	17.0800
13	Free-head	0.6000	-1183.	4251.	1271.	15.2500	17.0800
14	Free-head	0.6500	-1175.	4215.	1307.	15.2500	17.0800
15	Free-head	0.7000	-1167.	4179.	1343.	15.2500	17.0800
16	Free-head	0.7500	-1159.	4144.	1379.	15.2500	17.0800
17	Free-head	0.8000	-1152.	4109.	1414.	15.2500	17.0800
18	Free-head	0.8500	-1144.	4093.	1449.	15.2500	17.0800
19	Free-head	0.9000	-1136.	4199.	1484.	15.2500	17.0800
20	Free-head	0.9500	-1129.	4305.	1519.	15.2500	17.0800
21	Free-head	1.0000	-1121.	4411.	1553.	15.2500	17.0800
22	Free-head	1.0500	-1114.	4515.	1586.	15.2500	17.0800
23	Free-head	1.1000	-1106.	4619.	1620.	15.2500	17.0800
24	Free-head	1.1500	-1098.	4723.	1652.	15.2500	17.0800
25	Free-head	1.2000	-1091.	4827.	1687.	15.2500	17.0800
26	Free-head	1.2500	-1083.	4932.	1723.	15.2500	17.0800
27	Free-head	1.3000	-1076.	5037.	1759.	15.2500	17.0800
28	Free-head	1.3500	-1069.	5142.	1794.	15.2500	17.0800
29	Free-head	1.4000	-1061.	5245.	1829.	15.2500	17.0800
30	Free-head	1.4500	-1054.	5347.	1863.	15.2500	17.0800
31	Free-head	1.5000	-1046.	5449.	1897.	15.2500	17.0800

Table C-11: Analysis Results for Row 3 "With Failures" Condition

Pushover Point Number	Pile-head Fixity Condition	Pile-head Deflection meters	Pile-head Shear kN	Max Moment in Pile kN-m (abs)	Max Shear in Pile kN (abs)	Depth to Max Moment meters	Depth to Max Shear meters
1	Free-head	0.00	-515.7001	2036.	515.7001	13.9472	16.3728
2	Free-head	0.05000	-511.2181	2014.	511.2181	13.9472	16.3728
3	Free-head	0.10000	-506.7545	1993.	506.7545	13.9472	16.3728
4	Free-head	0.1500	-502.3073	1971.	503.0957	13.9472	16.3728
5	Free-head	0.2000	-497.8762	1950.	526.3711	13.9472	16.3728
6	Free-head	0.2500	-493.4593	1928.	549.6840	13.9472	16.3728
7	Free-head	0.3000	-489.0569	1907.	573.0287	13.9472	16.3728
8	Free-head	0.3500	-484.6678	1886.	596.3935	13.9472	16.3728
9	Free-head	0.4000	-480.2902	1866.	619.7661	13.9472	16.3728
10	Free-head	0.4500	-475.8267	1845.	642.6295	13.9472	16.3728
11	Free-head	0.5000	-471.3729	1825.	665.4858	13.9472	16.3728
12	Free-head	0.5500	-466.9356	1805.	688.3639	13.9472	16.3728
13	Free-head	0.6000	-462.5143	1785.	711.2552	13.9472	16.3728
14	Free-head	0.6500	-458.1077	1823.	734.1492	13.9472	16.3728
15	Free-head	0.7000	-453.7154	1879.	757.0371	13.9472	16.3728
16	Free-head	0.7500	-449.3364	1935.	779.9096	13.9472	16.3728
17	Free-head	0.8000	-444.9701	1991.	802.7573	13.9472	16.3728
18	Free-head	0.8500	-440.6155	2048.	825.5709	13.9472	16.3728
19	Free-head	0.9000	-436.2720	2104.	848.3411	13.9472	16.3728
20	Free-head	0.9500	-431.9386	2160.	871.0586	13.9472	16.3728
21	Free-head	1.0000	-427.6145	2216.	893.7139	13.9472	16.3728
22	Free-head	1.0500	-423.1728	2271.	915.7342	13.9472	16.3728
23	Free-head	1.1000	-418.7785	2326.	937.9002	13.9472	16.3728
24	Free-head	1.1500	-414.4310	2382.	960.1974	13.9472	16.3728
25	Free-head	1.2000	-410.1457	2437.	982.6976	13.9472	16.3728
26	Free-head	1.2500	-405.8782	2493.	1005.	13.9472	16.3728
27	Free-head	1.3000	-401.6276	2549.	1028.	13.9472	16.3728
28	Free-head	1.3500	-397.3924	2604.	1050.	13.9472	16.3728
29	Free-head	1.4000	-393.1716	2660.	1072.	13.9472	16.3728
30	Free-head	1.4500	-388.9644	2715.	1094.	13.9472	16.3728
31	Free-head	1.5000	-384.6889	2770.	1116.	13.9472	16.3728

Table C-12: Analysis Results for Row 4 "With Failures" Condition

Pushover Point Number	Pile-head Fixity Condition	Pile-head Deflection meters	Pile-head Shear kN	Max Moment in Pile kN-m (abs)	Max Shear in Pile kN (abs)	Depth to Max Moment meters	Depth to Max Shear meters
1	Free-head	0.00	-205.9116	889.3108	266.0096	13.7381	16.3688
2	Free-head	0.05000	-200.9735	864.7733	270.5585	13.7381	16.3688
3	Free-head	0.10000	-196.0953	840.5330	275.0666	13.7381	16.3688
4	Free-head	0.1500	-191.2681	816.5462	279.5435	13.7381	16.3688
5	Free-head	0.2000	-186.4884	818.2179	291.1473	13.7381	16.3688
6	Free-head	0.2500	-181.7507	878.3955	310.3290	13.7381	16.3688
7	Free-head	0.3000	-177.0510	938.2396	329.3270	13.7381	16.3688
8	Free-head	0.3500	-172.3871	997.7733	348.1510	13.7381	16.3688
9	Free-head	0.4000	-167.7543	1057.	366.8204	13.7381	16.3688
10	Free-head	0.4500	-163.1507	1116.	385.3406	13.7381	16.3688
11	Free-head	0.5000	-158.5743	1175.	405.7740	13.7381	16.3688
12	Free-head	0.5500	-154.0224	1233.	427.2497	13.7381	16.3688
13	Free-head	0.6000	-149.4464	1292.	448.5503	13.7381	16.3688
14	Free-head	0.6500	-144.8601	1350.	469.7330	13.7381	16.3688
15	Free-head	0.7000	-140.2974	1407.	490.9343	13.7381	16.3688
16	Free-head	0.7500	-135.7571	1465.	512.1464	13.7381	16.3688
17	Free-head	0.8000	-131.2381	1523.	533.3612	13.7381	16.3688
18	Free-head	0.8500	-126.7395	1580.	554.5704	13.7381	16.3688
19	Free-head	0.9000	-122.2601	1638.	575.7655	13.7381	16.3688
20	Free-head	0.9500	-117.7991	1695.	596.9378	13.7381	16.3688
21	Free-head	1.0000	-113.3551	1752.	618.0782	13.7381	16.3688
22	Free-head	1.0500	-108.9282	1809.	639.1779	13.7381	16.3688
23	Free-head	1.1000	-104.5169	1866.	660.2273	13.7381	16.3688
24	Free-head	1.1500	-100.1212	1922.	681.2170	13.7381	16.3688
25	Free-head	1.2000	-95.7391	1979.	702.1374	13.7381	16.3688
26	Free-head	1.2500	-91.3417	2035.	722.8837	13.7381	16.3688
27	Free-head	1.3000	-86.8754	2092.	743.2777	13.7381	16.3688
28	Free-head	1.3500	-82.4284	2148.	763.6085	13.7381	16.3688
29	Free-head	1.4000	-77.9998	2204.	783.8655	13.7381	16.3688
30	Free-head	1.4500	-73.5885	2260.	804.0386	13.7381	16.3688
31	Free-head	1.5000	-69.1938	2316.	824.1165	13.7381	16.3688

Table C-13: Analysis Results for Row 5 "With Failures" Condition

Pushover Point Number	Pile-head Fixity Condition	Pile-head Deflection meters	Pile-head Shear kN	Max Moment in Pile kN-m (abs)	Max Shear in Pile kN (abs)	Depth to Max Moment meters	Depth to Max Shear meters
1	Free-head	0.00	-81.5225	414.8708	173.7311	13.7232	16.2963
2	Free-head	0.05000	-62.4762	560.7596	192.2421	13.7232	16.2963
3	Free-head	0.10000	-44.6233	787.7095	219.5520	13.7232	16.2963
4	Free-head	0.1500	-27.5839	1007.	265.4777	13.7232	16.2963
5	Free-head	0.2000	-11.0859	1220.	313.1770	13.7232	16.2963
6	Free-head	0.2500	5.0293	1430.	362.3874	13.7232	16.2963
7	Free-head	0.3000	20.8549	1637.	414.5168	13.7232	16.2963
8	Free-head	0.3500	36.4552	1843.	467.8936	13.7232	16.2963
9	Free-head	0.4000	51.8713	2046.	520.8632	13.7232	16.2963
10	Free-head	0.4500	67.1323	2248.	575.3090	13.7232	16.2963
11	Free-head	0.5000	82.2589	2449.	631.7657	13.7232	16.2963
12	Free-head	0.5500	97.2673	2648.	688.0081	13.7232	16.2963
13	Free-head	0.6000	112.1686	2847.	743.9607	13.7232	16.2963
14	Free-head	0.6500	127.0639	3044.	799.3700	13.7232	16.2963
15	Free-head	0.7000	141.9054	3241.	854.2734	13.7232	16.2963
16	Free-head	0.7500	156.6491	3437.	908.7279	13.7232	16.2963
17	Free-head	0.8000	171.2979	3631.	965.8284	13.7232	16.2963
18	Free-head	0.8500	185.8544	3825.	1023.	13.7232	16.2963
19	Free-head	0.9000	200.3202	4020.	1079.	13.7232	16.2963
20	Free-head	0.9500	214.6968	4213.	1135.	13.7232	16.2963
21	Free-head	1.0000	228.9850	4406.	1190.	13.7232	16.2963
22	Free-head	1.0500	243.1859	4598.	1245.	13.7232	16.2963
23	Free-head	1.1000	257.3004	4790.	1299.	13.7232	16.2963
24	Free-head	1.1500	271.3796	4980.	1352.	13.7232	16.2963
25	Free-head	1.2000	285.5090	5169.	1404.	13.7232	16.2963
26	Free-head	1.2500	299.5387	5356.	1456.	13.7232	16.2963
27	Free-head	1.3000	313.4729	5543.	1510.	13.7232	16.2963
28	Free-head	1.3500	327.2876	5729.	1564.	13.7232	16.2963
29	Free-head	1.4000	340.8970	5914.	1617.	13.7232	16.2963
30	Free-head	1.4500	354.4162	6098.	1670.	13.7232	16.2963
31	Free-head	1.5000	367.8046	6282.	1722.	13.7232	16.2963

Table C-14: Analysis Results for Row 6 "With Failures" Condition

Pushover Point Number	Pile-head Fixity Condition	Pile-head Deflection meters	Pile-head Shear kN	Max Moment in Pile kN-m (abs)	Max Shear in Pile kN (abs)	Depth to Max Moment meters	Depth to Max Shear meters
1	Free-head	0.00	-53.3604	339.2546	171.2480	13.4750	15.9500
2	Free-head	0.05000	-43.2551	430.5646	181.0998	13.4750	15.9500
3	Free-head	0.10000	-33.5410	554.2463	190.5542	13.4750	15.9500
4	Free-head	0.1500	-24.0388	676.1899	220.4187	13.4750	15.9500
5	Free-head	0.2000	-14.8642	794.0675	249.1082	13.4750	15.9500
6	Free-head	0.2500	-5.9053	909.5741	273.8581	13.4750	15.9500
7	Free-head	0.3000	2.8850	1023.	301.0115	13.4750	15.9500
8	Free-head	0.3500	11.5356	1135.	328.2250	13.4750	15.9500
9	Free-head	0.4000	20.0705	1246.	354.4632	13.4750	15.9500
10	Free-head	0.4500	28.5515	1356.	384.8596	13.4750	15.9500
11	Free-head	0.5000	36.9909	1465.	414.9136	13.4750	15.9500
12	Free-head	0.5500	45.3540	1574.	444.6916	13.4750	15.9500
13	Free-head	0.6000	53.6491	1681.	474.2056	13.4750	15.9500
14	Free-head	0.6500	61.8822	1788.	503.8016	13.4750	15.9500
15	Free-head	0.7000	70.0593	1895.	536.3429	13.4750	15.9500
16	Free-head	0.7500	78.1852	2001.	568.7974	13.4750	15.9500
17	Free-head	0.8000	86.2642	2107.	601.1428	13.4750	15.9500
18	Free-head	0.8500	94.2983	2212.	633.3541	13.4750	15.9500
19	Free-head	0.9000	102.2913	2316.	665.4069	13.4750	15.9500
20	Free-head	0.9500	110.2456	2421.	697.2749	13.4750	15.9500
21	Free-head	1.0000	118.1634	2525.	728.9316	13.4750	15.9500
22	Free-head	1.0500	126.0628	2628.	760.3148	13.4750	15.9500
23	Free-head	1.1000	134.0390	2732.	791.2175	13.4750	15.9500
24	Free-head	1.1500	141.9745	2835.	822.7559	13.4750	15.9500
25	Free-head	1.2000	149.8714	2939.	855.7915	13.4750	15.9500
26	Free-head	1.2500	157.7312	3042.	888.6714	13.4750	15.9500
27	Free-head	1.3000	165.5553	3144.	921.3703	13.4750	15.9500
28	Free-head	1.3500	173.3450	3247.	953.8631	13.4750	15.9500
29	Free-head	1.4000	181.1016	3349.	986.1245	13.4750	15.9500
30	Free-head	1.4500	188.8259	3451.	1018.	13.4750	15.9500
31	Free-head	1.5000	196.5205	3552.	1050.	13.4750	15.9500

Table C-15: Analysis Results for Row 7 "With Failures" Condition

Pushover Point Number	Pile-head Fixity Condition	Pile-head Deflection meters	Pile-head Shear kN	Max Moment in Pile kN-m (abs)	Max Shear in Pile kN (abs)	Depth to Max Moment meters	Depth to Max Shear meters
1	Free-head	0.00	-29.5492	217.3111	138.5842	13.3104	15.0096
2	Free-head	0.05000	-18.5783	352.7310	149.4898	13.3104	15.0096
3	Free-head	0.10000	-8.1307	482.8781	170.6536	13.3104	15.0096
4	Free-head	0.1500	2.0465	611.2219	204.8098	13.3104	15.0096
5	Free-head	0.2000	11.8219	734.6701	234.2822	13.3104	15.0096
6	Free-head	0.2500	21.4621	857.3821	265.1484	13.3104	15.0096
7	Free-head	0.3000	30.7842	976.0658	295.4073	13.3104	15.0096
8	Free-head	0.3500	39.9536	1092.	320.5026	13.3104	15.0096
9	Free-head	0.4000	48.9574	1207.	342.8470	13.3104	15.0096
10	Free-head	0.4500	57.8220	1319.	369.1571	13.3104	15.0096
11	Free-head	0.5000	66.5699	1431.	395.1496	13.3104	15.0096
12	Free-head	0.5500	75.2167	1542.	420.3266	13.3104	15.0096
13	Free-head	0.6000	83.7752	1651.	448.1072	13.3104	15.0096
14	Free-head	0.6500	92.2547	1760.	477.3567	13.3104	15.0096
15	Free-head	0.7000	100.6651	1869.	506.3267	13.3104	15.0096
16	Free-head	0.7500	109.0111	1976.	535.0131	13.3104	15.0096
17	Free-head	0.8000	117.2993	2083.	563.4147	13.3104	15.0096
18	Free-head	0.8500	125.5341	2190.	592.2117	13.3104	15.0096
19	Free-head	0.9000	133.7193	2296.	623.8158	13.3104	15.0096
20	Free-head	0.9500	141.8582	2401.	655.2712	13.3104	15.0096
21	Free-head	1.0000	149.9534	2506.	686.5517	13.3104	15.0096
22	Free-head	1.0500	158.1111	2611.	717.4258	13.3104	15.0096
23	Free-head	1.1000	166.2375	2715.	748.0656	13.3104	15.0096
24	Free-head	1.1500	174.3190	2819.	778.4769	13.3104	15.0096
25	Free-head	1.2000	182.3569	2923.	808.6300	13.3104	15.0096
26	Free-head	1.2500	190.3527	3026.	838.4944	13.3104	15.0096
27	Free-head	1.3000	198.3075	3129.	868.0392	13.3104	15.0096
28	Free-head	1.3500	206.2224	3231.	897.2333	13.3104	15.0096
29	Free-head	1.4000	214.0984	3333.	928.9265	13.3104	15.0096
30	Free-head	1.4500	221.9368	3435.	960.5466	13.3104	15.0096
31	Free-head	1.5000	229.7384	3536.	991.9099	13.3104	15.0096

Table C-16: Analysis Results for Row 8 "With Failures" Condition

Pushover Point Number	Pile-head Fixity Condition	Pile-head Deflection meters	Pile-head Shear kN	Max Moment in Pile kN-m (abs)	Max Shear in Pile kN (abs)	Depth to Max Moment meters	Depth to Max Shear meters
1	Free-head	0.00	-8.3595	92.5118	80.8193	13.9026	12.4236
2	Free-head	0.05000	10.2064	327.3178	98.6526	13.9026	12.4236
3	Free-head	0.10000	26.8879	544.8637	137.6153	13.9026	12.4236
4	Free-head	0.1500	42.6098	752.2704	182.4279	13.9026	12.4236
5	Free-head	0.2000	57.8106	954.2160	229.0278	13.9026	12.4236
6	Free-head	0.2500	72.6742	1153.	277.4924	13.9026	12.4236
7	Free-head	0.3000	87.2959	1348.	326.8990	13.9026	12.4236
8	Free-head	0.3500	101.7236	1542.	377.0472	13.9026	12.4236
9	Free-head	0.4000	115.9846	1734.	426.6179	13.9026	12.4236
10	Free-head	0.4500	130.0926	1926.	477.3078	13.9026	12.4236
11	Free-head	0.5000	144.1086	2116.	527.7862	13.9026	12.4236
12	Free-head	0.5500	158.1170	2304.	577.3408	13.9026	12.4236
13	Free-head	0.6000	171.9795	2491.	626.1084	13.9026	12.4236
14	Free-head	0.6500	185.6940	2676.	675.2702	13.9026	12.4236
15	Free-head	0.7000	199.2578	2859.	724.5605	13.9026	12.4236
16	Free-head	0.7500	212.6675	3040.	773.0577	13.9026	12.4236
17	Free-head	0.8000	225.9172	3220.	820.6672	13.9026	12.4236
18	Free-head	0.8500	239.0253	3399.	867.2517	13.9026	12.4236
19	Free-head	0.9000	252.0174	3577.	914.8726	13.9026	12.4236
20	Free-head	0.9500	265.0109	3752.	961.7005	13.9026	12.4236
21	Free-head	1.0000	277.9048	3925.	1008.	13.9026	12.4236
22	Free-head	1.0500	290.5819	4097.	1053.	13.9026	12.4236
23	Free-head	1.1000	303.1212	4267.	1097.	13.9026	12.4236
24	Free-head	1.1500	315.5224	4436.	1142.	13.9026	12.4236
25	Free-head	1.2000	327.7857	4602.	1187.	13.9026	12.4236
26	Free-head	1.2500	339.8796	4767.	1230.	13.9026	12.4236
27	Free-head	1.3000	351.7692	4931.	1273.	13.9026	12.4236
28	Free-head	1.3500	363.8089	5093.	1315.	13.9026	12.4236
29	Free-head	1.4000	375.7433	5254.	1358.	13.9026	12.4236
30	Free-head	1.4500	387.5813	5414.	1399.	13.9026	12.4236
31	Free-head	1.5000	399.2740	5573.	1439.	13.9026	12.4236